LA-4725 (ENDF-173)

$c.3$

An Evaluation of the

Neutron and Gamma-Ray Production Cross Sections for Nitrogen

los alamos
scientific laboratory
of the University of California
LOS ALAMOS, NEW MEXICO 87544

los alamos
scientific laboratory
of the University of California
LOS ALAMOS, NEW MEXICO 87544

An Evaluation of the
Neutron and Gamma-Ray Production
Cross Sections for Nitrogen

by

P. G. Young
D. G. Foster, Jr.

CONTENTS
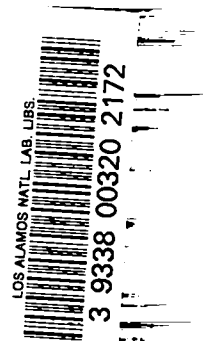
AN EVALUATION OF THE NEUTRON AND

GAMMA-RAY-PRODUCTION CROSS SECTIONS FOR NITROGEN

by

P. G. Young and D. G. Foster, Jr.

ABSTRACT

This report describes a complete evaluation of the neutron
cross sections of ^{14}N from 10^{-5} eV to 20 MeV, including photon-
production cross sections and energy and angular distributions of
secondary neutrons and photons. The recommended data are based
mainly on experiment, augmented by calculations from nuclear
models where appropriate. The evaluated data are available on
magnetic tape in ENDF/B(III) format.

---

1. INTRODUCTION

All neutron-induced reactions with ^{14}N have
been evaluated for the neutron energy region from
10^{-5} eV to 20 MeV.[*] The evaluation includes energy
and angular distributions for secondary neutrons and
photons, as well as neutron- and photon-production
cross sections. The evaluated data are in ENDF/B
(III) format as MAT 1133 and have been provided to
the Radiation Shielding Information Center at Oak
Ridge and to the National Neutron Cross Section Cen-
ter at Brookhaven.

The evaluation is based primarily upon experi-
mental measurements. All available experimental
information for neutron-induced reactions with
nitrogen was compiled for the study. Our bibliog-
raphy is reasonably complete for measurements re-
ported before the fall of 1970, but not all of it
is included in this report. The evaluation was com-
pleted around the end of 1970. Since then several
new results have appeared in the literature, and we
comment on the most important of these in the text.
We also comment on areas that might be improved,
either in light of new information or because of
oversights in the original evaluation.

The more general features of the study are re-
viewed in Sec. 2. The detailed considerations that
went into the evaluation are described in Secs. 3 –
5. Section 3 is devoted to cross sections, Sec. 4
to neutron angular distributions, and Sec. 5 to
secondary-photon angular distributions. Sec. 3 also
gives implicit information on neutron and photon
energy distributions, because all (n,n') reactions
are represented as discrete level-excitation cross
sections and all gamma rays are given as discrete
transitions. In addition, explicit information on
(n,2n) energy distributions is given in Sec. 3.
Finally, Sec. 6 includes a capsule summary of esti-
mated uncertainties in the evaluated quantities, to-
gether with a brief discussion of areas where the
evaluation might be improved.

2. GENERAL FEATURES OF THE EVALUATION

The neutron-induced reactions with ^{14}N that
have two or three outgoing particles are summarized
in Table I, together with the reaction Q-values[*]
and thresholds. The most important reactions are
also shown schematically in Fig. 1. The "E_{lab}"
scales at the right and left boundaries of Fig. 1

---

[*] Because natural nitrogen consists of 99.63% ^{14}N
and only 0.37% ^{15}N, it can be treated as ^{14}N for
most practical applications.

[*] All Q-values in this evaluation are from the 1964
mass tables of Mattauch et al. (Ma65). A new set
of mass tables (Wa71) has recently become available.

indicate laboratory neutron energy and can be used to determine the thresholds for the various reactions. The energies associated with the level diagrams are in the center-of-mass system. Going from left to right, the following processes are represented: $^{14}N(n,n')^{14}N$, $^{14}N(n,np)^{13}C$, $^{14}N(n,p)^{14}C$, $^{14}N(n,d)^{13}C$, $^{14}N(n,t)^{12}C$, $^{14}N(n,\alpha)^{11}B$, $^{14}N(n,2\alpha)^{7}Li$, and $^{14}N(n,2n)^{13}N$.

TABLE I

Q-VALUE AND THRESHOLD

FOR SEVERAL NITROGEN REACTIONS

Reaction	Q-value (MeV)	Threshold (MeV)
$^{14}N(n,n)^{14}N$	0	0
$^{14}N(n,\gamma)^{15}N$	10.835	0
$^{14}N(n,p)^{14}C$	0.626	0
$^{14}N(n,d)^{13}C$	-5.325	5.709
$^{14}N(n,t)^{12}C$	-4.015	4.304
$^{14}N(n,^{3}He)^{12}B$	-17.366	18.617
$^{14}N(n,\alpha)^{11}B$	-0.157	0.168
$^{14}N(n,n')^{14}N*$	-2.313	2.480
$^{14}N(n,n'p)^{13}C$	-7.550	8.094
$^{14}N(n,n'd)^{12}C$	-10.272	11.012
$^{14}N(n,n'\alpha)^{10}B$	-11.613	12.450
$^{14}N(n,p\alpha)^{10}Be$	-11.386	12.206
$^{14}N(n,d\alpha)^{9}Be$	-15.976	17.127
$^{14}N(n,t\alpha)^{8}Be$	-11.384[a]	12.204
$^{14}N(n,2\alpha)^{7}Li$	-8.822	9.457
$^{14}N(n,2n)^{13}N$	-10.553	11.313

[a]^{8}Be is unstable by 95 keV to breakup into two alpha particles.

We determined the cross sections for the (n,p_0), (n,d_0), (n,t_0), (n,α_0), $(n,2\alpha)$, and $(n,2n)$ reactions from direct experimental measurements. The excitation cross sections for the various gamma-ray-producing levels, which are mostly the levels shown below the thresholds for particle emission in Fig. 1, are also based largely on experimental measurements. For the higher levels, we used Hauser-Feshbach (Ha52) and evaporation-model calculations to supplement the measurements. We determined the total cross section over the entire energy region from experimental data. Below 10 MeV, the elastic cross section was obtained by subtracting the sum of the nonelastic partials from the total cross section. At higher energies, however, the nonelastic cross section be-

comes less and less certain owing to uncertainty in the (n,n') cross section to highly excited levels of ^{14}N. Therefore, above 10 MeV we joined the elastic cross section smoothly to the elastic measurements, and adjusted the (n,n') cross section to the particle-unstable states (predominantly the (n,np) reaction), so that the nonelastic partial cross sections summed to the correct total nonelastic cross section.

The gross features of the evaluated cross sections are shown in Figs. 2-5. Fig. 2 gives the total, elastic, (n,p), and (n,γ) cross sections from 10^{-11} to 0.1 MeV. The (n,p) reaction accounts for most of the neutron absorption at these energies. Figure 3 gives an overview of the structure in the total, elastic, and nonelastic cross sections in the MeV region. Figure 4 shows the (n,γ), (n,α), (n,2α), and (n,2n) cross sections over the MeV region. We obtained the (n,α) cross section by summing the discrete (n,α) excitation cross sections for the first 11 states of ^{11}B. The (n,γ) reaction is relatively unimportant at these energies, whereas the (n,α) cross section is reasonably large over much of the MeV region. The (n,2α) reaction also becomes important at higher energies. Finally, Fig. 5 compares the (n,n'), (n,p), (n,d), and (n,t) cross sections in the MeV region. The (n,n') cross section is the sum of all (n,n') reactions and includes the (n,n'p), (n,n'd), and (n,n'α) processes. The (n,p), (n,d) and (n,t) cross sections result from summing the excitation cross sections to particle-stable levels for these reactions and are seen to have relatively small cross sections at energies above ~ 6 MeV.

We determined the elastic angular distributions below 8 MeV from a single-level resonance-theory analysis that incorporated resonance energies and total widths from our analysis of the total cross section and reaction widths from our analysis of the partial cross sections. With the resonance parameters fixed, we obtained the $\ell = 0$ and $\ell = 1$ potential phase shifts by fitting the available angular-distribution measurements. A total of 33 resonances are included in the analysis. From 8 to 15 MeV, we determined the elastic angular distributions by fitting the available measurements with Legendre expansions, and above 15 MeV we used optical-model calculations to estimate the angular
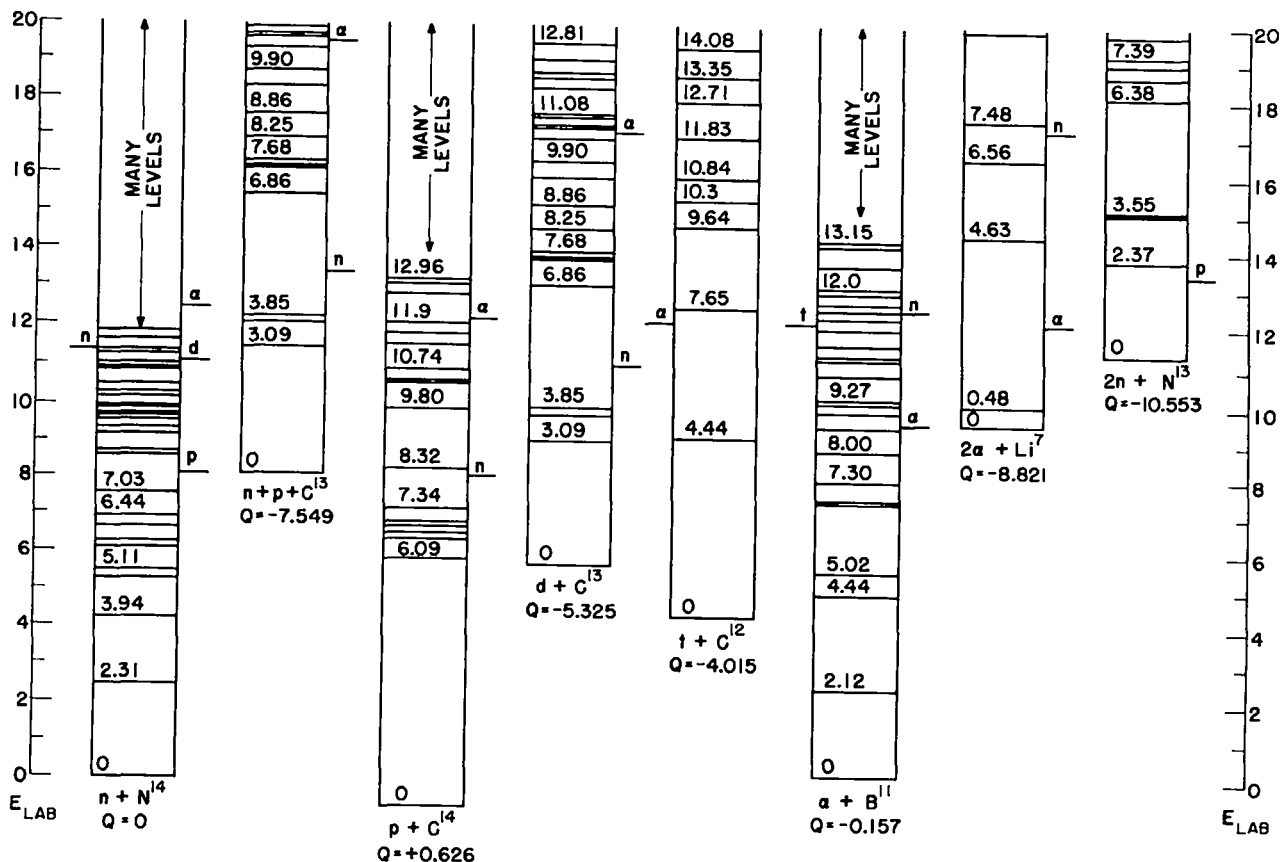
Fig. 1. Composite energy-level diagram for the residual nuclei of major interest in this evaluation. Except for the "E_{lab}" scales, the energies are in the center-of-mass system, and all energies are in MeV. The separation energies for secondary-particle emission are shown by short lines at the side of each diagram.

distributions. The inelastic neutron angular distributions are based almost entirely upon measured (p,p') angular distribtuions, making use of an equivalence theorem due to Lutz and Anderson (Lu66) and Anderson et al. (An67) which is based upon the charge symmetry of nuclear forces.

3. NEUTRON AND PHOTON-PRODUCTION CROSS SECTIONS AND SECONDARY-ENERGY DISTRIBUTIONS

3.1 Total Cross Section

We constructed the free-atom total cross section in the eV region from the scattering and absorption cross sections. The absorption cross section was assumed to have a 1/v energy dependence and was based upon a measurement of the thermal (n,γ) cross section by Jurney and Motz (Ju63) and upon a composite of four measurements of the thermal

(n,p) cross section (Co49,[*] Ba49,[*] Cu51,[*] Ha61[*]). We assumed the scattering cross section to be constant at these energies and obtained it by fitting a straight line as a function of $E_n^{-\frac{1}{2}}$ to Melkonian's (Me49) time-of-flight total-cross-section measurement between 1 and 79 eV, augmented by a single point at 0.0253 eV derived from the absorption cross section and an estimate of the scattering cross section. Two iterations of this procedure were made to obtain the scattering cross section, and the results are summarized for $E_n = 0.0253$ eV in Table II. In this way we found that molecular effects in N_2 gas are perceptible in the total cross section at all energies below 2 eV, in approximate agreement with Melkonian's original conclusions (Me49).

---

[*]These results have been renormalized to a boron (n,α) cross section of 759b for thermal neutrons.
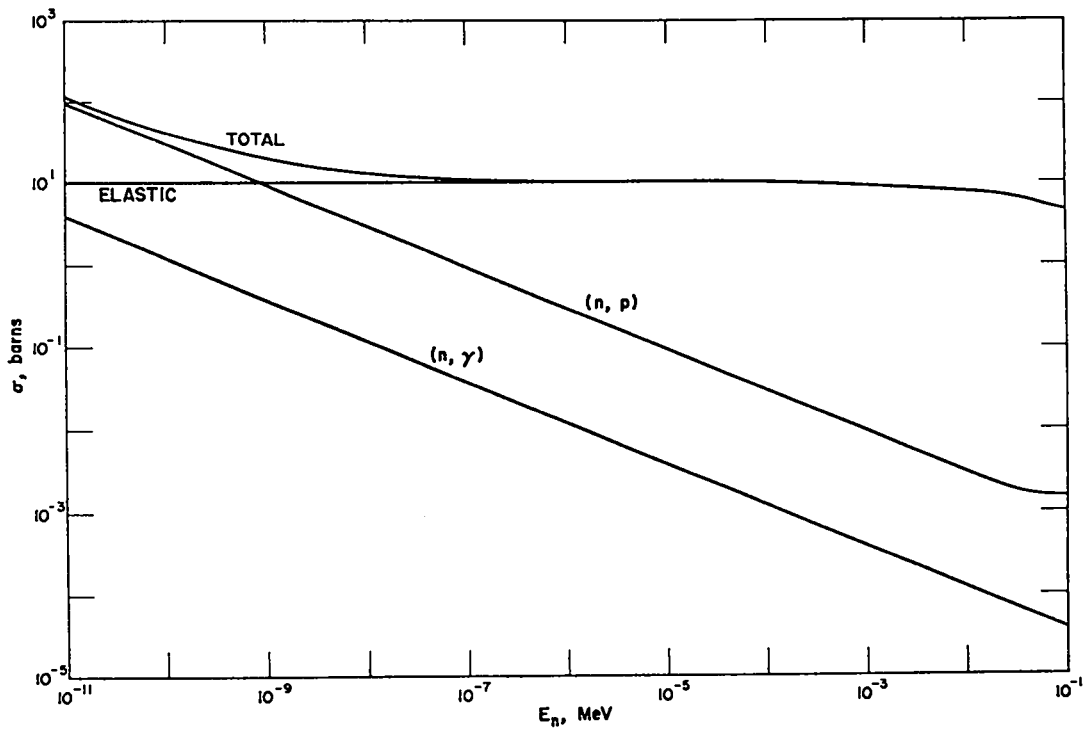
Fig. 2. Evaluated total cross section and its constituent partial cross sections from 10^{-11} to 10^{-1} MeV.
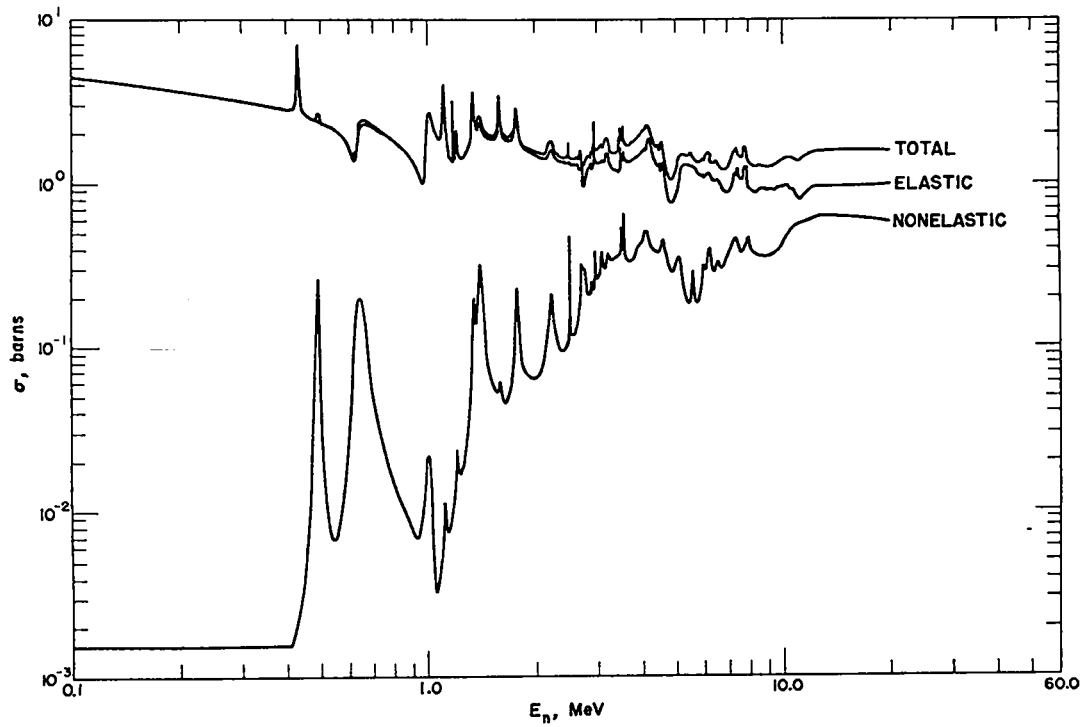
Fig. 3. Evaluated total cross section and its constituent elastic and nonelastic cross sections from 0.1 to 20 MeV.

4
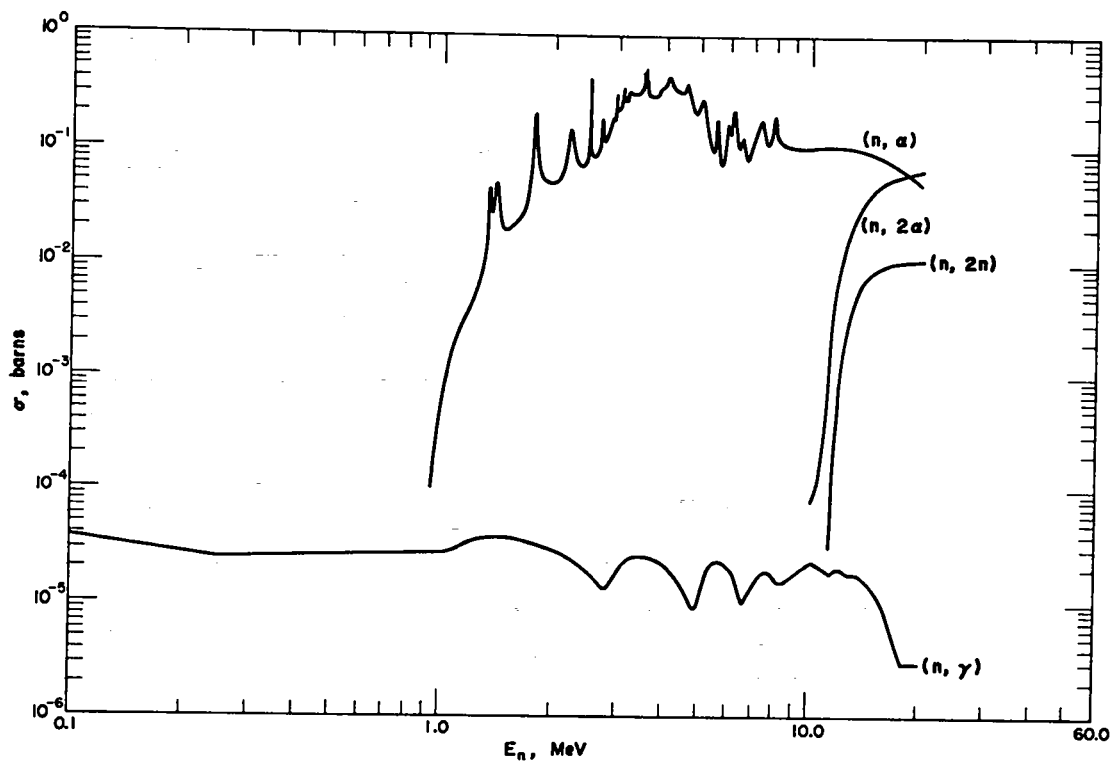
Fig. 4. Evaluated (n,γ), (n,α), $(n,2\alpha)$, and $(n,2n)$ cross sections from 0.1 to 20 MeV.
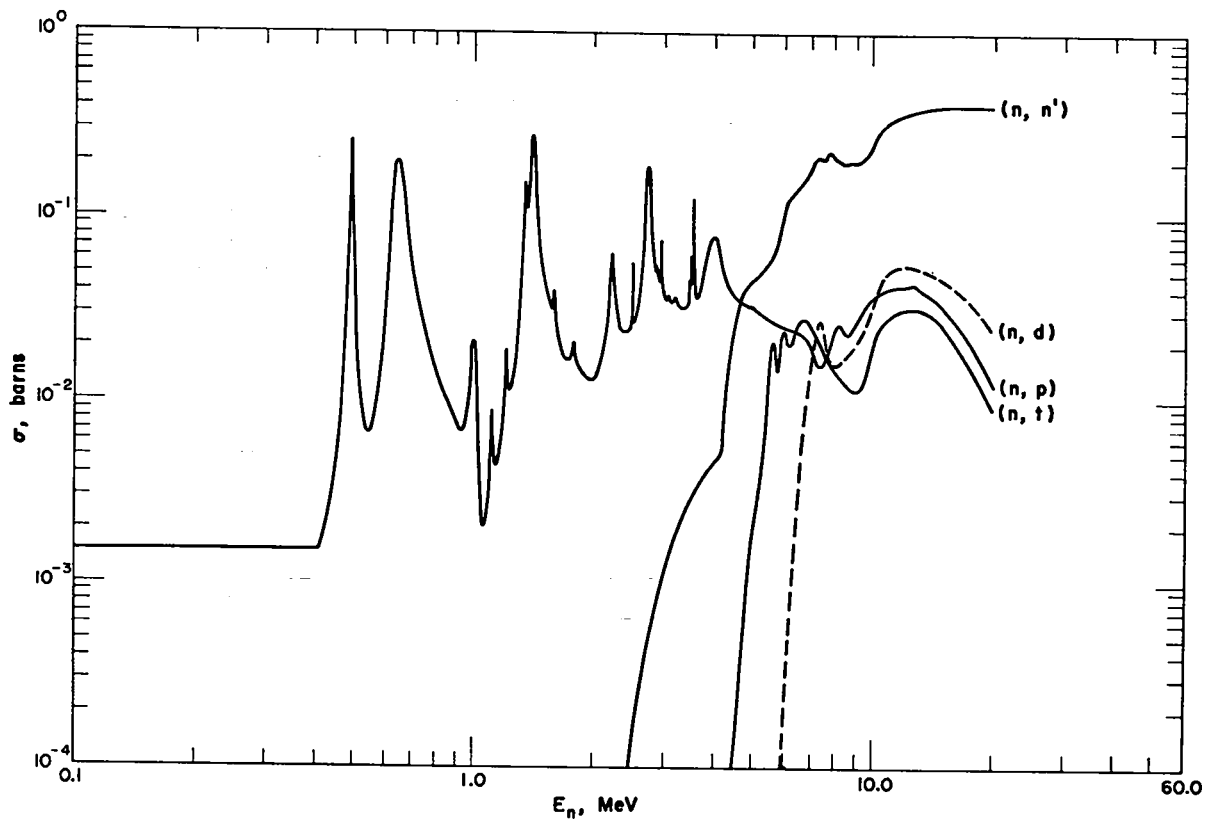
Fig. 5. Evaluated cross sections from 0.1 to 20 MeV for inelastic scattering and the (n,p), (n,d), and (n,t) reactions. As discussed in the text, the (n,n') cross section includes $(n,n'p)$, $(n,n'd)$, and $(n,n'\alpha)$ reactions.

Accordingly, we included only the total cross-section data between 1.3 and 79 eV in the fit. Aside from any unknown systematic errors in the total or absorption cross sections, the extrapolation of the total cross section to 10^{-5} eV is accurate to within 5%.

TABLE II

2200-m/sec CROSS SECTIONS OF NITROGEN

Reaction	σ (barns)	$\Delta\sigma$[a] (barns)	Reference
(n,p)	1.819	0.036	Co49,Ba49,Cu51,Ha61
(n,γ)	0.075	0.0075	Ju63
Absorption	1.894	0.037	Sum of (n,γ) and (n,p)
Scattering	9.957	0.040	Present Analysis
Total	11.851	0.054	Present Analysis

[a] Does not include estimates of systematic errors. See Sec. 6 for more realistic error estimates.

The evaluated total cross section from 10^{-5} eV to 10 keV is compared to the available measurements in Fig. 6. Melkonian's data below 0.3 eV, which are severely influenced by molecular effects, have been omitted from Fig. 6. Above 80 eV, we fitted a quadratic in log E_n to Melkonian's data from 85 to 653 eV and to our evaluated composite (described below) from 10 to 20 keV. Melkonian's two points above 653 eV are clearly inconsistent with the other measurements and have been discarded.

The foundation for the evaluated total cross section in the MeV region is the recent time-of-flight measurements by Heaton et al. (He70) at the National Bureau of Standards, Carlson and Cerbone (Ca70) at Gulf General Atomic (GGA), and Foster and Glasgow (Fo71) at Hanford. These three measurements, which span the energy region from 0.5 to 25 MeV, are in such dramatically good agreement (better than 0.5% on the average after allowance for differences in resolution) that we discarded nine older measurements between 2 and 15 MeV. The Heaton and Carlson energy scales agree to within ±0.5 keV at all energies where a close comparison can be made. We therefore used the time-of-flight energy scale to correct the energy scales of the older measurements that overlap it at the low-energy end. Further, the time-of-flight measurements served as a standard for judging the quality of the older measurements that overlapped at lower energies.

Between 10 and 500 keV, the measurements of Hinchey et al. (Hi52) and Huddleston and Mooring (Hu61) are flanked by two unpublished measurements (Bi59, Bi62) from Duke which disagree by 8% in their overlap region. However, a composite of these four measurements, after normalization to their weighted average, provides a substantial overlap with the time-of-flight measurements by Heaton et al. (He70) and Carlson and Cerbone (Ca70), and the composite agrees with the Heaton data to within a few tenths of one percent. We therefore used this composite for the evaluated total cross section from 10 to 500 keV. Figure 7 compares the evaluated and experimental data from 10 to 410 keV before normalization.

The only significant disagreement in the time-of-flight measurements occurs at the low-energy end of the Heaton (He70) and Carlson (Ca70) measurements, roughly from 0.5 to 0.7 MeV. This difference, which is a maximum of 5% at 500 keV, arises from dead-time errors in the high-intensity time-of-flight systems and is always greatest at the lowest energy. The error in the Heaton (He70) data is intrinsically larger, but the correction is more accurately known. Because the Heaton data agree so well with the normalized composite of the Hinchey (Hi52), Huddleston (Hu61), and Bilpuch (Bi59, Bi62) measurements at lower energies, we based our evaluated curve from 0.5 to 0.75 MeV entirely on the Heaton (He70) results. Additional NBS measurements (made after this part of the evaluation was completed) directed specifically at resolving this discrepancy indicate that our composite should be lowered by 1.5% at 500 keV, which would reduce the discrepancy between the GGA and NBS measurements to 3.5%.

The total-cross-section results from 0.4 to 0.7 MeV, including the unnormalized data, are shown in Fig. 8. This energy region includes the first three resonances in nitrogen at 434, 493, and 647 keV. We found the energy of the lowest resonance to be 433.6 ± 0.4 keV after correcting the energy scales of the lower-energy measurements to agree with the Heaton (He70) and Carlson (Ca70) time-of-flight data. The second resonance at 493 keV has a rather small neutron width ($\Gamma_n/\Gamma \sim 0.3$) and is seen more clearly in the (n,p) reaction than in the total cross section. This point is better illustrated in Fig. 3 where the first peak in the non-elastic cross section is entirely due to the 493-keV resonance in the (n,p) cross section.
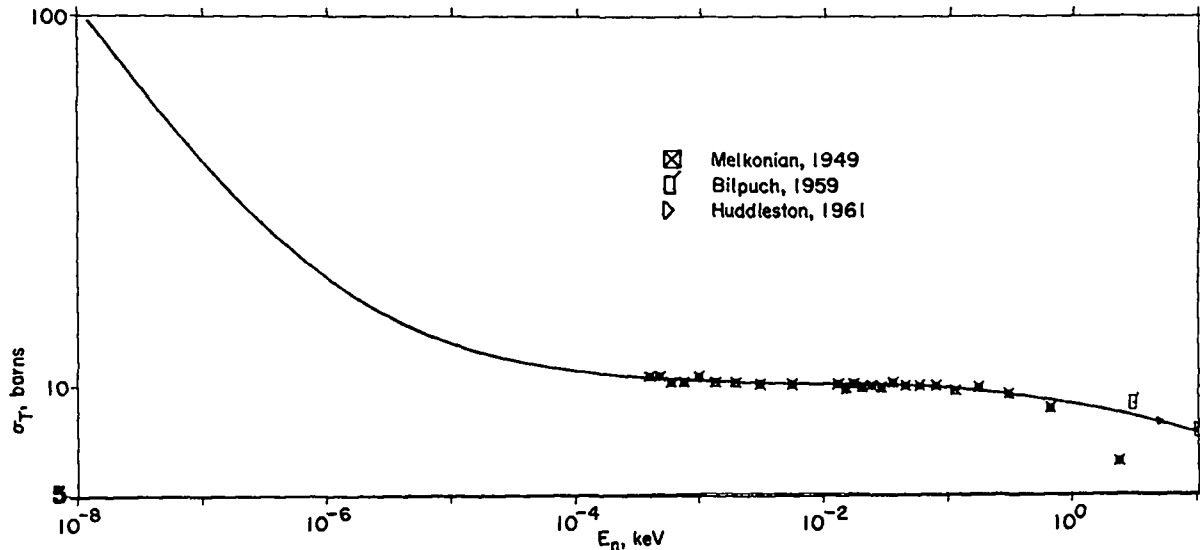
Fig. 6. Evaluated total cross section below 10 keV with the data on which it is based.
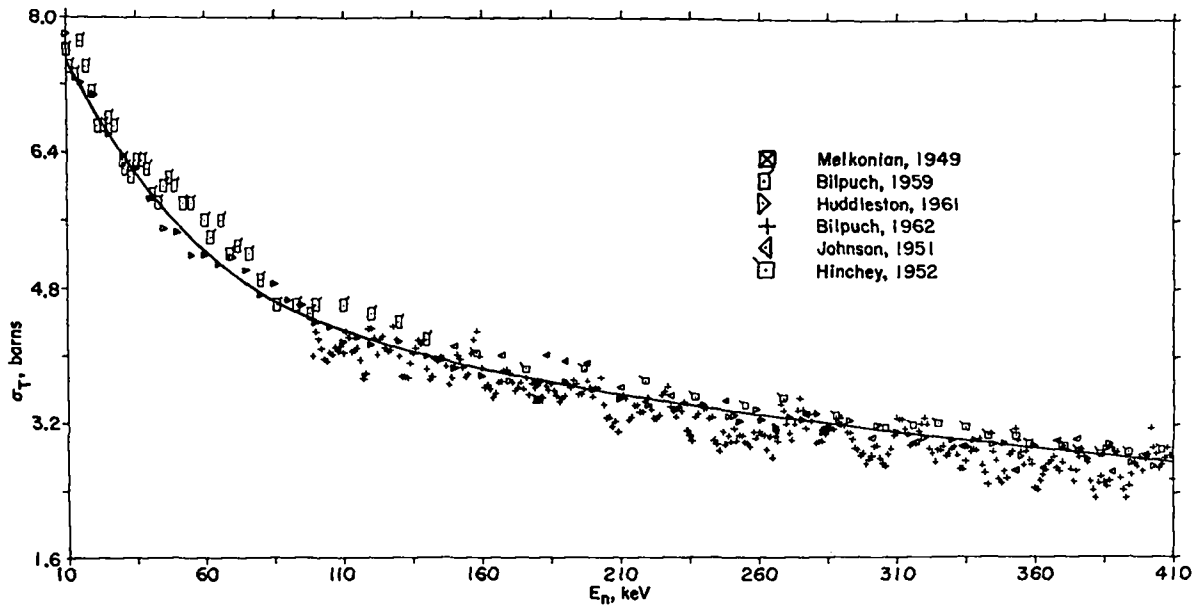
Fig. 7. Evaluated total cross section from 10 to 410 keV with the measurements on which it is based.

For smoothing purposes, we have represented the peaks in the total cross section up to about 8 MeV by single-level Breit-Wigner fits above straight-line backgrounds. These fits also served to establish resonance energies and widths for other parts of the evaluation. Where the cross section is smooth, that is, between resonances and at energies > 8 MeV, we generated the evaluated curve by sliding polynomial fits to the composite experimental data.

From 0.75 to 25 MeV, we used a composite of the three time-of-flight measurements by Heaton et al.

(He70), Carlson and Cerbone (Ca70), and Foster and Glasgow (Fo71) to represent the total cross section. The evaluated curve was obtained by smoothing the composite results, as described above. Generally, we used the Carlson data alone to fit the Breit-Wigner shapes over sharp structure because these data have the best resolution; the Heaton results, on the other hand, dominate the composite at other energies because of their better precision. There was serious disagreement between some of the older measurements and the time-of-flight composite, with

differences of up to 20%. Most of the older data between 4 and 15 MeV lie systematically higher than the composite. The evaluated total cross section from 0.7 to 30 MeV is compared to all available experimental measurements in Figs. 9-18. Again, we show all of the data in their original (unnormalized) form. We estimate the accuracy of the evaluated total in this energy region to be ~ 1% except near fine structure.

Pronounced structure is observed in the total cross section up to about 8 MeV. A complete description of the resonances in the total cross section is given in Sec. 4.1.1, which deals with the resonance-theory analysis used to obtain the elastic angular distributions. Evidence for this structure is seen in most of the figures, but perhaps the best example occurs in Fig. 10 which shows the 1.116-, 1.184-, 1.209-, 1.349-, and 1.406-MeV resonances. The sharp structure in this figure, particularly the 1.184-MeV resonance (width = 2.1 keV), illustrates the excellent agreement between the energy scales of the Heaton (He70) and Carlson (Ca70) measurements, as well as the superior energy resolution of the

Carlson measurements. These points are also illustrated in Fig. 13 which includes several resonances over the energy region 2.65 to 3.375 MeV. The Foster and Glasgow time-of-flight data (Fo71) in Fig. 13 have poorer resolution than either the Heaton or Carlson measurements.

Examples of disagreement between older measurements and the recent time-of-flight results (Ca70), He70, Fo71) occur in all figures, but the most apparent involve the data of Johnson et al. (Jo51) in Fig. 9, the data of Johnson et al. (Jo52, Jo68) in Fig. 12, the data of Johnson et al.(Jo68) and Meier et al. (Me53) in Figs. 13 and 14, and the data of Nereson and Darden (Ne54) and Becker and Barschall (Be56) in Figs. 14-16. Most of these data are fairly old, and the differences are not too surprising. Examples of extremely good agreement between older measurements and the recent time-of-flight data are the Coon measurement (Co52) at 14.1 MeV in Fig. 17 and the Peterson et al.measurements (Pe60) above 15 MeV in Fig. 18.

The time-of-flight data of Foster and Glasgow (Fo71) begin in Fig. 12 near 2.3 MeV. The statistics in these data are poor at the low-energy end, and
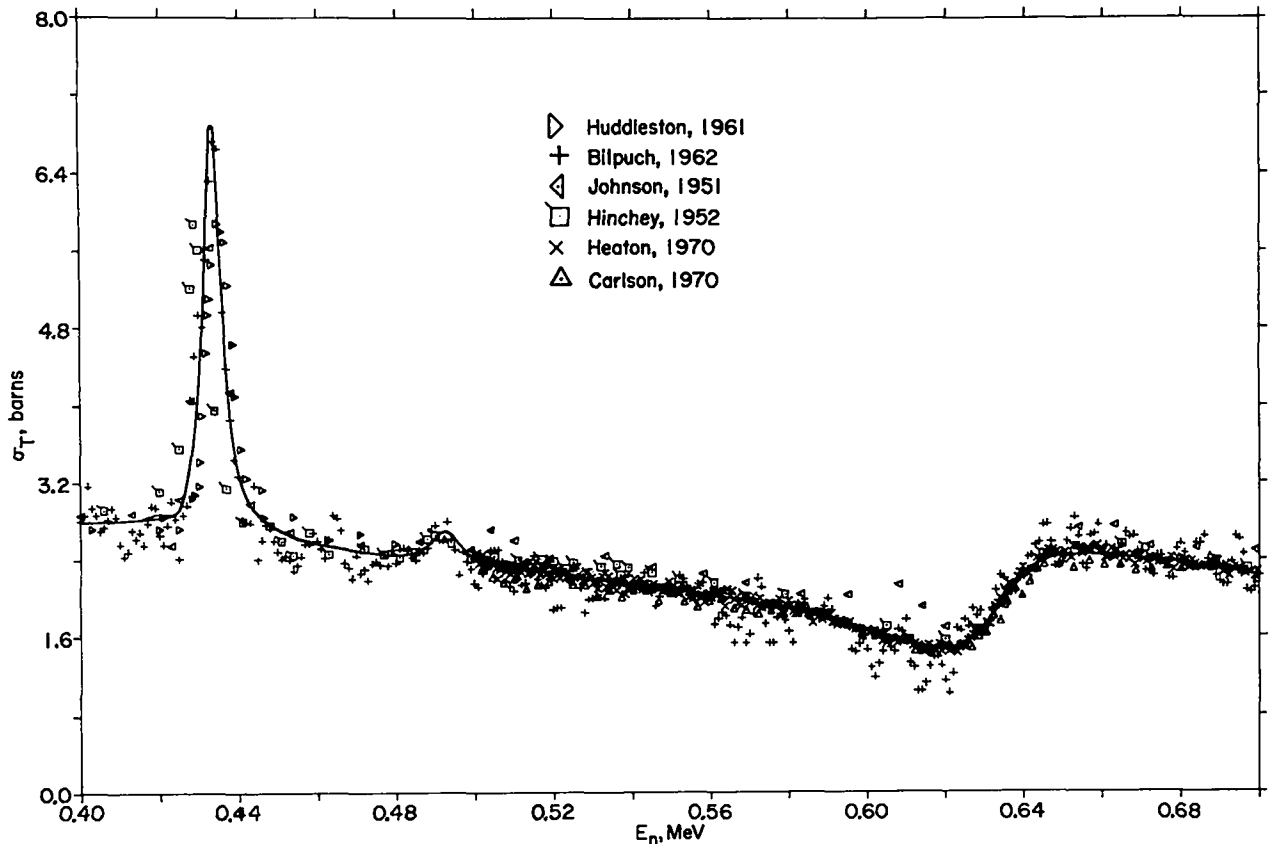
Fig. 8. Evaluated total cross section from 400 to 700 keV with the data on which it is based.

the results seem somewhat lower than the Heaton (He70) and Carlson (Ca70) measurements near 2.4 MeV. At energies above 2.7 MeV, however, the three time-of-flight measurements agree very well.

Figure 16 gives the total cross section from 6 to 9 MeV, which spans the energy region of the famous nitrogen discrepancy. This discrepancy, which was pointed out by Stewart (St69) and Dickens and Perey (Di69), occurs because the elastic cross sec-

tion obtained near 8 MeV by subtracting the sum of the nonelastic partial cross sections from the total cross section lies some 200 mb higher than the elastic measurement by Bauer et al. (Ba67). This problem is discussed further in Sec. 3.10. In Fig. 16, the time-of-flight measurements of Heaton (He70), Carlson (Ca70), and Foster (Fo71) again agree reasonably well, and, although some of the older data (Be56, Ne54) disagree with the evaluated curve,

Fig. 9. Measured and evaluated total cross section between 0.7 and 1.1 MeV.
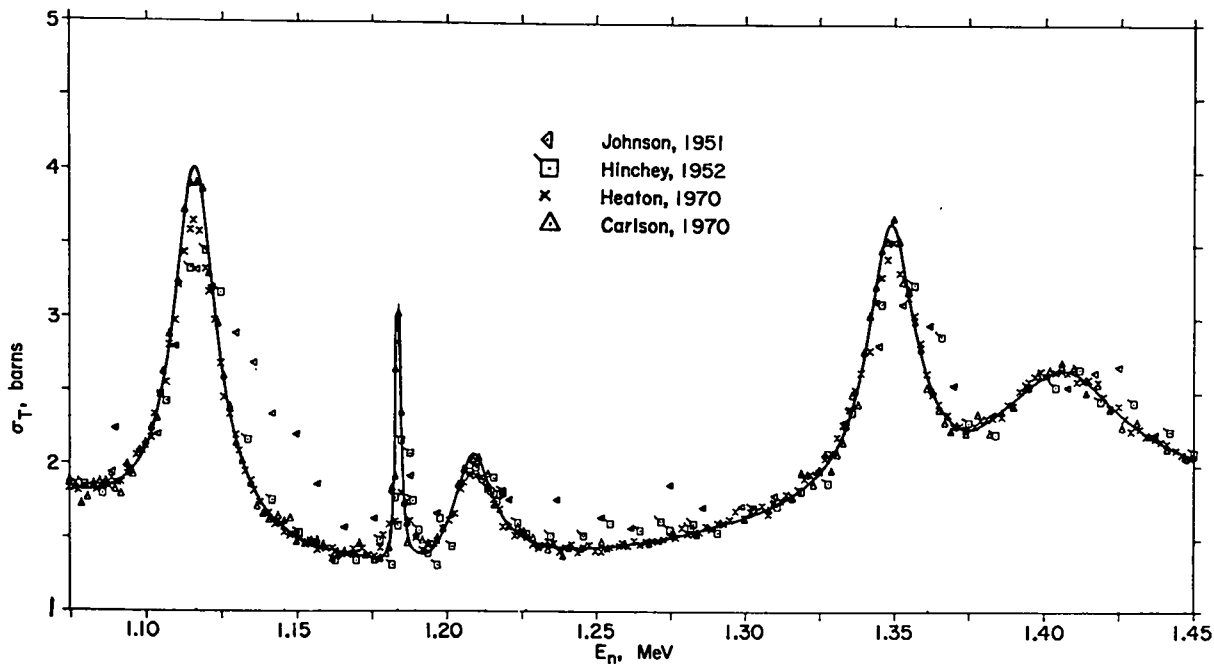
Fig. 10. Measured and evaluated total cross section between 1.1 and 1.45 MeV.

9

these earlier measurements are generally higher than the evaluation which is in the wrong direction to explain the discrepancy in the cross sections.

The Carlson (Ca70) measurement ends at 9 MeV (Fig. 16), and near this energy the statistics in the data are poor. The Foster (Fo71) and Heaton (He70) results agree well up to 15 MeV where the Foster measurement ends (Fig. 17). The Heaton measurement continues to 25 MeV and is seen to agree well with the older Peterson measurement (Pe60) above 15 MeV (Fig. 18). We extended the evaluated total cross section to 150 MeV by fitting all available measurements above 24 MeV with a cubic in log E_n; these results are presented in Fig. 19. The worst statistical uncertainty in the fit is less than 2% near 45 MeV.

3.2 The $^{14}N(n,\gamma)^{15}N$ Cross Section

The thermal (n,γ) cross section for nitrogen has been measured as 80 ± 20 mb by Bartholomew (Ba57) and as 75 ± 7.5 mb by Jurney and Motz (Ju63). The 75-mb value was accepted for this evaluation. The energy dependence of the (n,γ) cross section is assumed to be 1/v up to 250 keV, as the first resonance in nitrogen does not occur until 434 keV.

The (n,γ) reaction is the inverse of the nuclear photoeffect and is expected to exhibit the photonuclear giant resonance near $E_n = 11$ MeV. Because of lack of experimental data in the MeV region, we
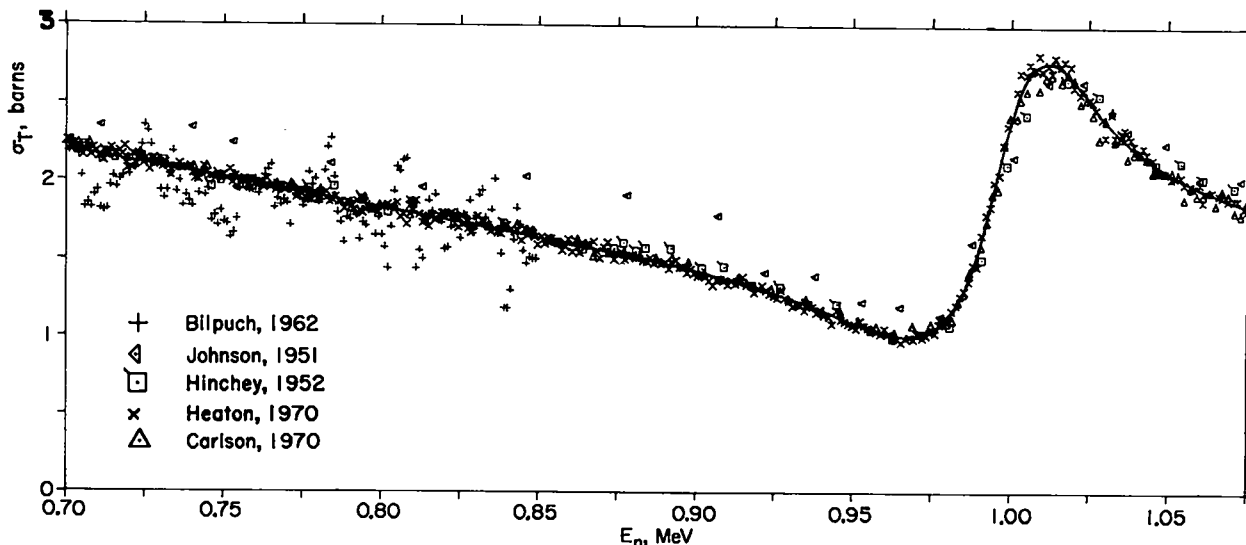
Fig. 11. Measured and evaluated total cross section between 1.45 and 2.05 MeV.
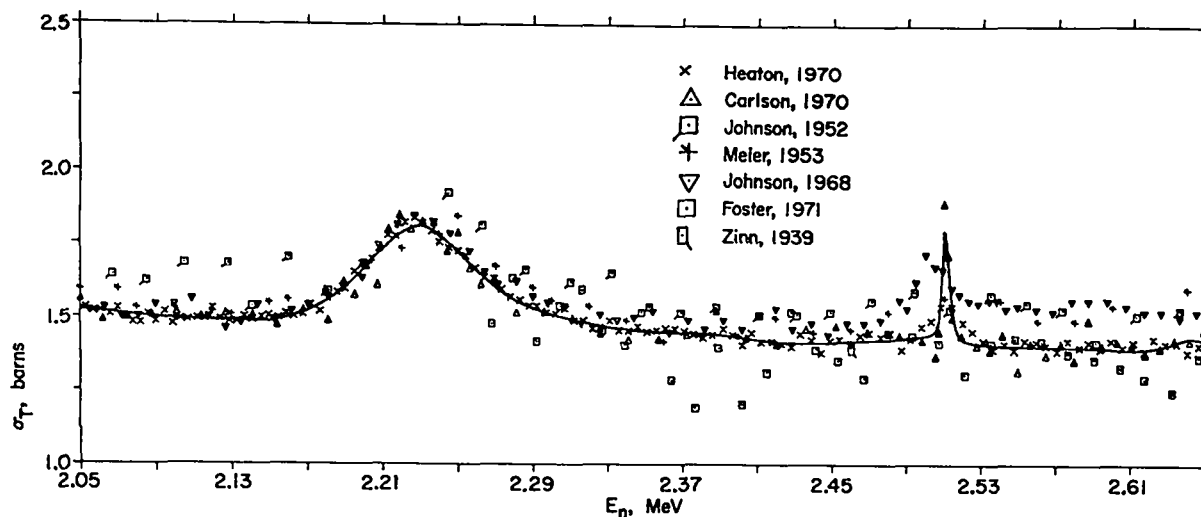
Fig. 12. Measured and evaluated total cross section between 2.05 and 2.65 MeV.

10

assume that the cross section for the $^{14}N(n,\gamma)^{15}N$ reaction is equal to the cross section for the $^{14}N(p,\gamma)^{15}O$ charge-conjugate reaction. This assumption is made because the (n,γ) and the (p,γ) reactions excite the same isospin states, and ^{15}N and ^{15}O are mirror nuclei. In addition to adjusting the (n,γ) and (p,γ) data to the same excitation energies in the compound nucleus, we have introduced a linear shift in the neutron-energy scale which decreases from about 2 MeV near $E_n = 1$ MeV to zero near $E_n = 15$ MeV. This realignment of the energies in the mirror nuclei matches the observed structure in the (p,γ) cross section below the giant resonance to groups of peaks in the neutron total cross section.

The best available evidence on the (p,γ) reaction in this region comes from measurements by Kuan et al. (Ku70). The (p,γ) cross section is 6 to 8 times greater than the (n,γ) cross section extrapolated from thermal. The evaluated $^{14}N(n,\gamma)$ cross section from 10^{-11} to 20 MeV is shown in Fig. 20.

We obtained the capture gamma-ray energy spectrum at thermal-neutron energy by evaluating a decay scheme for the particle-stable levels of ^{15}N, using charged-particle data as well as direct (n,γ) spectrum measurements. The results of this analysis are shown schematically in Fig. 21. The primary transition probabilities and level-branching ratios are based mainly upon the $^{14}N(n,\gamma)$ spectrum measurements
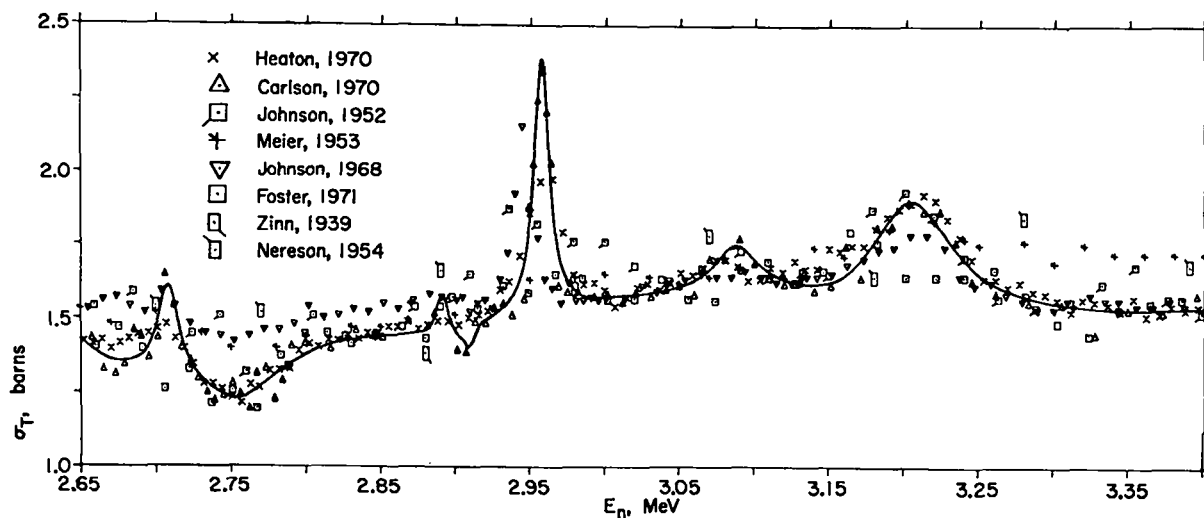
Fig. 13. Measured and evaluated total cross section between 2.65 and 3.4 MeV. The weak structure at 2.9 MeV is barely significant statistically.
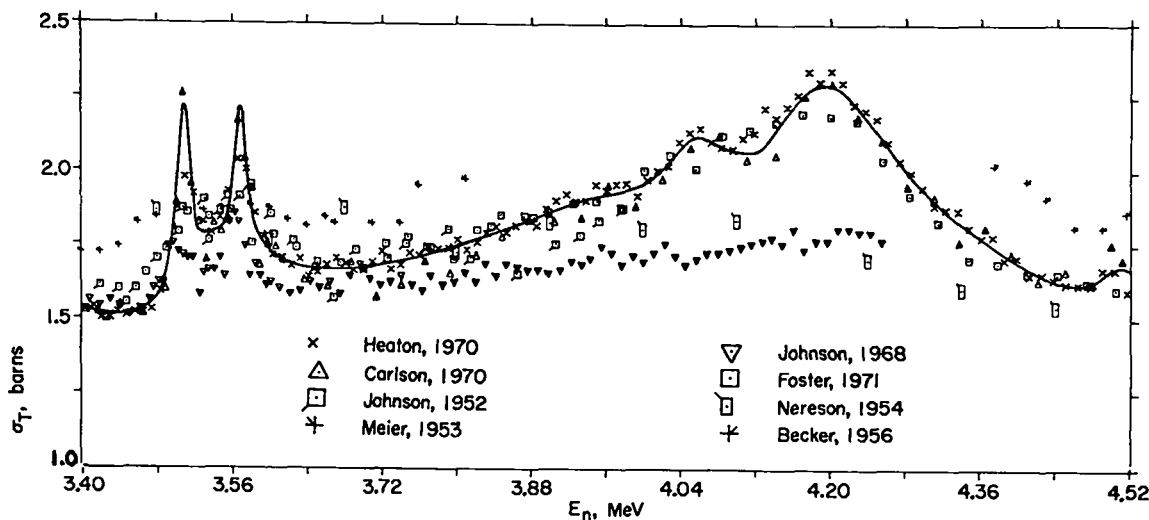
Fig. 14. Measured and evaluated total cross section from 3.4 to 4.5 MeV.

by Jonsson and Hardell (Jo69), Thomas et al. (Th67), and Motz et al. (Mo62), together with $^{13}C(^{3}He,p\gamma)^{15}N$ coincidence measurements by Phillips et al. (Ph67), $^{14}C(p,\gamma)^{15}N$ measurements by Siefken et al. (Si69), $^{13}C(^{3}He,p\gamma)^{15}N$ measurements by Warburton et al. (Wa66), and the $^{14}N(d,p\gamma)^{15}N$ and $^{13}C(^{3}He,p\gamma)^{15}N$ studies of Warburton et al. (Wa65a). We obtained branching information for the 9.15-MeV doublet from Greenwood's $^{14}N(n,\gamma)$ measurement (Gr68), as well as from Jonsson and Hardell (Jo69). The excitation energies in Fig. 21 are from measurements by Greenwood (Gr68), Jonsson and Hardell (Jo69), Gallman

et al. (Ga66), and Warburton et al. (Wa66), in decreasing order of emphasis.

In Table III, we compare the evaluated capture gamma-ray spectrum to measurements by Motz et al. (Mo62), Thomas et al. (Th67), Jonsson and Hardell (Jo69), and Orphan et al. (Or70). The column labeled E_γ contains the transition energy without correction for the energy of the recoiling ^{15}N nucleus. Thomas et al. (Th67) tabulate the recoil energy, which is a maximum of 4.2 keV for the 10.835-MeV transition, for the various lines. The total multiplicity of the evaluated thermal spectrum is 2.166. In Table III the evaluated spectrum and the
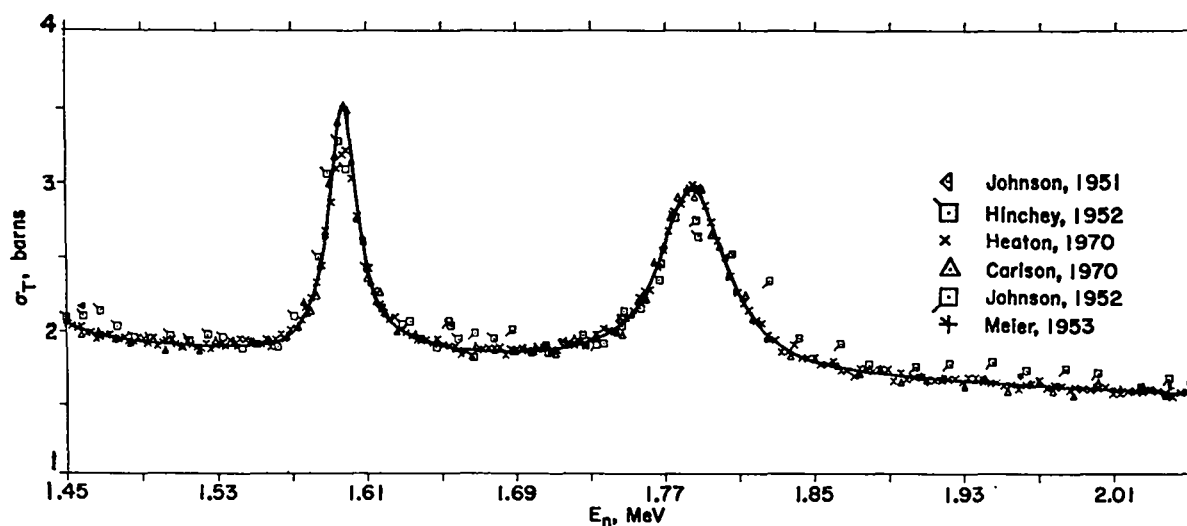

Fig. 15. Measured and evaluated total cross section from 4.5 to 6.0 MeV.

Fig. 16. Measured and evaluated total cross section between 6 and 9 MeV. The small peak near 7.3 MeV is probably not statistically significant.
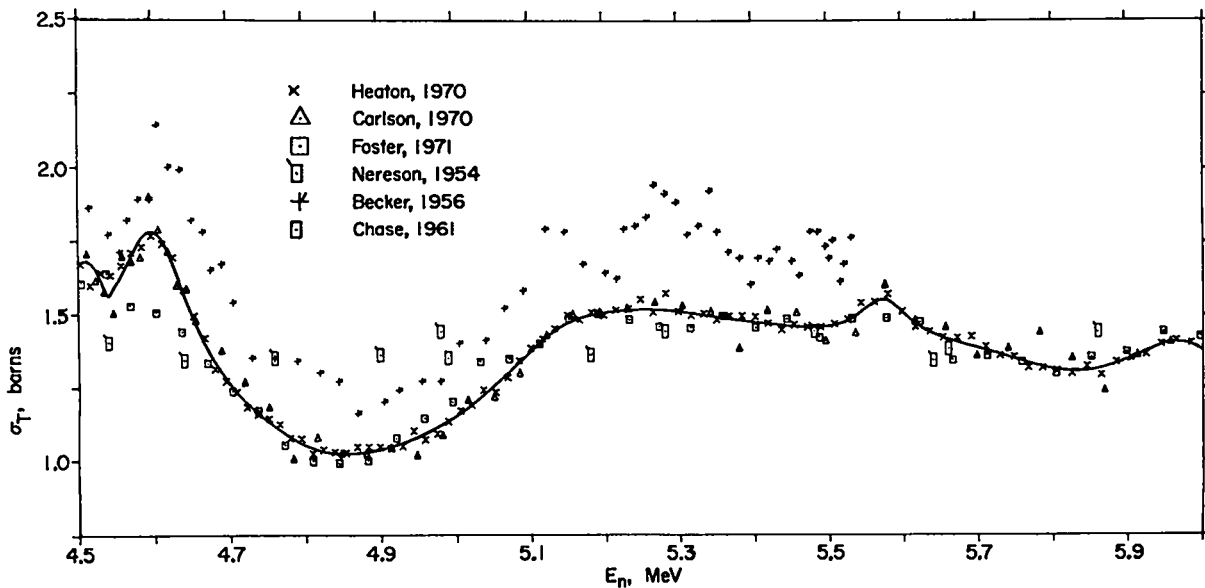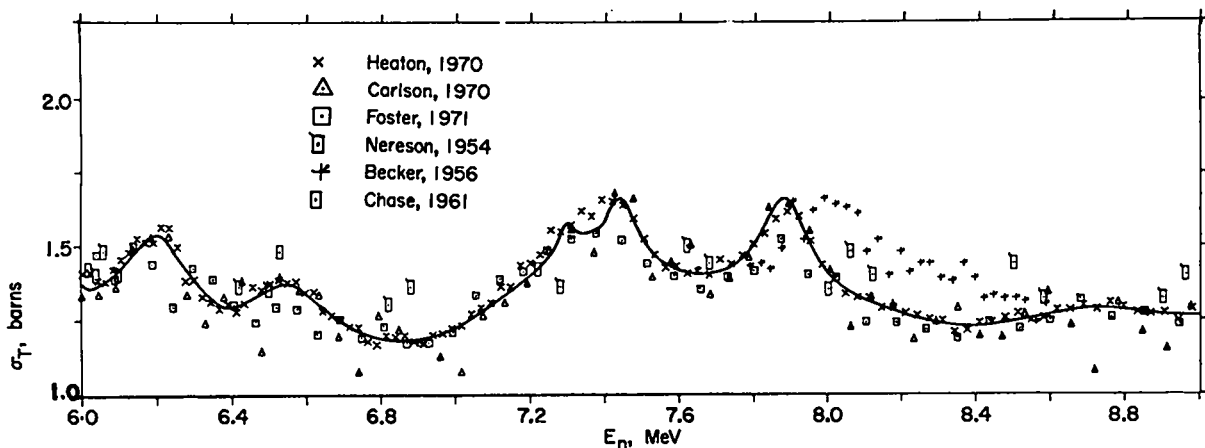
12

measurements by Motz et al. (Mo62), Thomas et al. (Th67), and Jonsson and Hardell (Jo69) agree reasonably well. The measurements by Orphan et al. (Or70) for some of the lines (for example, E_γ = 1.8849, 2.523, and 5.2701 MeV) differ significantly from the other experimental data. Further, Orphan reports several reasonably strong lines (not included in Table III) that were not seen in the other measurements. The evaluated (n,γ) spectrum and cross section are reasonably consistent with Maerker and Muckenthaler's (Ma69) thermal-neutron measurements.

The thermal spectrum is assumed to hold up to a neutron energy of 250 keV. Again, we believe this is a reasonable assumption because the first resonance in nitrogen does not occur until 434 keV. From 250 keV to 1 MeV, the thermal spectrum is phased into a single ground-state transition, and at all higher energies the spectrum is assumed to consist of a single ground-state transition. This behavior is suggested by the ^{14}N(p,γ) measurements by Kuan et al. (Ku70) who observed no significant transition to oth-

er than the ground state. The evaluated capture cross section and spectrum imply that 14-MeV neutrons produce 24-MeV photons with a cross section of 15 μb.

3.3 Neutron Inelastic-Scattering Cross Sections

The usual procedure in neutron cross-section evaluations is to separate inelastic neutron scattering into cross sections to discrete levels of the target nucleus and to a continuum of levels. In the former case, the (n,n') cross sections to individual levels are tabulated separately as functions of incident neutron energy, with separate angular distributions provided for each level. In the continuum case, a composite energy distribution is given at each incident energy to represent inelastic neutrons from a continuum of states (generally highly excited) of the target nucleus, and each distribution is given an average angular distribution.

We have departed from this procedure in that we have specified all inelastic scattering as (n,n') reactions to discrete states or groups of states,
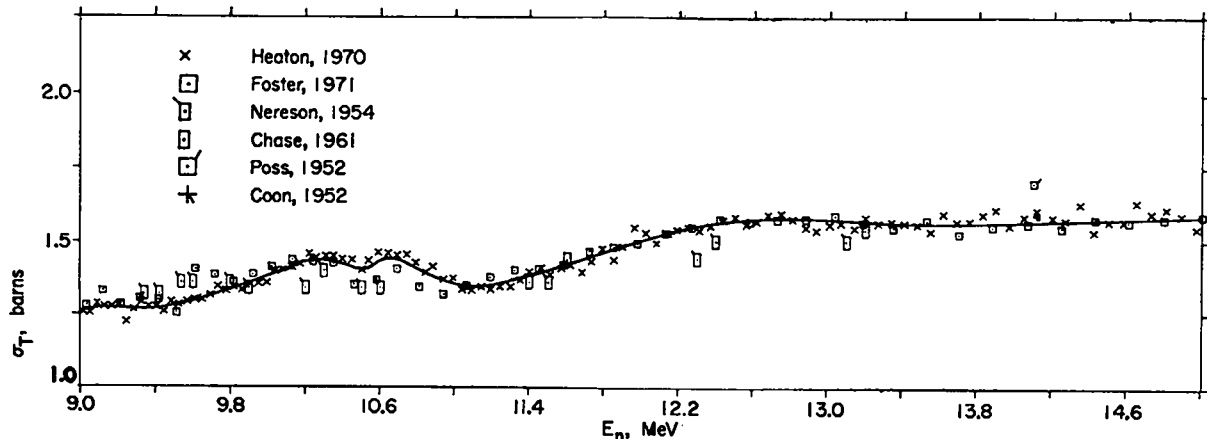

Fig. 17. Measured and evaluated total cross section between 9 and 15 MeV. The structure in this region appears to match that deduced for the inverse photonuclear giant resonance (Sec. 3.2 and Fig. 20).
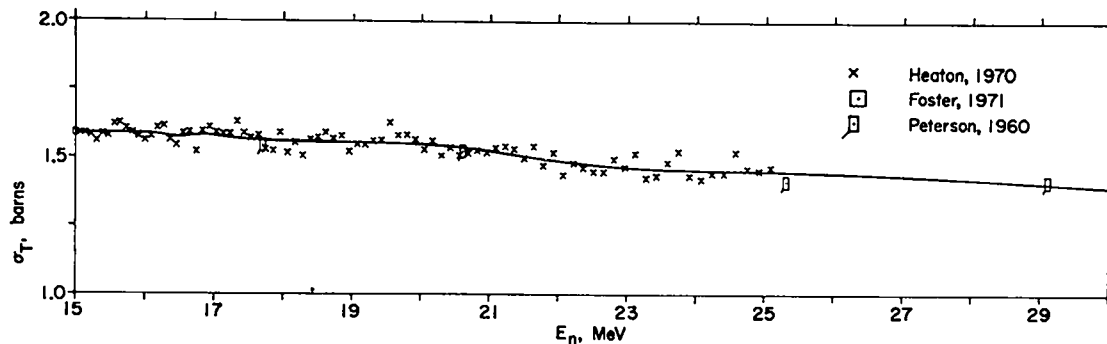
Fig. 18. Measured and evaluated total cross section from 15 to 30 MeV.

13
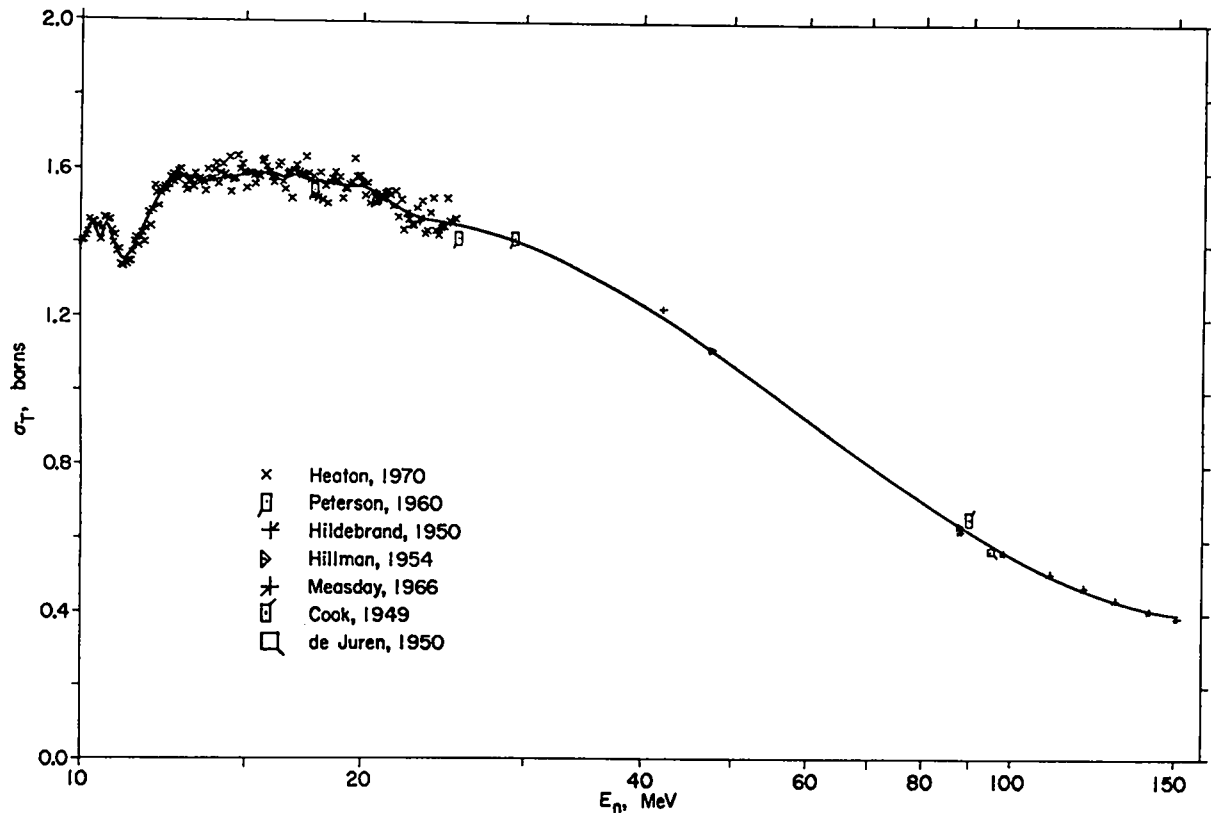
Fig. 19. Measured and evaluated total cross section from 10 to 150 MeV.

and do not use an (n,n') continuum representation. This approach allows more accurate representation of the energy-angle relationships of outgoing neutrons without actually incorporating complicated energy-angle correlations like those, for example, provided for in File 6 of ENDF/B. The use of average angular distributions for composite energy spectra is limited because angular distributions of inelastic neutrons can be strong functions of outgoing neutron energy, particularly for the lighter elements. Because the largest effects occur at the lowest outgoing neutron energies, this problem is made more important by the fact that (n,n') energy distributions frequently peak at relatively low outgoing neutron energies. A more accurate representation of the outgoing neutrons is clearly attained by allowing the (n,n') reactions for different excitation levels of the residual nucleus to have different angular distributions.

A crude example of the above effect is shown in Fig. 22 where relative angular distributions in the laboratory frame of reference are shown for the

$^{14}N(n,n')^{14}N^*$ reaction to fictitious states in ^{14}N between 10- and 13-MeV excitation for 14-MeV incident neutron energy. The angular distributions are assumed to be isotropic in the center-of-mass system, so the departure from isotropy of the laboratory distributions is due entirely to center-of-mass motion. The different excitation energies correspond approximately to different outgoing laboratory neutron energies. The angular distributions vary appreciably with excitation energy, and, although we do not regard the effect as severe in this case, it is clearly significant even for a nucleus as heavy as nitrogen.

We evaluated the (n,n') cross sections as a function of neutron energy in two stages:

1. We evaluated the excitation cross sections to the first 12 levels of $^{14}N(E_x<8.5$ MeV) from threshold to 20 MeV, mainly using (n,n'γ) experimental data together with the level-decay scheme for ^{14}N.

2. We estimated the relative (n,n') cross sections to states in ^{14}N above 8.5-MeV exci-

14

Fig. 20. Evaluated cross section for radiative capture from 10^{-5} eV to 20 MeV.

Fig. 21. Decay scheme and branching ratios for thermal radiative capture. The numbers in parentheses at the top of the diagram are transitions per 100 captures to the designated states.
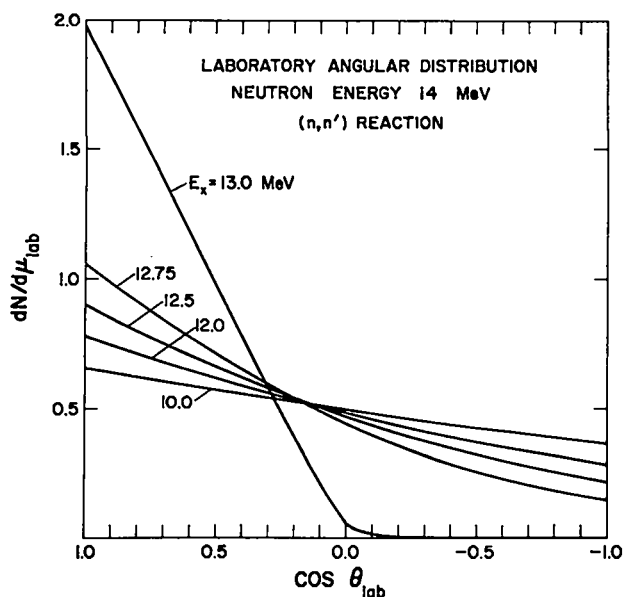
Fig. 22. Calculated angular distributions in the laboratory system corresponding to isotropic inelastic scattering in the c.m. system for 14-MeV incident neutrons and final states of excitation energy E_x in ^{14}N. The curves are normalized so that the area under each is unity.
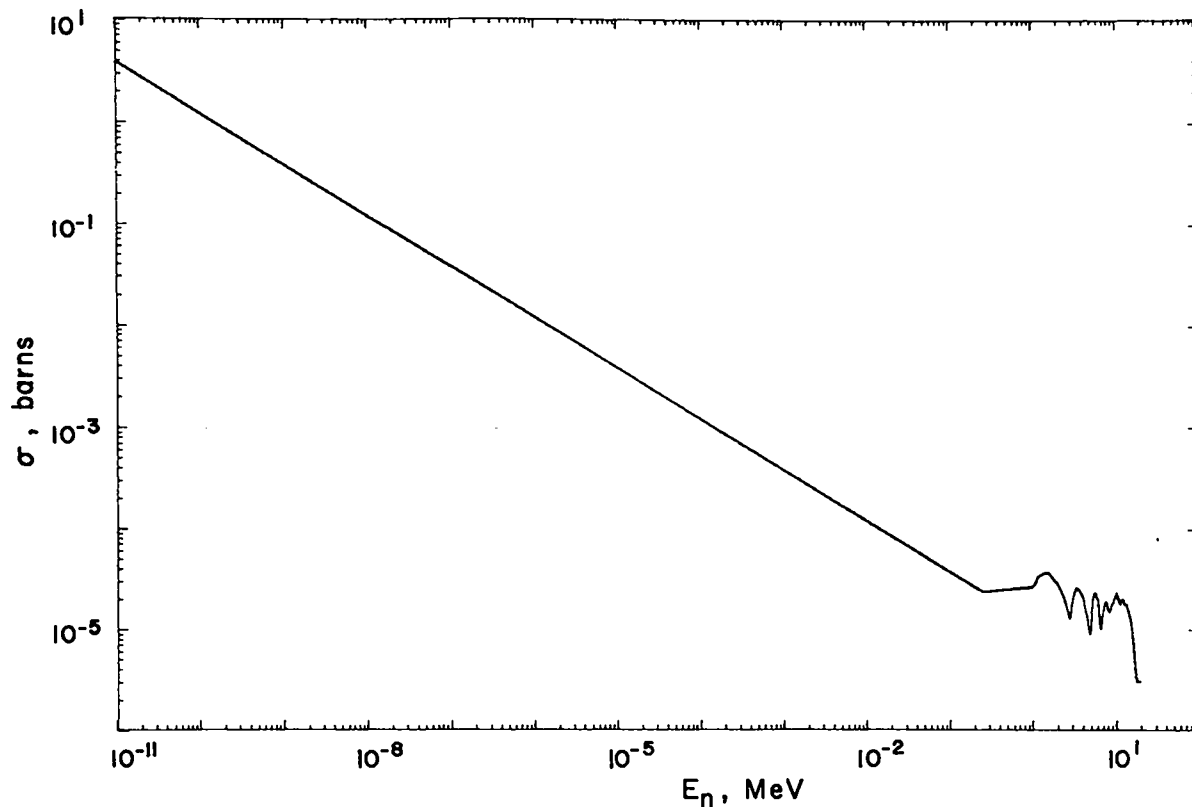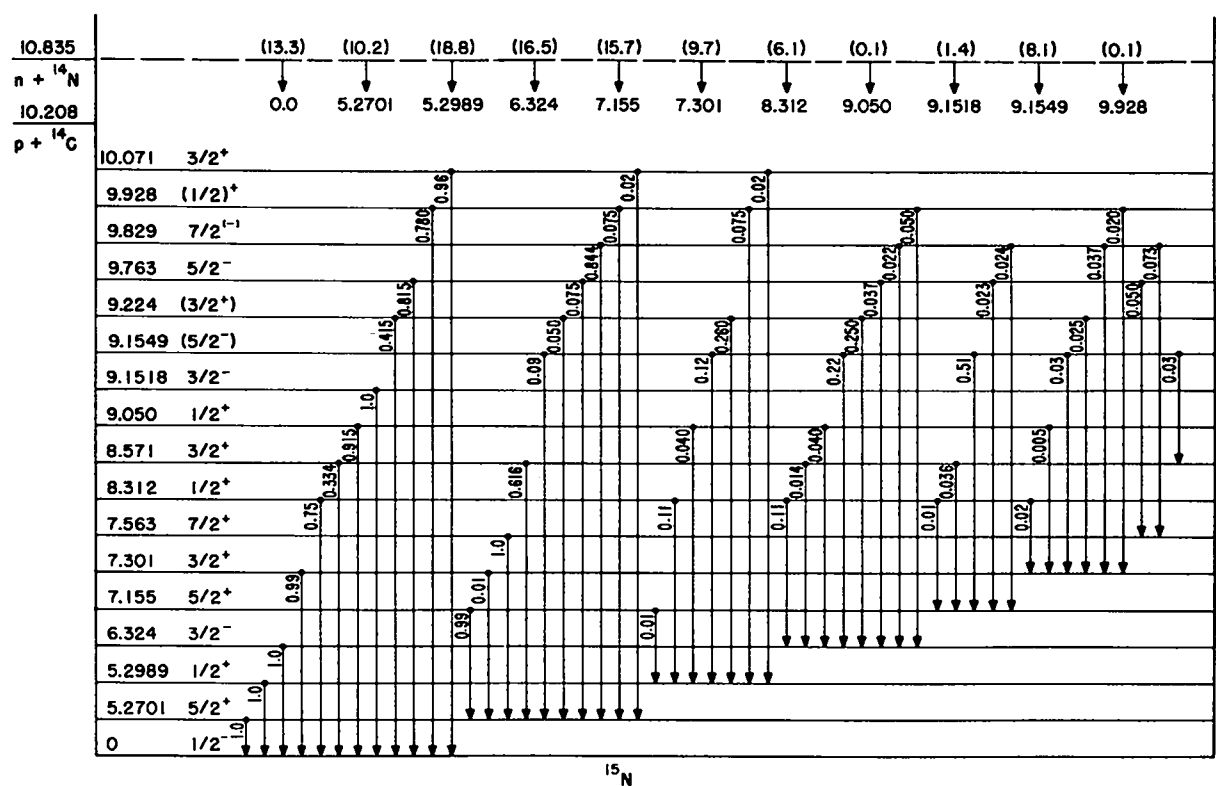
tation energy from Hauser-Feshbach (Ha52) and evaporation-model calculations, and normalized the composite at all incident neutron energies so that the sum of the partial reaction cross sections agreed with the evaluated elastic and total cross sections. We grouped the (n,n') cross sections into 0.5-MeV-wide excitation bins and represented them as some 20 discrete (n,n') reactions to ficitious levels at the average excitation energies of the bins. This information replaces the more-usual continuum representation.

3.3.1 The ^{14}N(n,n') and ^{14}N(n,n'γ) Cross Sections for $E_x(^{14}$N)<8.5 MeV

Except for limited data near 14 MeV (Ba63, Bo62, An64), no direct measurements of (n,n') cross sections were available when we completed this evaluation.[*] Consequently, we based the (n,n') excitation cross sections to all states in ^{14}N below an excitation energy of 8.5 MeV almost entirely upon

---

* Some data have subsequently become available from measurements at 9 and 11 MeV by Nellis et al. (Ne71).

gamma-ray production measurements. The decay scheme for ^{14}N, which relates the (n,n') excitation cross sections to the gamma-ray production measurements, is given in Fig. 23. We took the level energies, spins, and parities from Ajzenberg-Selove's compilation (Aj70). The branching ratios were obtained mainly from Carlson's ^{10}B(^{6}Li,dγ)^{14}N coincidence measurements (Ca66), the ^{12}C(^{3}He,pγ)^{14}N measurements by Gorodetzky et al. (Go66), and the ^{12}C(^{3}He,pγ)^{14}N measurements by Warburton et al. (Wa64, Wa65), although several other sources also provided input (see Aj70 for a compilation of the measured branching ratios).

Unfortunately, we did not become aware of the recent work by Young, Phillips, and Marion (Yo69) until the Ajzenberg-Selove (Aj70) compilation, which cites their results, appeared in its final form late in 1970. Because our (n,n') cross-section evaluation was already complete, we did not include the Young results in Fig. 23. Doing so would generally lower the total (n,n') cross section by at most a few percent, with a maximum decrease of perhaps 5-10% for the (n,n') level-excitation cross sections to the 5.106- and 5.834-MeV levels. In view of the

Fig. 23. Decay scheme for ^{14}N used in interpreting the (n,n'γ) measurements. The levels are labeled with their isospin as well as ordinary spin and parity. Note that the energy scale is distorted.

TABLE III

CAPTURE GAMMA-RAY SPECTRUM FOR THERMAL NEUTRONS ON NITROGEN

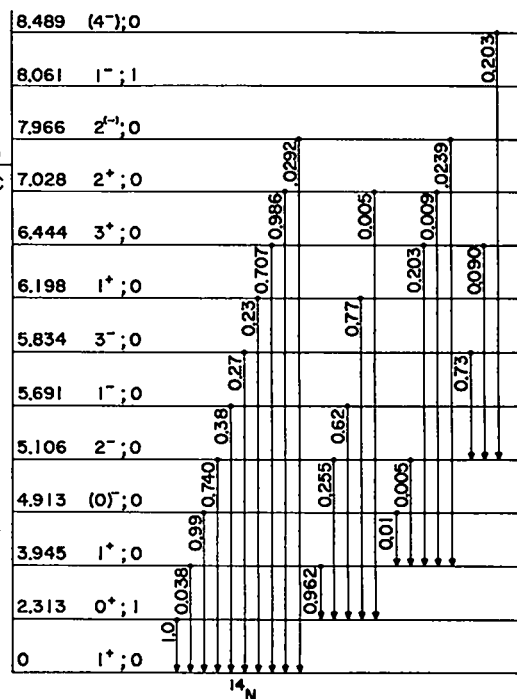| $E_\gamma{}^a$ (MeV)	$E_{initial}$ (MeV)	E_{final} (MeV)	Photons per 100 Captures				
			Motz 1962	Thomas 1967	Jonsson 1969	Orphan 1970	Present Work
10.835[b]	10.835	0.	14.	13.3±2.0	14.	14.9	13.3
9.928	9.928	0.			0.2±0.1		0.1
9.1518	9.1518	0.	1.4	1.7±0.2	1.6±0.2	1.7	1.4
9.050	9.050	0.	0.5	0.2±0.03	0.2±0.1		0.1
8.571	8.571	0.		0.2±0.03	0.1±0.05		0.1
8.312	8.312	0.	4.	4.4±0.4	3.8±0.4	4.2	4.5
7.301	7.301	0.	9.	10.0±0.5	9.2±1.0	8.3	9.9
6.324	6.324	0.	18.	18.8±0.9	18.4±1.3	16.5	19.0
5.5649[b]	10.835	5.2701	11.	10.3±0.5	10.4±0.7	9.0	10.2
5.5361[b]	10.835	5.2989	21.	18.8±0.9	18.5±1.3	17.6	18.8
5.2989	5.2989	0.	21.	21.4±1.1	21.4±1.5	18.4	20.7
5.2701	5.2701	0.	32.	30.6±1.5	31.4±2.2	25.2	30.9
4.511[b]	10.835	6.324	16.	16.6±0.8	16.5±1.2	15.7	16.5
3.8848	9.1549	5.2701		0.8±0.1	0.9±0.2		0.7
3.856	9.1549	5.2989	0.5	1.0±0.1	1.0±0.2	1.4	1.0
3.680[b]	10.835	7.155	<23.	15.9±0.8	15.0±1.4	15.4	15.7
3.534[b]	10.835	7.301	9.	9.9±0.5	9.3±0.6	9.5	9.7
3.3009	8.571	5.2701			0.2±0.1		0.2
3.0131	8.312	5.2989			0.7±0.2		0.7
2.8309	9.1549	6.324	1.5	2.0±0.2	2.0±0.3		1.8
2.523[b]	10.835	8.312	6.	6.1±0.3	6.0±0.4	9.4	6.1
2.0309	7.301	5.2701					0.1
1.9999	9.1549	7.155	4.	4.6±0.2	4.2±0.3		4.1
1.988	8.312	6.324		1.5±0.3	0.5±0.2		0.7
1.8849	7.155	5.2701	21.	19.7±1.0	18.3±1.5	27.2	19.7
1.8561	7.155	5.2989		0.8±0.2	0.4±0.2		{0.2
1.8539	9.1549	7.301					0.2
1.785[b]	10.835	9.050					0.1
1.6832[b]	10.835	9.1518	12.	9.2±0.5	{1.7±0.4	6.0	{1.4
1.6801[b]	10.835	9.1549			8.0±1.0}		8.1
1.157	8.312	7.155					0.1
1.011	8.312	7.301					0.1
0.907[b]	10.835	9.928					0.1
0.5839	9.1518	8.571					0.3

[a] No correction has been made for the energy of the recoiling ^{15}N nucleus.

[b] Primary transitions.

overall uncertainty in the (n,n') cross sections, we do not regard the omission of the Young branching-ratio information as serious.

The branching ratios shown in Fig. 23 for states above the p + ^{13}C threshold at 7.55 MeV have been multiplied by the probability that the levels decay by gamma-ray emission, taken to be the ratio of the gamma-ray width to the total width for each level. The largest uncertainty in Fig. 23 is for the branches from the 7.966-MeV level. There the ratio of the two branches is well known, but the relative probability of photon emission is unknown. In the evaluation, we assumed that the 7.966-MeV level decays 5.3% by gamma emission. This assumption, coupled with Dickens and Perey's (n,xγ) measurements (Di69) for the 7.966-MeV line, suggests

an (n,n') excitation cross section somewhat larger than that predicted by Hauser-Feshbach calculations.[*] However, the analysis by Hebbard and Vogl (He60), who studied the ^{13}C(p,p) and ^{13}C(p,γ) reactions, suggests that the 7.966-MeV level decays by gamma emission less than 1% of the time, which leads to a much larger (n,n') cross section for this level when it is combined with Dickens and Perey's (n,xγ) results (Di69). The ∼ 5% value we used is therefore a compromise between these considerations.

We surveyed the states in ^{14}N above the p + ^{13}C threshold to determine whether these particle-unstable levels make significant contributions to the (n,xγ) cross sections. We made this study using the gamma-

[*] These calculations are discussed in detail in Appendix A.

ray and total widths compiled by Ajzenberg-Selove (Aj70) together with the experimental results of Gallmann et al. (Ga67). In addition to the contributions from the 7.966- and 8.489-MeV states shown in Fig. 23, we found the states at 8.963 and 9.172 MeV in ^{14}N to have gamma-ray decay probabilities of 19.6% and 9.1%, respectively. Almost all the remaining states above the p + ^{13}C threshold have total widths in the keV range. Because the largest gamma-ray width in the Ajzenberg-Selove compilation is 43 eV, we expect the (n,n'γ) contribution from these higher states to be negligible. We therefore assumed that no gamma rays result from states in ^{14}N above an excitation energy of 8.5 MeV. We estimate the maximum (n,xγ) contributions from the 8.963- and 9.172-MeV levels, which we did not include in the evaluation, to be ~3 mb for the 8.963- →6.444-MeV transition and ~0.5 mb for the 9.172- → 0-MeV transition near a neutron energy of 13 MeV. Table IV summarizes the gamma rays from (n,n') reactions that appear in our evaluation. The brackets indicate transitions that were combined into one (n,xγ) cross section.

TABLE IV

GAMMA RAYS FROM ^{14}N(n,n'γ)^{14}N REACTIONS

E_γ (MeV)	$E_{initial}$ (MeV)	E_{final} (MeV)
7.966	7.966	0
7.028	7.028	0
6.444	6.444	0
6.198	6.198	0
5.834	5.834	0
5.691	5.691	0
5.106	5.106	0
4.913	{4.913 / 7.028	0 / 2.313}
3.98	{7.966 / 3.945	3.945 / 0}
3.885	6.198	2.313
3.38	{8.489 / 5.691	5.106 / 2.313}
2.793	{7.028 / 5.106	3.945 / 2.313}
2.499	6.444	3.945
2.313	2.313	0
1.632	3.945	2.313
1.25	{6.444 / 5.106	5.106 / 3.945}
0.728	{4.913 / 5.834	3.945 / 5.106}

Most of the ^{14}N(n,xγ) experimental data are from measurements performed at one angle; Table V is a summary of the angles and detectors used in the various measurements considered in the evalua-

tion. Except for some of the results of Morgan et al. (Mo64), the experimental (n,xγ) data described here are single-angle measurements multiplied by 4π. This procedure should not lead to large errors for nitrogen because at most energies the 55 and 125° measurements by Dickens and Perey (Di69) and Orphan and Hoot (Or69) were emphasized in the evaluation.[*] Near 15 MeV we stressed Nyberg's (Ny69) 80° measurements; many of the gamma-ray angular distributions are isotropic within 10% at these energies (Bu71; also see Mo64). The Morgan results (Mo64) that we give for the 1.632-, 2.124-, 2.313-, 3.684-, 3.854-, and 5.1-MeV gamma rays were obtained by integrating the measured angular distributions; all other gamma-ray cross sections from this source are 90° measurements multiplied by 4π.

TABLE V

SUMMARY OF GAMMA-RAY PRODUCTION MEASUREMENTS USED IN THE EVALUATION

Reference	Measurement Angles	Neutron Energy Range (MeV)	Detector
Bostrom, 1959	77°	4.2	NaI
Buchanan,[a] 1969	55°	14.8	NaI
Clayeux, 1969	90°	14.1	Ge(Li)
Condé, 1968	55°	4.5–7.0	Ge(Li)
Dickens, 1969	55°, 90°	5.8–11.0	Ge(Li)
Engesser, 1967	90°	14.7	NaI
Hall, 1959	90°	4.7–8.1	CsI
Maslov, 1968	90°	14.1	NaI
Morgan,[a] 1963	90°	14.8	NaI
Morgan,[a] 1964	30°–140° (8 angles)	14.8	NaI
Nyberg, 1969	80°	15.0	Ge(Li)
Orphan, 1969	125°	2–16	Ge(Li)

[a]The 1963 and 1964 Morgan data are largely superseded by the 1969 Buchanan results but are included for completeness. These data were obtained using a NaI anticoincidence shield.

We wish to emphasize that the Morgan measurements (Mo63,Mo64) and the Buchanan results (Bu69) were all obtained by Texas Nuclear Corporation (TNC), and the 1969 reference apparently supersedes the

[*]If a photon angular distribution can be represented by an expression of the form $\sigma(\mu) = a_0 + a_2 P_2(\mu)$, where μ is the cosine of the reaction angle and $P_2(\mu)$ is the $\ell = 2$ Legendre polynomial, then the integrated cross section is identically equal to 4π times the differential cross section at 54.7 or 125.3° (zeros of the second Legendre polynomial). This is true for many of the gamma rays from nitrogen.

earlier results. Accordingly, we largely ignored the 1963 and 1964 data in our evaluation of the (n,xγ) cross sections; however, for completeness we included these results in our figures. After we completed the evaluation, a new compilation of TNC results (Bu71), which supersedes the three previous communications, became available. The new compilation includes a reanalysis of the nitrogen (n,xγ) measurements, and the results for some lines differ significantly from Buchanan's 1969 compilation. The new cross sections, which are not included in our figures, are generally higher than the older values and usually agree better with the evaluation. We have included specific comments in the text where we consider the new TNC results most significant.

The 2.313-MeV level of ^{14}N is a T = 1 level with $J^{\pi} = 0^{+}$. Consequently, the (n,n') cross section to this level is relatively small, and there is little direct information about its magnitude. Further, the (n,xγ) cross section for the 2.313-MeV photon, which results from the decay of this level, is composed mainly of cascade contributions from the higher 3.945-, 5.106-, 5.691-, and 6.198-MeV levels (Fig. 23). Consequently, we based the evaluated (n,n') cross section for the 2.313-MeV level mainly upon (p,p') measurements to this level by Oda et al. (Od60), Hansen et al. (Ha70), Freemantle et al. (Fr54), and Boreli et al. (Bo68), augmented by the

(n,n'γ) measurements and a single (n,n') measurement at 14 MeV by Bauer et al. (Ba63).[*] Our decision to use (p,p') measurements in the absence of (n,n') data results from arguments by Lutz and Anderson (Lu66) and Anderson et al. (An67) which are based upon charge symmetry of the nuclear two-body force (see Sec. 4.2 for further discussion). Indeed, we allowed the available (p,p') results to influence our evaluation of the (n,n') cross sections for some of the stronger transitions in energy regions where (n,xγ) measurements were lacking or were in disagreement.

The evaluated (n,n'γ) cross section for the 2.313-MeV gamma ray is compared to the available measurements in Fig. 24. As noted above, the curve is determined mainly by cascade contributions from higher levels and is not very sensitive to the small (n,n') cross section to the 2.313-MeV level. The evaluated curve and the measurements in Fig. 24 agree reasonably well, although we biased our evaluation of the (n,n'γ) data somewhat in the high direction to try to reconcile the "discrepancy" in the cross sections near 8-MeV neutron energy (St69, Di69). This problem is discussed further in Sec. 3.10.

[*]The (n,n') measurement by Bobyr et al. (Bo62) is more than an order of magnitude higher than the other measurements and is not included here.
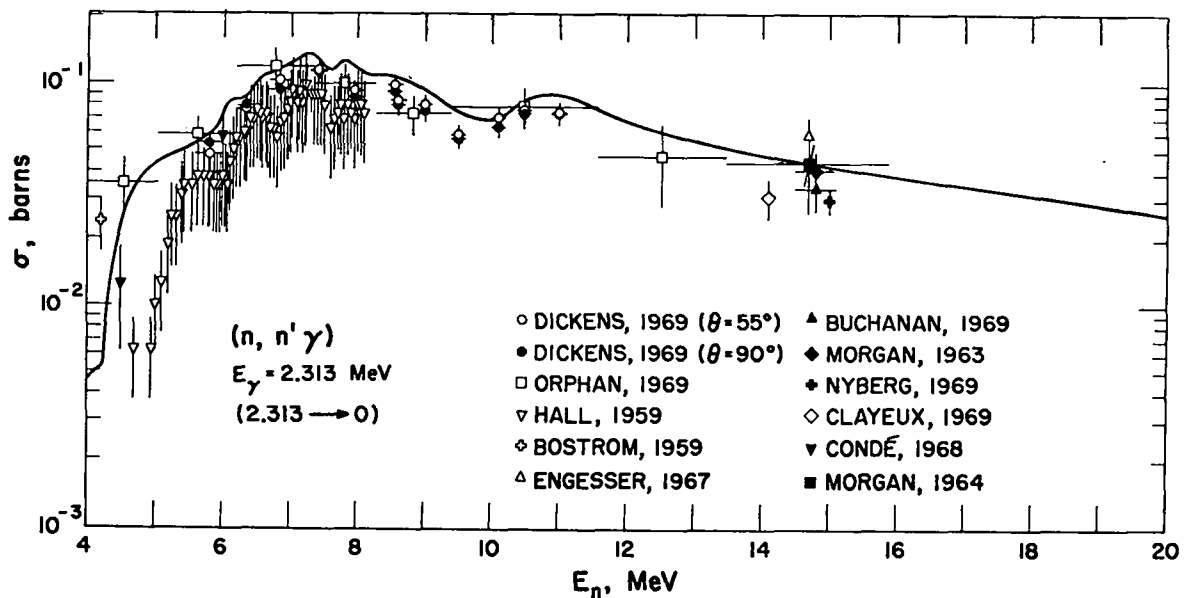

Fig. 24. Measured and evaluated photon-production cross section from 4 to 20 MeV for the 2.313-MeV gamma ray.

The gamma-ray production cross sections for the 1.632- and 4.913-MeV gamma rays are given in Fig. 25. We used the experimental data shown in the figure to estimate the (n,n') cross sections to the 3.945- and 4.913-MeV levels in ^{14}N, incorporating also, of course, the decay scheme given in Fig. 23. We have combined a small contribution (<0.2 mb) from the 7.028- → 2.313-MeV transition (E_γ = 4.715 MeV) into the (n,n'γ) cross section for the 4.913-MeV gamma ray. The evaluated (n,n') cross section (19 mb) for the 3.945-MeV level near 14 MeV agrees well with the direct (n,n') measurement (19 mb) by Bauer et al. (Ba63). The extensions of both evaluated curves from 15 to 20 MeV are simple extrapolations of the lower energy results. This is true of all (n,n'γ) results shown.

The evaluated (n,n'γ) cross sections for the 2.793- and 5.106-MeV gamma rays are compared to the available measurements in Fig. 26. Both these gamma rays result from decay of the 5.106-MeV level.

We determined the evaluated (n,n') excitation cross section to this level mainly from the 5.106-MeV gamma-ray measurements. The good agreement of the evaluated curve with the 2.793-MeV measurements supports the branching ratios used for this level and the (n,n'γ) experimental data for both these photons. The new TNC compilation (Bu71) gives a point at 14.8 MeV for the 2.793-MeV photon which agrees closely with the curve.

The gamma-ray production cross sections for the 3.378- and 5.691-MeV gamma rays are given in Fig. 27. Both of these gamma rays result from decay of the 5.691-MeV level. We based the evaluated curves in the figures primarily upon measurements of the 3.378-MeV gamma ray, which is the predominant branch in the decay. The cross section for the 3.378-MeV photon also includes a small contribution from the 8.489- → 5.106-MeV transition (E_γ = 3.383 MeV). The 3.378- and 3.383-MeV photons are close enough in energy so that they were certainly unresolved

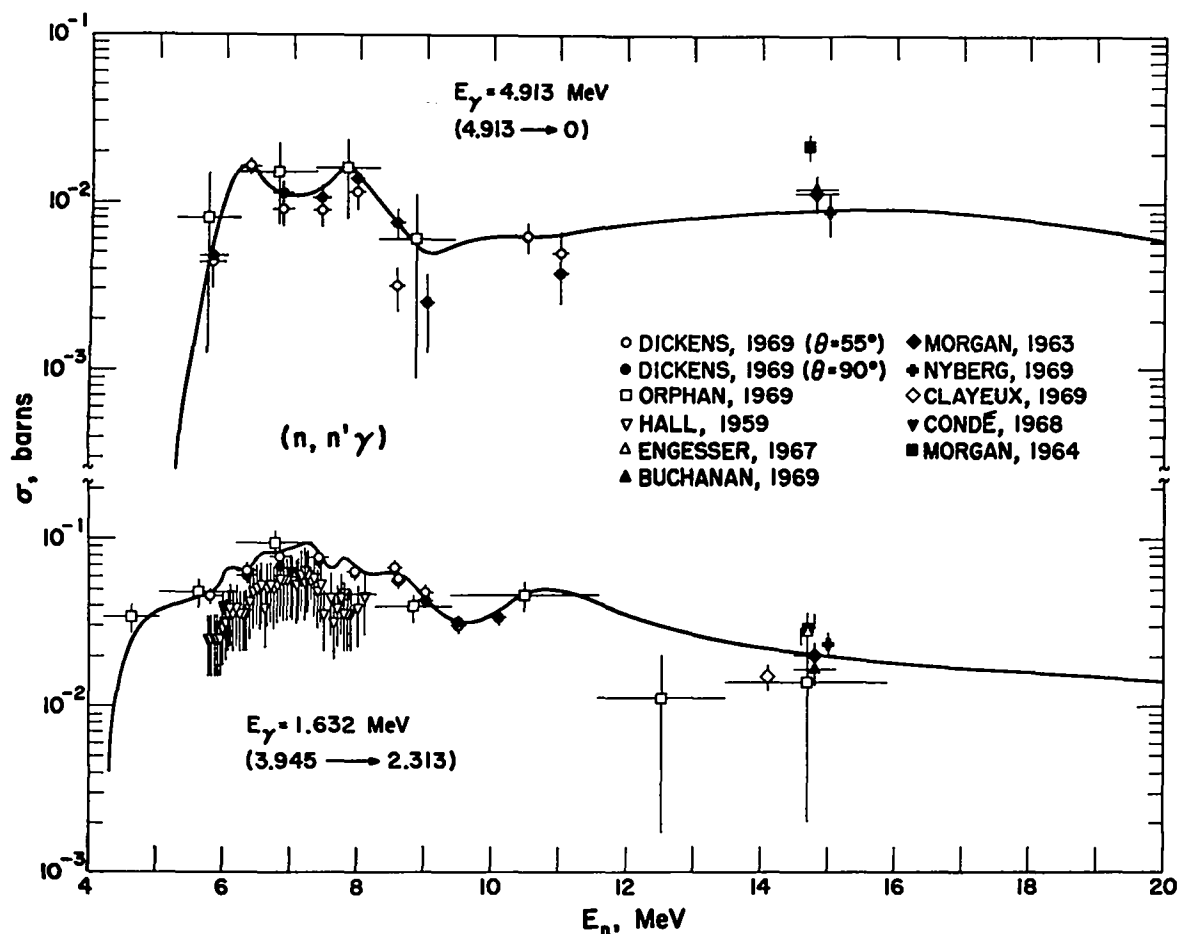Fig. 25. Measured and evaluated photon-production cross sections for the predominant gamma rays from the second and third excited states in ^{14}N.
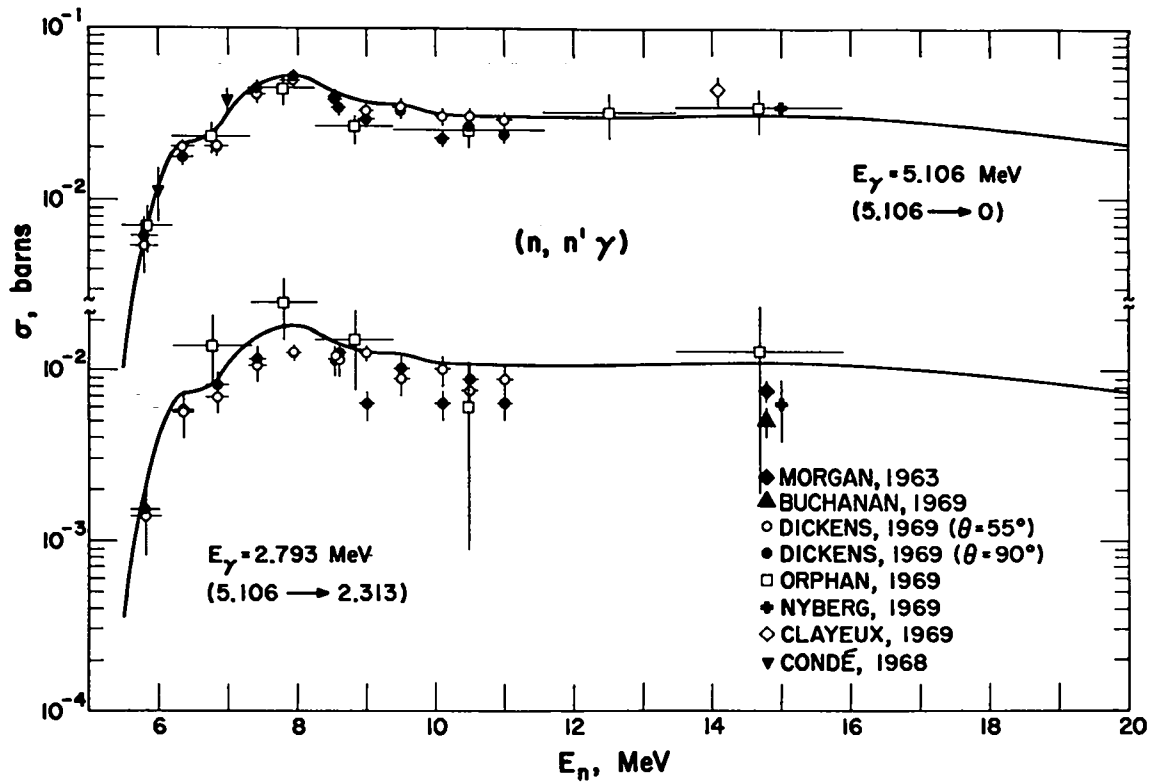
Fig. 26. Measured and evaluated photon-production cross sections for the predominant gamma rays from the 5.106-MeV level in ^{14}N.
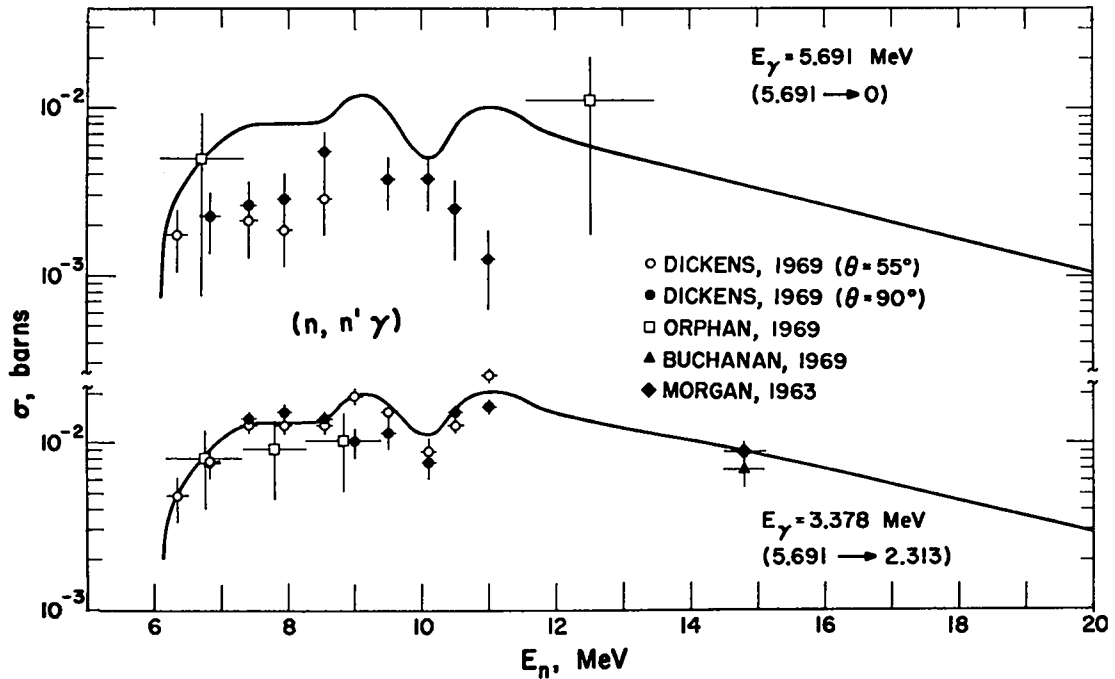

Fig. 27. Measured and evaluated photon-production cross sections for two gamma rays from the 5.691-MeV level in ^{14}N.

in the measurements made with NaI detectors and prob-
ably unresolved in the Ge(Li) measurements as well.
The lack of agreement between the evaluated curve
and most of the 5.691-MeV experimental data may re-
flect an error in the branching ratios used or a
problem in the measurements. The latter is more
probable, and the problem probably lies in the 5.691-
MeV data because most of the measured cross sections
for this photon are quite small (~ a few mb).

The (n,n'γ) cross sections for the 0.728- and
5.834-MeV gamma rays from the 5.834-MeV level are
given in Fig. 28. The evaluated curves and, con-
sequently, the evaluated excitation cross section,
are based mainly upon the 0.728-MeV gamma-ray data.[*]
Again, the agreement of the evaluated curve with
the 5.834-MeV gamma-ray experimental data gives us
confidence in the branching ratios used for this
level and in the experimental data for both the
0.728- and 5.834-MeV photons.

_____

[*] The new TNC compilation (Bu71) gives a 14.8-MeV
point for the 0.728-MeV line which is 10 mb higher
than the curve.

The (n,n'γ) measurements used in determining
the excitation cross section for the 6.198-MeV level
are shown in Fig. 29. In this case, experimental
data are available only for the 3.885-MeV gamma ray.
The shape of the evaluated curve to 14 MeV is based
upon a Hauser-Feshbach calculation (described in
Appendix A). The evaluated cross section for the
weaker 6.198-MeV gamma ray is also included in Fig.
29.

The evaluated cross sections for the 2.499- and
6.444-MeV gamma rays from the 6.444-MeV level in ^{14}N
are compared to experiment in Fig. 30. The predomi-
nant branch is the ground-state transition, and the
(n,n') excitation cross section to this level is
based upon the (n,n'γ) measurements for the 6.444-
MeV photon. As discussed above, the earlier TNC
data (Mo63, Mo64) have been superseded by more re-
cent results, so we ignored the single Morgan datum
near 15 MeV in our evaluation of the cross section
for the 6.444-MeV photon. The new TNC compilation
(Bu71) cites 24 mb for the interval E_γ = 6.0 to 6.5
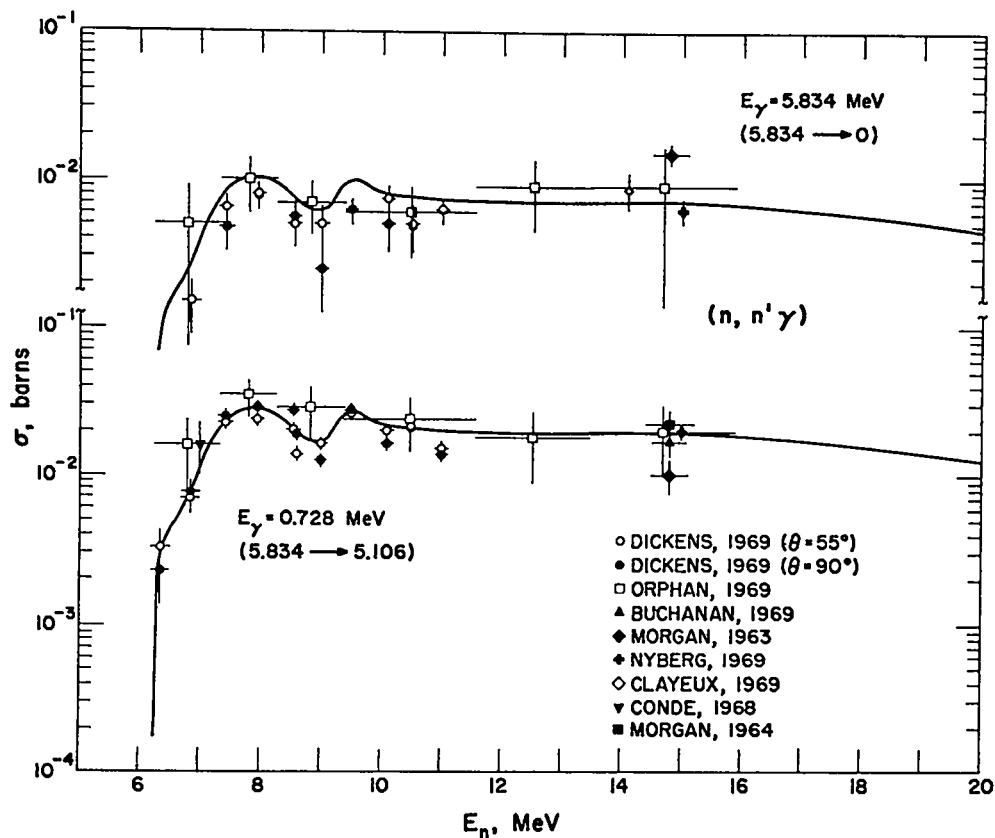MeV which is much more consistent with our results.

Fig. 28. Measured and evaluated photon-production cross sections for two gamma rays from the 5.834-MeV
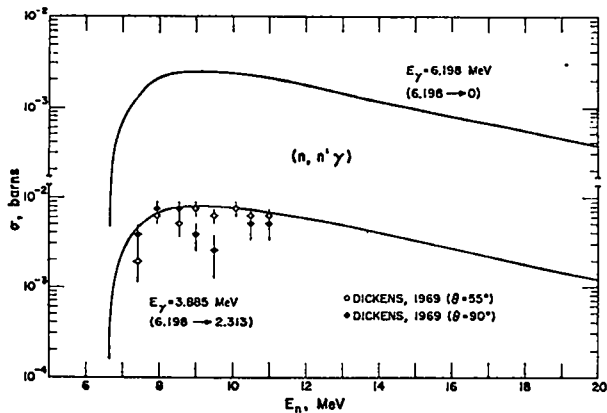level in ^{14}N.

Fig. 29. Measured and evaluated photon-production cross section for the 3.885-MeV gamma ray from the 6.198-MeV level in ^{14}N, together with the evaluated cross section for the unobserved 6.198-MeV gamma transition to the ground state.
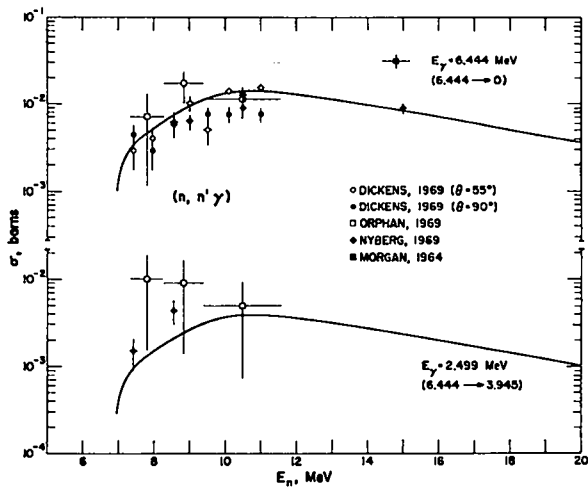

Fig. 30. Measured and evaluated photon-production cross sections for the predominant gamma rays from the 6.444-MeV level in ^{14}N.

Figure 31 shows the (n,n'γ) cross sections for the 7.028- and 7.966-MeV gamma rays. The shape of the evaluated curve up to 14 MeV for the 7.966-MeV line is based again upon a Hauser-Feshbach calculation, as described in Appendix A. We determined the (n,n') excitation cross sections to the 7.028- and 7.966-MeV levels from these data.

Finally, Fig. 32 gives the gamma-ray production cross sections for gamma rays of 3.98- and 1.25-MeV energy. The 3.98-MeV line is a composite of the 3.945- → 0- and 7.966- → 3.945-MeV transitions, and the 1.25-MeV gamma is a sum of the contributions from the 5.106- → 3.945-, and 6.444- →

5.106-MeV transitions. The curves were computed from the evaluated level-excitation cross sections to the four levels involved.

The ^{14}N(n,n') level-excitation cross sections that result from the foregoing analysis are presented in Figs. 33-35. Figure 33 gives the cross sections for the 2.313- and 3.945-MeV levels up to E_n = 5 MeV, Fig. 34 contains the results for levels with E_x < 6 MeV for E_n = 5 to 20 MeV, and Fig. 35 gives the cross sections for 6 < E_x < 8.5 MeV out to E_n = 20 MeV. The cross sections for the 8.061- and 8.489-MeV levels in Fig. 35 are based entirely upon the Hauser-Feshbach calculations. There are no experimental (n,n') nor (n,xγ) data for these two levels; however, the integrated (p,p') measurements by Hansen et al. (Ha70) at E_p = 14.6 MeV lie approximately 35% below the evaluation for the 8.061-MeV level and within a few percent for the (n,n') cross section to the 8.489-MeV level.
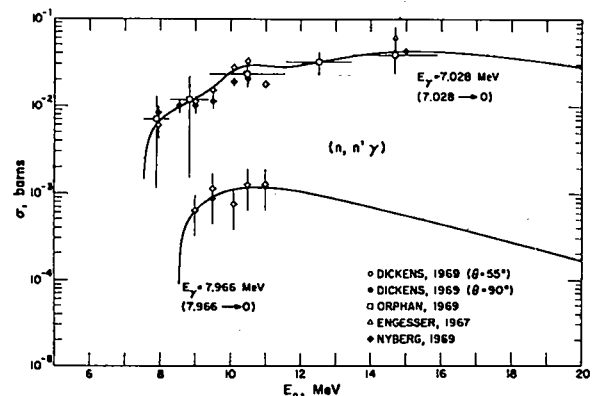

Fig. 31. Measured and evaluated photon-production cross sections for the ground-state gamma rays from the 7.028- and 7.966-MeV levels in ^{14}N.
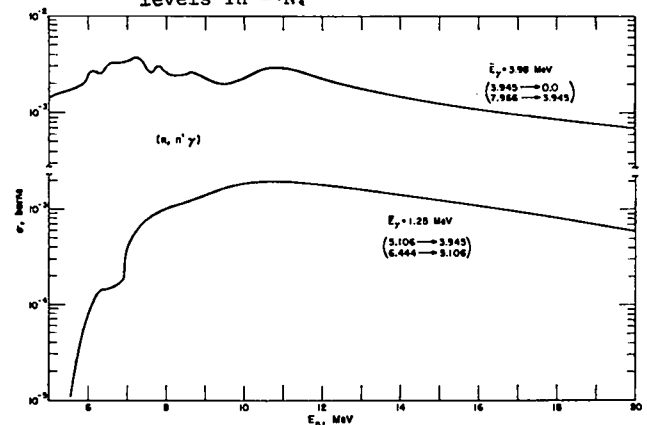

Fig. 32. Evaluated cross sections for the production of two weak photon doublets following inelastic scattering from ^{14}N.
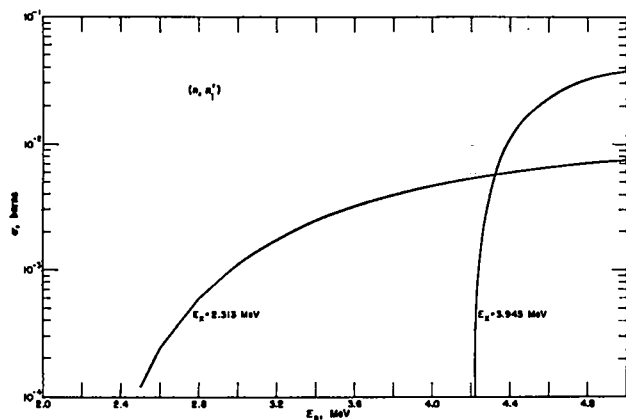
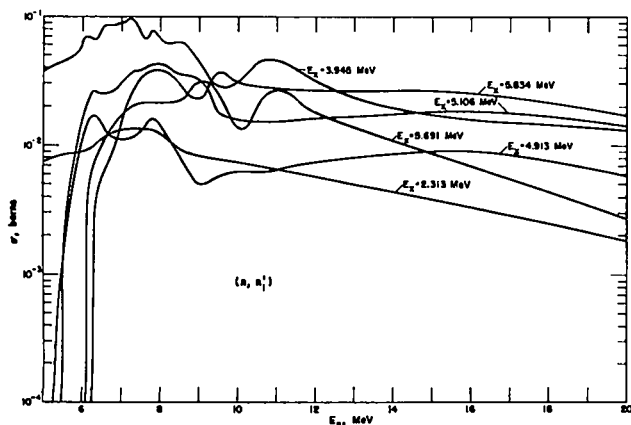Fig. 33. Evaluated cross sections up to 5 MeV for inelastic scattering to the first two excited states in ^{14}N.

Fig. 34. Evaluated cross sections from 5 to 20 MeV for inelastic scattering to levels in ^{14}N with $E_x < 6$ MeV.
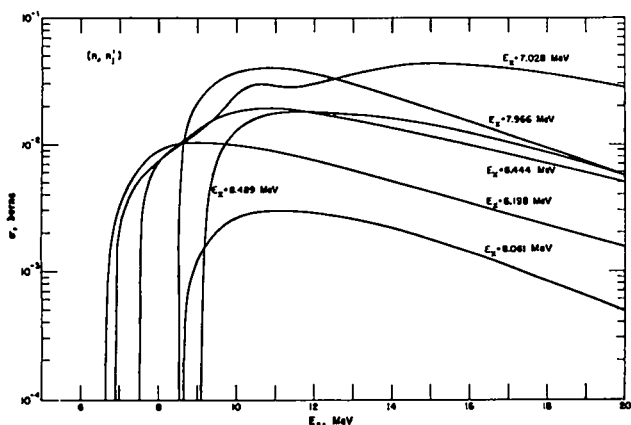

Fig. 35. Evaluated cross sections for inelastic scattering to levels in ^{14}N with E_x between 6 and 8.5 MeV.

3.3.2 The ^{14}N(n,n') Cross Section for $E_x(^{14}N) > 8.5$ MeV

As noted previously, at neutron energies above 9 to 10 MeV many new levels in ^{14}N become available for (n,n') reactions. Because almost no experimental information is available on the cross sections to these highly excited levels, it becomes increasingly difficult to estimate all the reaction cross sections at these energies. Therefore, in the 10- to 12-MeV region the elastic cross section, which was obtained at lower energies by subtracting the sum of the partial reaction cross sections from the total cross section, was joined smoothly to the available elastic measurements, and we obtained a nonelastic cross section by subtracting the evaluated elastic from the total cross section. At neutron energies above 10 MeV we adjusted the (n,n') cross section to levels in ^{14}N with $E_x > 8.5$ MeV so that the total (n,n') cross section and the evaluated (n,γ), (n,p), (n,d), (n,t), (n,α), (n,2α), and (n,2n) cross sections sum to the correct nonelastic cross section.

Implicit in the above procedure is the assumption that neutrons from ^{14}N(n,p)^{14}C*(n)^{13}C and ^{14}N(n,d)^{13}C*(n)^{12}C reactions are adequately represented in this way (or can be neglected), because these processes are lumped into the (n,n') reactions. We feel that this assumption is reasonable because the (n,p) and (n,d) cross sections to highly excited states in ^{14}C and ^{13}C are undoubtedly quite small. A second implied assumption is that the ^{14}N(n,t)3α cross section is negligible; this approximation is supported by the measurement by Mösner et al. (Mo67) at 15.7 MeV which gives a value of 0.8 ± 0.5 mb for the (n,t)3α cross section. No similar problem arises for the (n,α) reaction to highly excited states of ^{11}B because these states decay mainly by alpha emission and are included in our estimate of the (n,2α) cross section.

We generated the spectrum of inelastic neutrons from (n,n') reactions to states in ^{14}N above 8.5-MeV excitation energy in three steps:

(1) We estimated the relative (n,n') cross sections to levels between 8.5- and 13-MeV excitation energy from Hauser-Feshbach calculations. At these excitation energies, the level structure of ^{14}N is reasonably well understood, and spin and parity assignments have been made for most

of the levels. We performed the calculations, described in more detail in Appendix A, with the code JANE (Fe68), employing some 50 levels in ^{14}N and using the level information compiled by Ajzenberg-Selove (Aj70).

(2) For excitation energies greater than 13 MeV, we estimated the (n,n') energy distributions from a simple evaporation model using the expression

$$\sigma_{n,n'}(\epsilon) \propto \epsilon \exp[-\epsilon/T],$$

where ϵ is the outgoing neutron energy in the center-of-mass system. We chose the nuclear temperature T so that the shape calculated from this expression agreed with the Hauser-Feshbach calculation below $E_x = 13$ MeV. The temperatures we used are given by

$$T = 0.307\sqrt{E} \quad (MeV),$$

where E is the laboratory neutron energy in MeV. We normalized the evaporation energy spectra at each incident neutron energy to match the (n,n') cross sections calculated from Hauser-Feshbach theory for 8.5 MeV $< E_x <$ 13 MeV.

(3) The final step was to normalize the composite Hauser-Feshbach nuclear-temperature energy spectrum for $E_x > 8.5$ MeV so that all the reaction cross sections summed to the proper nonelastic cross section at all incident neutron energies, as described earlier.

We grouped the inelastic cross sections resulting from this treatment into 0.5-MeV-wide excitation-energy bins and represented them as (n,n') reactions to fictitious levels at 8.75, 9.25, 9.75, ..., 18.25 MeV. The results are shown in Figs. 36-39. The curves become more systematic for $E_x > 13$ MeV where we used the evaporation-model calculations.

The only experimental result available to use in checking our evaluation of (n,n') cross sections for levels with $E_x > 8$ MeV is the 14-MeV neutron-spectrum measurement by Anderson and McClure (An64). These results, which have been renormalized to give an integrated cross section of 0.54 b (St65),[*] are compared in Fig. 40 to a histogram constructed from our evaluated (n,n') cross sections. We determined the evaluated results above $E_n^c = 4.2$ MeV from the various (n,n'γ) measurements and from the (n,n')

---

[*] This renormalization is a rough correction for multiple-scattering effects. A detailed calculation was not made.

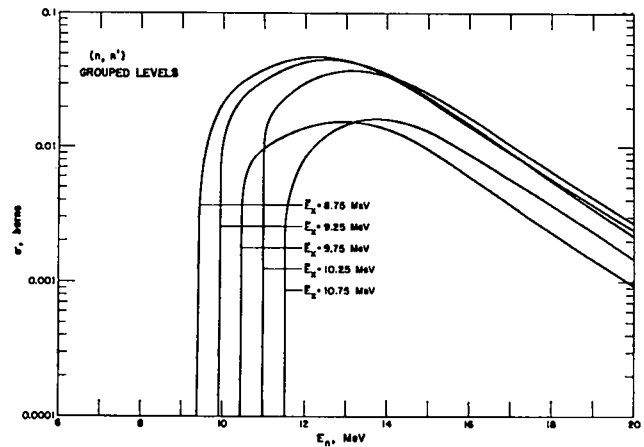Fig. 36. Evaluated cross sections for inelastic scattering to groups of known levels in ^{14}N with E_x between 8.5 and 11 MeV. Each half-MeV in excitation energy is represented as a single fictitious level.
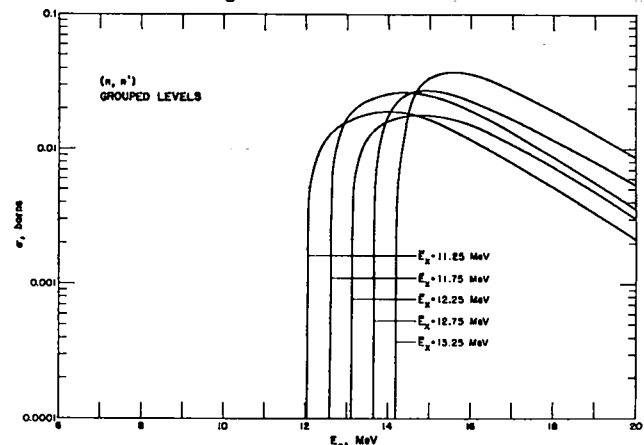

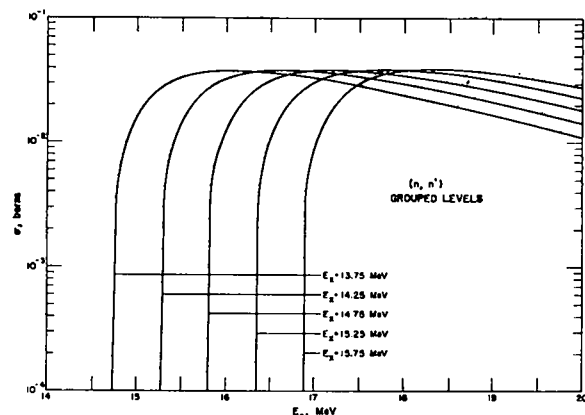Fig. 37. Evaluated (n,n') cross sections to groups of levels in ^{14}N between 11 and 13.5 MeV.

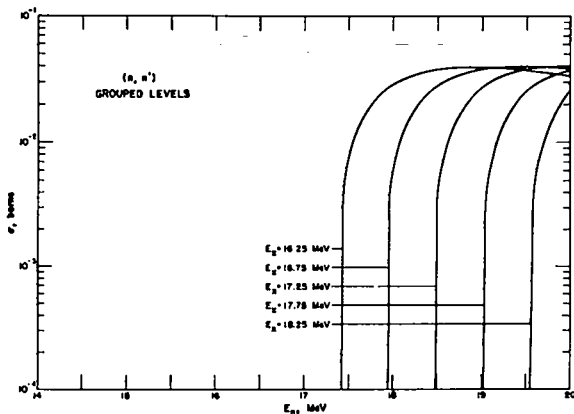Fig. 38. Evaluated (n,n') cross sections to groups of levels in ^{14}N between 13.5 and 16 MeV.

25

Fig. 39. Evaluated (n,n') cross sections to groups
of levels in ^{14}N between 16 and 18.5 MeV.

measurement at 14 MeV by Bauer et al. (Ba63), as de-
scribed in Sec. 3.3.1. The evaluated spectrum be-
low E_n^c = 4.2 MeV results from our renormalized Hau-
ser-Feshbach calculations, as discussed above. The
gaps in the histogram are regions where there are
no levels in ^{14}N; the fact that the measured spec-
trum does not dip near the gaps indicates that the
resolution of the measurements was fairly broad.

The agreement between evaluation and measure-
ment is only fair, and significant differences occur
for E_n^c < 2 MeV. The difference may indicate that
the level structure of ^{14}N for 8.5 < E_x < 13 MeV is
not adequately known; however, the problem may very
well be in the measurement because the experimental
uncertainties are probably greatest at the lowest

neutron energies. A second difficulty in the compar-
ison is that the total (n,n') cross section from the
measurement is 0.54±0.11 b (St65), whereas the eval-
uated total (n,n') cross section is 0.4 b. If the
measured value of 0.54 b is accepted, the elastic
cross section at 14 MeV (described in Sec. 3.10) must
be decreased substantially ($\sim$ 0.14 b), and this is
difficult to reconcile with most of the elastic mea-
surements. If we assume that the measured spectrum
is wrong below E_n^c = 2.3 MeV and compare the inte-
grated cross sections for the evaluated and measured
spectra only for E_n^c > 2.3 MeV, the difference between
the evaluated and measured values decreases from
roughly 30 to 20%.

3.3.3 The ^{14}N(n,n'p)^{13}C and ^{14}N(n,n'α)^{10}B Cross Sec-
tions

States at high excitation energies in ^{14}N decay
predominantly by proton, deuteron, and alpha emission,
corresponding to the ^{14}N(n,n'p)^{13}C, ^{14}N(n,n'd)^{12}C,
and ^{14}N(n,n'α)^{10}B reactions with thresholds at 8.09,
11.01, and 12.45 MeV, respectively. In this evalua-
tion we assume that levels above 8.5-MeV excitation
in ^{14}N decay entirely by emission of either protons
or alpha particles. Because there is virtually no
available experimental information on these proces-
ses, we have very crudely divided the (n,n') cross
sections into (n,n'p) and (n,n'α) components by as-
suming that states in ^{14}N emit particles with decay
probabilities proportional to $(2s+1)(2J+1)\Delta E_c$, where
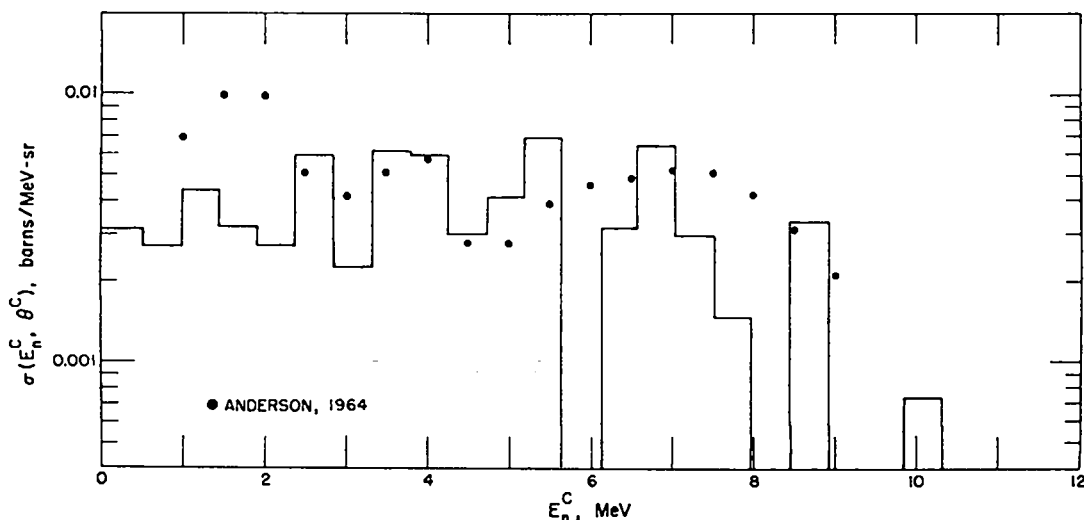s is the spin of the emitted particle, J is the spin

Fig. 40. Measured and evaluated secondary-neutron spectra in the c.m. system for 14-MeV (lab) incident
neutrons.

of the new state, and ΔE_c is the center-of-mass energy released in the reaction. We performed this calculation using all the states available for particle decay. The resulting (n,n'p) and (n,n'α) cross sections are given in Fig. 41 together with the total (n,n') and (n,n'$_\gamma$) cross sections, where the latter is defined to be the (n,n') cross section that results in photon emission. We have combined the (n,n'd) cross section, which is relatively small, into our estimate for the (n,n'p) cross section.
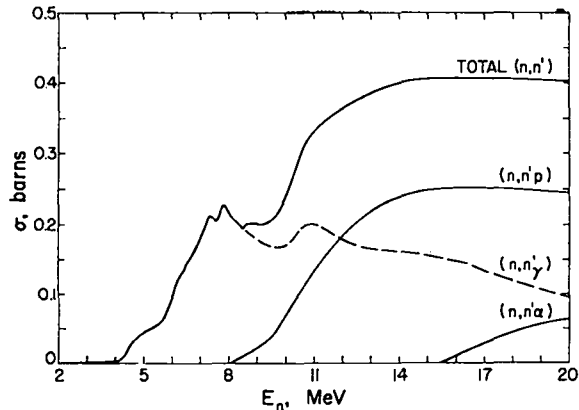

Fig. 41. Total inelastic-scattering cross section and its constituent photon- and charged-particle-emission cross sections. This curve is compounded from the results shown in Figs. 34-39.

The (n,n'p) and the (n,n'α) cross sections are included in the ENDF/B evaluation by flagging certain of the (n,n') level-excitation cross sections in File 3 as decaying by either proton or alpha emission. Because the number of discrete levels allowed by the format is limited, this representation necessarily produces artificial structure in the (n,n'p) and (n,n'α) cross sections. This structure is not included in Fig. 41.

3.4 The $^{14}N(n,p)^{14}C$ and $^{14}N(n,p\gamma)^{14}C$ Cross Sections

We evaluated the thermal (n,p$_o$) cross section to be 1.819±0.036 b from a composite of measurements by Coon and Nobles (Co49), Batchelor and Flowers (Ba49), Cüer et al. (Cu51), and Hanna et al (Ha61). The uncertainty in the thermal value is based upon the quoted errors in the measurements. The (n,p$_o$) cross section is assumed to vary as 1/v up to 10 keV and is then joined smoothly to measurements by Gibbons and Macklin (Gi59) and Johnson and Barschall (Jo50) between 0.03 and 0.3 MeV. These results are

given in Fig. 42. Again, we feel that the 1/v assumption up to 10 keV is reasonable because the first resonance does not occur until 434 keV.
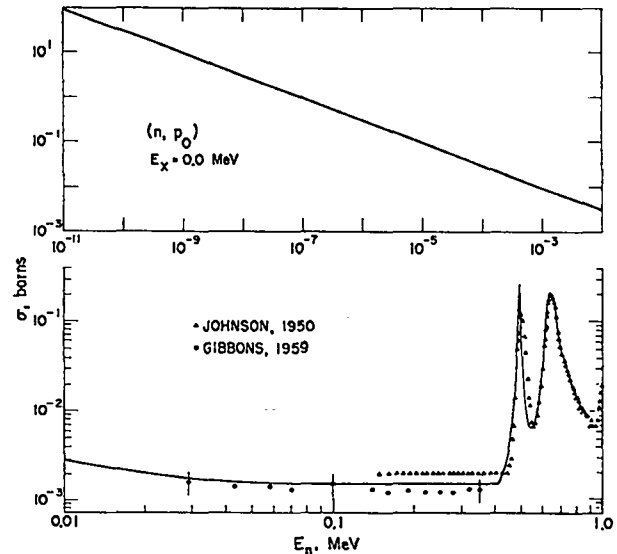
Fig. 42. Measured and evaluated (n,p) cross section to the ground state of ^{14}C from 10^{-5} eV to 1 MeV. The top figure is based on a composite of four measurements at thermal energy (not shown).

The (n,p$_o$) cross section up to 6 MeV is shown in Fig. 43. In the regions between resonances, the curve is a smooth fit to the measured data, with greatest emphasis placed on the results of Johnson (Jo50) and Gabbard et al. (Ga59)[*] up to 4 MeV. Over many of the sharper resonances, we obtained the curve from a Breit-Wigner shape using the resonance energy and width from the total-cross-section analysis and normalizing the area under the curve to the (n,p$_o$) measurements.

At neutron energies from 4 to 13 MeV, we used the measurement of the inverse $^{14}C(p,n)^{14}N$ reaction by Wong et al. (Wo67) to determine the (n,p$_o$) cross section. The results from 6 to 20 MeV are given in Fig. 44. Because of the paucity of experimental information, the structure in the (n,p$_o$) cross section in this energy region is largely unknown.

Also shown in Fig. 44 are the (n,p) excitation cross sections for the six particle-stable excited levels of ^{14}C, with the first, second, and fourth levels combined into one curve. Except for (n,p$_5$),

---

[*] All the results of Gabbard et al. (Ga59) have been increased 20% to account for a calibration error (Ga63).
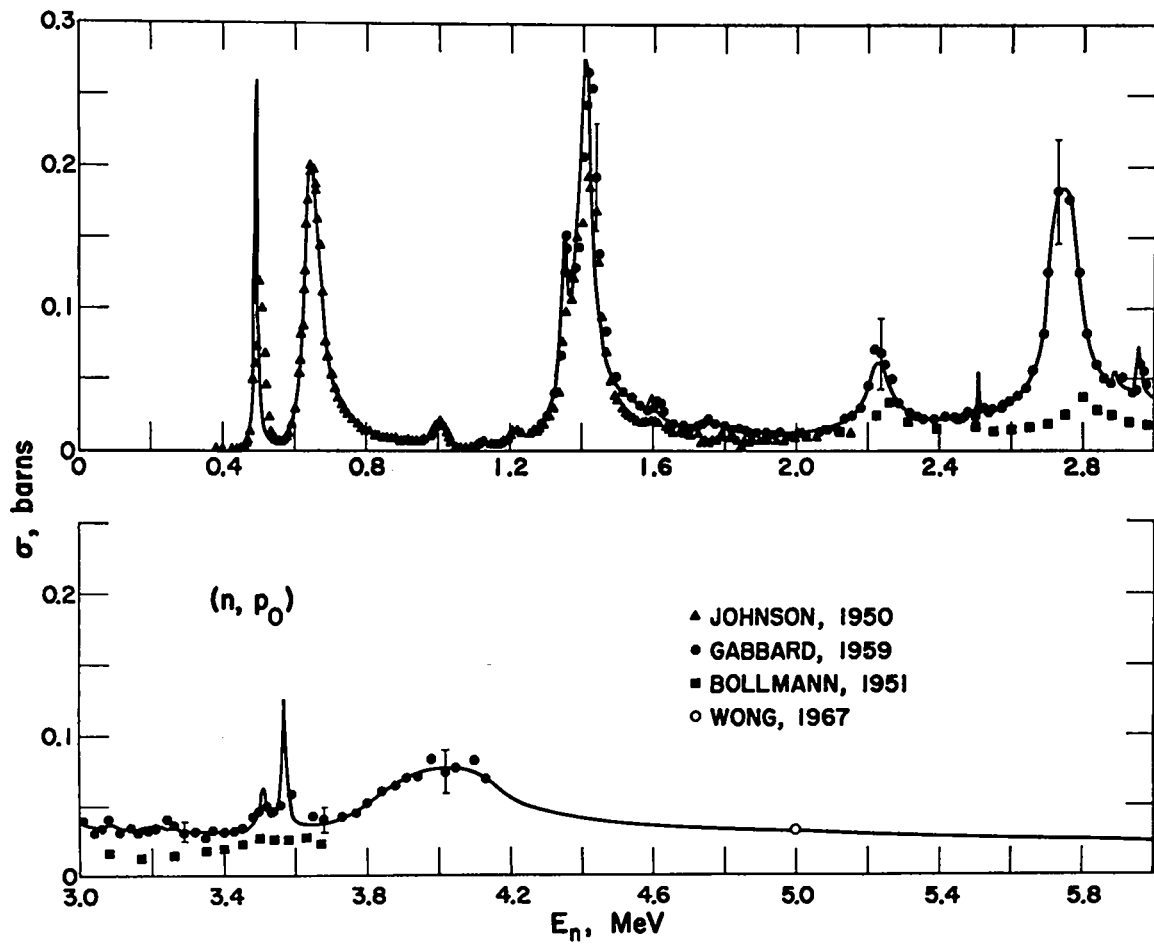
Fig. 43. Evaluated cross section for the (n,p$_0$) reaction from 400 keV to 6 MeV, with the measurements on which it is based.
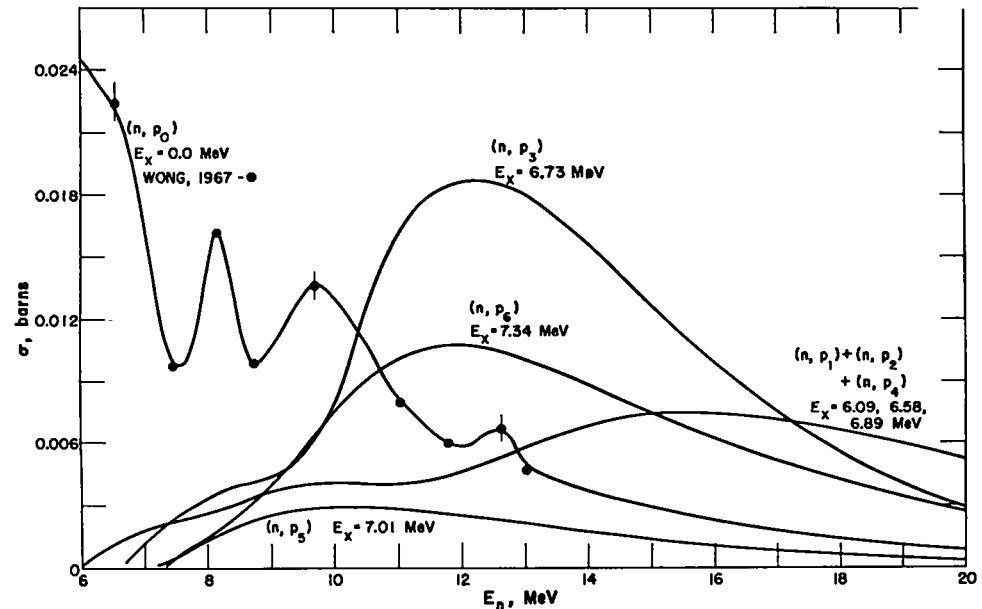
Fig. 44. Evaluated cross sections from 6 to 20 MeV for the (n,p) reaction to the six particle-stable excited states in ^{14}C, together with the (n,p$_0$) cross section and the data on which it is based.

we obtained the excited-level excitation cross sections from measurements of gamma-ray production cross sections, together with the decay scheme for ^{14}C, as described below. We obtained the curve for (n,p_5) from a compound-nucleus reaction-theory calculation, as described in Appendix A. We adjusted the calculated shape for (n,p_5) by the same factor required to produce agreement between the calculated shape of (n,p_6) and the $(n,p\gamma)$ measurements for the 1.242-MeV gamma ray from the sixth excited state of ^{14}C. The (n,p_5) cross section is relatively small, in qualitative agreement with the fact that a 7.012-MeV gamma ray is not observed in the gamma-ray production measurements.

The decay scheme for ^{14}C, which relates the (n,p) level excitation cross sections to the gamma-ray production measurements, is given in Fig. 45. The branching ratios are a composite of ^{13}C(d,p)^{14}C measurements by Alburger et al. (A166), ^{12}C(t,p)^{14}C measurements by Bell et al. (Be68), and Carlson's ^{9}Be(^{7}Li,d)^{14}C measurements (Ca66). The level energies, spins, and parities are from Ajzenberg-Selove's energy-level compilation for A = 13-15 (Aj70). The 6.583- and 6.894-MeV levels decay entirely to the 6.095-MeV level in ^{14}C. Therefore, because we had determined the (n,p) level excitation cross sections from $(n,p\gamma)$ measurements, we combined the (n,p_1), (n,p_2), and (n,p_4) excitation cross sections in the evaluation. Table VI is a summary of the gamma-ray transitions included in the evaluation. Two of the transitions have been combined, as indicated.
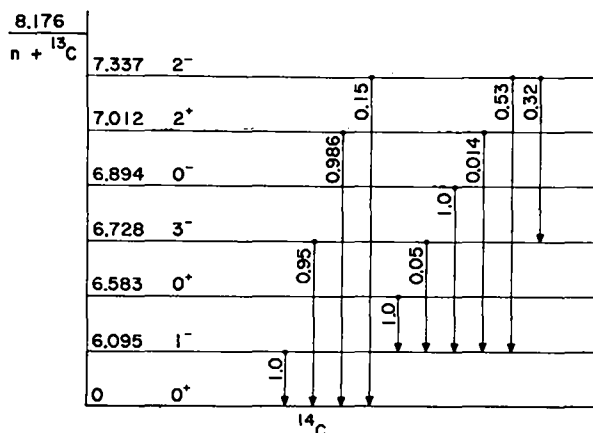
Fig. 45. Decay scheme for ^{14}C used in correlating the $(n,p\gamma)$ cross sections with the level-excitation cross sections. Note that the energy scale is grossly distorted.

Neutron emission is possible for ^{14}C states above 8.176-MeV excitation energy, and we have assumed that all states in ^{14}C above this energy decay entirely by particle emission. This assumption is supported by the fact that none of the levels in ^{14}C in this energy region have significant ratios of photon width to total width in either charged-particle- or neutron-induced reactions (Aj70). We do not give the (n,pn) cross section proceeding through these highly excited levels in ^{14}C explicitly in the evaluation, but it is included roughly in our estimates of (n,n') cross sections to levels in ^{14}N that decay by proton emission (see Sec. 3.3.3). Of the ^{14}N $(n,p)^{14}C^*(n)^{13}C$ and $^{14}N(n,n')^{14}N^*(p)^{13}C$ processes, the latter is expected to dominate. The total (n,p) cross section shown in Fig. 5 was obtained by summing the (n,p) level excitation cross sections for the first seven levels of ^{14}C.

In Fig. 46, the evaluated $(n,p\gamma)$ cross sections for the 6.094- and 6.728-MeV gamma rays are compared to the available measurements. We determined the excitation cross sections of the 6.094- and 6.728-MeV levels from these curves. The curves are based primarily upon measurements by Dickens and Perey (Di69), Orphan et al. (Or69), and Nyberg et al. (Ny69).

The $(n,p\gamma)$ cross sections for the 0.609-, 0.634-, 1.242-, 7.012-, and 7.337-MeV gamma rays are given in Fig. 47. The 0.634-MeV line is determined from the 6.728-MeV data of Fig. 46 using the decay scheme of Fig. 45. The 0.609- and 7.337-MeV lines are determined by the curve through the E_γ = 1.242-MeV measurements, and we obtained the 7.012-MeV line from the calculated (n,p_5) excitation cross section discussed previously.
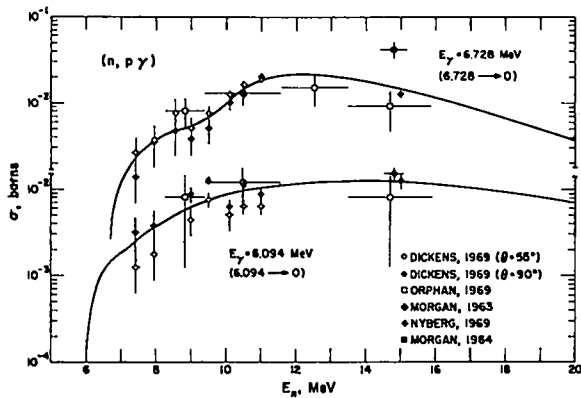
Fig. 46. Measured and evaluated cross sections for the ground-state gamma rays from de-excitation of the 6.094- and 6.728-MeV levels in ^{14}C.
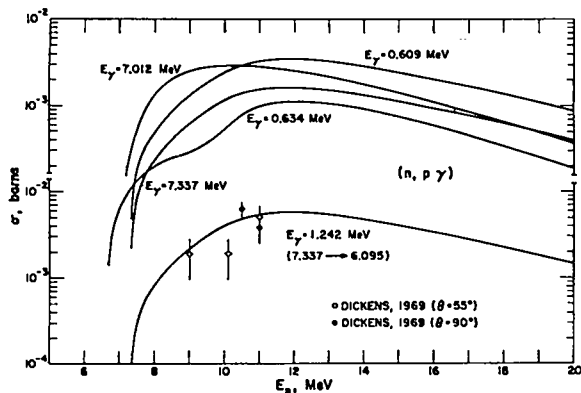
Fig. 47. Evaluated cross sections for some of the weaker $(n,p\gamma)$ gamma rays.

3.5 The ^{14}N$(n,d)^{13}$C, ^{14}N$(n,d\gamma)^{13}$C, and ^{14}N$(n,n'p\gamma)$ ^{13}C Cross Sections

The threshold for the ^{14}N$(n,d_o)^{13}$C reaction occurs at 5.71 MeV. In Fig. 48, the evaluated curve for the (n,d_o) cross section from threshold to 20 MeV is compared to the available measurements. The experimental data of Chase et al. (Ch61) and Benenson and Yaramis (Be63) consist of ^{13}C$(d,n)^{14}$N measurements that have been converted to ^{14}N(n,d_o) cross sections by means of the reciprocity theorem for nuclear reactions (B152). The single point at 14 MeV is a composite of ^{14}N(n,d_o) angular-distribution measurements by Fessenden and Maxson (Fe67), Carlson (Ca57), Miljanic et al. (Mi68), Zatzick and Maxson (Za63), and Lindsay and Veit (Li67). We de-emphasized Lindsay and Veit's measurements because they lie roughly a factor of 2 below the other

data. From these measurements, we estimate the (n,d_o) cross section at 14 MeV to be 20±4 mb. A smooth extrapolation of the evaluated curve was made from 14 to 20 MeV.
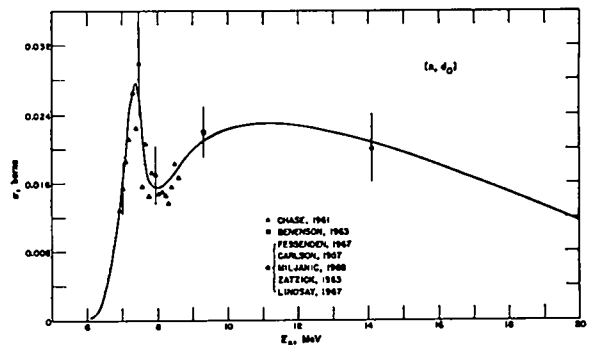
Fig. 48. Measured and evaluated (n,d) cross sections to the ground state of ^{13}C. The 14-MeV point is a composite of five measurements.

The level-decay scheme for ^{13}C, which relates the gamma-ray production measurements to the (n,d) and (n,np) level-excitation cross sections, is given in Fig. 49. We took the level energies, spins, and parities from the Ajzenberg-Selove (Aj70) A = 13-15 energy-level compilation. The branching ratios are a composite of ^{10}B$(\alpha,p\gamma)^{13}$C results of Mackin et al. (Ma56), Pixley et al. (Pi60), and Kane et al. (Ka60), and the ^{12}C$(d,p\gamma)^{13}$C results of Gorodetzky et al. (Go66). Table VII gives a list of the gamma rays that can result from de-excitation of ^{13}C levels. In this evaluation, we assume that levels in ^{13}C above the n + ^{12}C threshold at 4.947 MeV decay entirely by particle emission. We obtained the total (n,d) cross section shown in Fig. 5 by summing the (n,d) excitation cross sections for the four states given in Fig. 49.
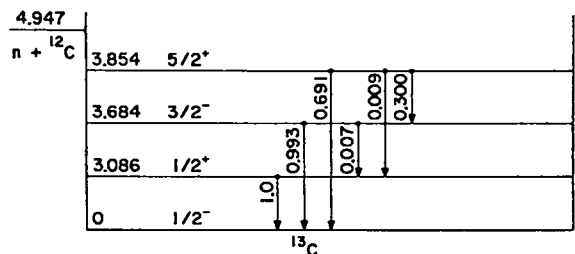

Fig. 49. Decay scheme for ^{13}C used in interpreting the $(n,d\gamma)$ and $(n,np\gamma)$ cross sections. Note that the energy scale is grossly distorted.

TABLE VII

GAMMA RAYS FROM $^{14}N(n,d)^{13}C$

AND $^{14}N(n,np)^{13}C$ REACTIONS

E_γ (MeV)	$E_{initial}$ (MeV)	E_{final} (MeV)
3.854	3.854	0
3.684	3.684	0
3.086	3.086	0
0.68	$\begin{cases} 3.854 \\ 3.684 \end{cases}$	$\begin{cases} 3.086 \\ 3.086 \end{cases}$
0.170	3.854	3.684

In evaluating the (n,xγ) cross sections, one must realize that levels in ^{13}C can be excited by (n,np) reactions as well as by (n,d) reactions. To estimate the (n,d) excitation cross sections, we assumed that the shapes of the excitation cross sections were similar to (n,p) cross sections for similar Q-values, as calculated using compound-nucleus reaction theory (Appendix A). We then normalized these calculated shapes so that they resulted in (n,xγ) cross sections that agreed with measurements around 10 MeV. Although the threshold for the (n,npγ) reaction is 9.02 MeV, substantial contributions from this source are not expected for an MeV or so above the threshold.

We estimated the excitation of ^{13}C levels through (n,np) reactions by roughly dividing the (n,n') cross section to particle-unstable levels in ^{14}N among the various states that can be reached in ^{13}N (neutron emission), ^{13}C (proton emission), ^{12}C (deuteron emission), and ^{10}B (alpha emission). As described in Sec. 3.3.3, we made this calculation assuming the decay probabilities to be proportional to $(2s + 1)(2J +1) \Delta E_c$, where the symbols have the same meaning as in Sec. 3.3.3. We then normalized the resulting (n,np) excitation functions for the three excited levels of ^{13}C by a common factor (~ 0.8) so that the sums of the (n,d) and (n,np) excitation cross sections resulted in (n,xγ) cross sections that agreed better with measurements near 14 MeV, where the (n,npγ) contributions are dominant.

Figure 50 shows the results of this analysis for the (n,d_1) cross sections and for the (n,xγ) cross section for the 3.086-MeV gamma ray. The rapid rise in the (n,xγ) cross section near 12 MeV results from the (n,npγ) contribution. The disagreement between the evaluation and the Morgan (Mo63)

and Buchanan (Bu69) experimental results in Fig. 50 is largely eliminated by the recently revised TNC compilation (Bu71). The new result, which supersedes the older data, is 14 mb at 14.8 MeV, in reasonable agreement with the 18 mb evaluated result.
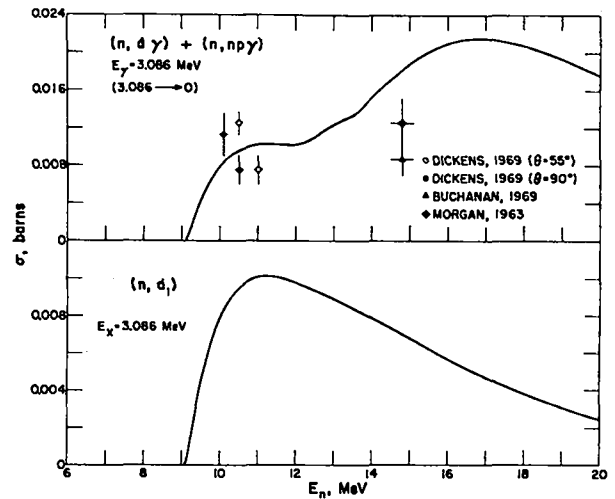
Fig. 50. Evaluated (n,d_1) cross section and the photon-production data for the 3.086-MeV photon. The rise in the upper curve above 12 MeV is due to the (n,npγ) contribution to the same gamma transition. The lower curve has a calculated shape normalized to the photon-production measurements below the effective (n,n'pγ) threshold.

The results of our analysis for the (n,d_2) excitation cross section to the 3.684-MeV level and the (n,xγ) cross section for the 3.684-MeV photon are given in Fig. 51. Again, the rise in the (n,xγ) cross section near 12 MeV is due to contributions from (n,npγ) reactions. The evaluated curve and the measurements agree reasonably well.

Fig. 51. Evaluated (n,d_2) cross section and the photon-production data for the 3.684-MeV photon. (See caption to Fig. 50.)

The (n,d_3) cross section to the 3.854-MeV level and the (n,xγ) cross section for the 3.854-MeV line are given in Fig. 52. The evaluated (n,xγ) curve and the measurements again agree reasonably well. The sum of our evaluated (n,d_2) and (n,d_3) cross sections (20 mb) agrees well with a rough estimate of this cross section (15 to 25 mb) from (n,d_2) + (n,d_3) partial angular distribution measurements by Fessenden and Maxson (Fe67), Zatzick and Maxson (Za63), and Carlson (Ca57).
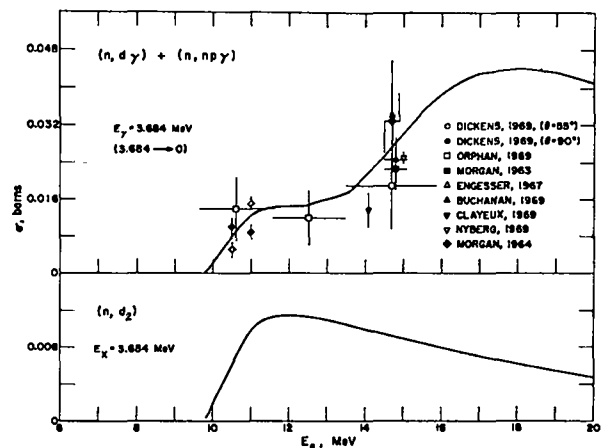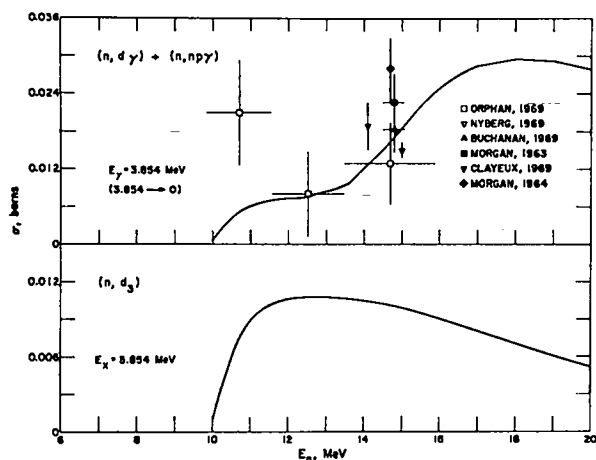
Fig. 52. Evaluated (n,d_3) cross section and the photon-production data for the 3.854 MeV photon. (See Caption to Fig. 50.)

The photon-production cross sections for photons of 0.170- and 0.68-MeV energy are given in Fig. 53. The latter is a composite of 3.684- → 3.086-MeV (E_γ = 0.598 MeV) and 3.854- → 3.086-MeV (E_γ = 0.768 MeV) transitions. In each case, we computed the (n,xγ) cross sections from the evaluated level-excitation cross sections.
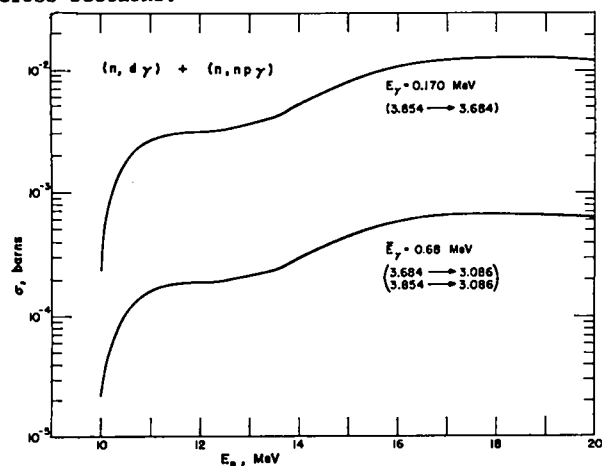
Fig. 53. Evaluated photon-production cross sections for the low-energy gamma rays from cascades in ^{13}C, as reconstructed from the level-excitation cross sections.

3.6 The $^{14}N(n,t)^{12}C$ and $^{14}N(n,tγ)^{12}C$ Cross Sections

The threshold for the $^{14}N(n,t_o)^{12}C$ reaction occurs at 4.304 MeV. The evaluated curve for the (n,t_o) reaction is compared to the available measurements in Fig. 54. Considering the uncertainties associated with the Gabbard et al. (Ga59) and Scobel et al. (Sc66) measurements, the agreement between the experiments is reasonable. The open triangle at 14.5 MeV is our evaluated result (6.5 ± 1.3 mb), based primarily upon (n,t_o) angular-distribution measurements by Fessenden and Maxson (Fe67) and Rendic (Re67); we also considered Lindsay and Veit's (Li67) measurement. but it is a factor of 2 lower than the other results.

Also shown in Fig. 54 is the evaluated curve for the $^{14}N(n,t_1)$ reaction to the 4.439-MeV state in ^{12}C. The curve is based upon a compound-nucleus reaction-theory calculation for the (n,p) reaction with a similar Q-value (see Appendix A) which has been normalized to our evaluated result at 14.5 MeV. The estimated cross section at 14.5 MeV for the (n,t_1) reaction is 21 ± 7 mb, based on the Fessenden (Fe67) and Rendic (Re67) measurements.

The only particle-stable excited state in ^{12}C is the 4.439-MeV level, which decays entirely by gamma-ray emission to the ground state of ^{12}C. The gamma-ray production cross section for the 4.439-MeV line is given in Fig. 55. We obtained the curve from the evaluated $^{14}N(n,t_1)^{12}C^*$ cross section and from an estimate of the $^{14}N(n,n'd)^{12}C^*$ cross section to the first excited state of ^{12}C. We made the latter estimate in the manner described in Sec. 3.5 for the (n,n'pγ) reactions. We obtained the evaluated total (n,t) cross section by summing the (n,t_o) and (n,t_1) contributions.

3.7 The $^{14}N(n,α)^{11}B$ and $^{14}N(n,αγ)^{11}B$ Cross Sections

The threshold for the (n,$α_o$) reaction occurs at 0.168 MeV; the (n,$α_o$) reaction does not become significant, however, until above 1.2 MeV. The evaluated (n,$α_o$) cross section from 1 to 7 MeV is compared to the available measurements in Fig. 56. The curve is based mainly on measurements by Johnson and Barschall (Jo50) at lower energies and on the results of Gabbard et al. (Ga59) at higher energies. The results of Haddad (Ha59a) and Mani and Dutt (Ma66) were obtained from measurements of the inverse $^{11}B(α,n)^{14}N$ reaction, using the reciprocity
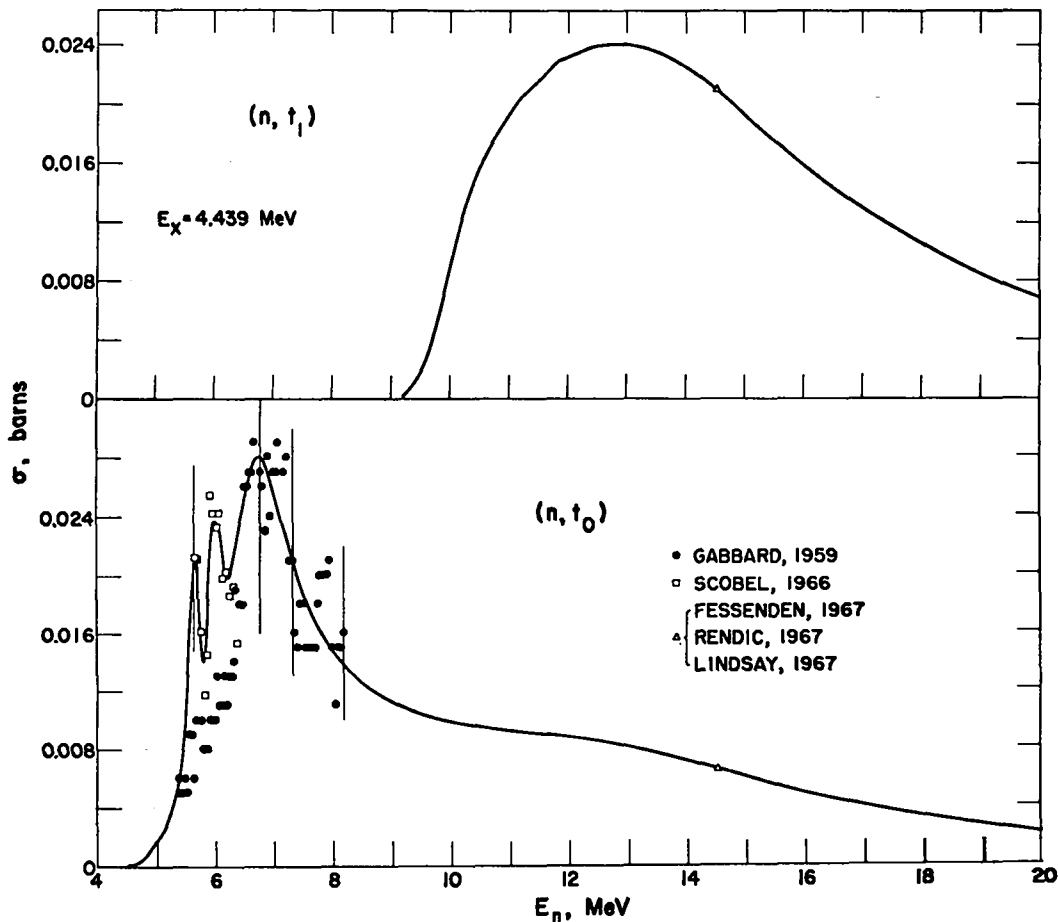
Fig. 54. Measured and evaluated (n,t) cross sections to the ground and first excited states of ^{12}C.
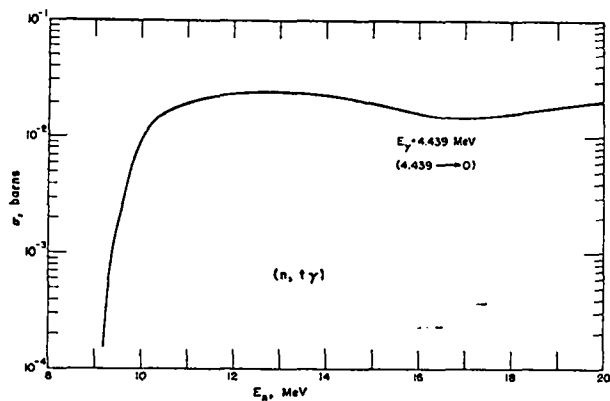
Fig. 55. Evaluated cross section for the photon decay of the first excited state in ^{12}C following (n,t) and (n,n'd) reactions.

theorem (B152). As was the case with (n,p_0), we obtained the shape of the (n,α_0) curve over many of the sharper resonances from a Breit-Wigner expression, using the resonance energy and width from the total-cross-section analysis and normalizing to the peak area in the (n,α_0) measurements. We used a similar treatment for several peaks in the (n,α_1), (n,α_2), and (n,α_3) reactions described below.

The (n,α_0) cross section from 7 to 20 MeV is given in Fig. 57. The open triangle at 14.5 MeV is the result of our evaluation of (n,α) experiments by Lillie (Li52), Leroux et al. (Le68), Bachinger and Uhl (Ba68), and Maxson and Murphy (Ma68). Lillie's measurement was made with a cloud-chamber, the Leroux and Bachinger data were obtained with nuclear emulsions, and the Maxson measurement employed a counter telescope. The four measurements do not agree well over the entire spectrum, and our results are a composite of the four, taking into account to a limited

33
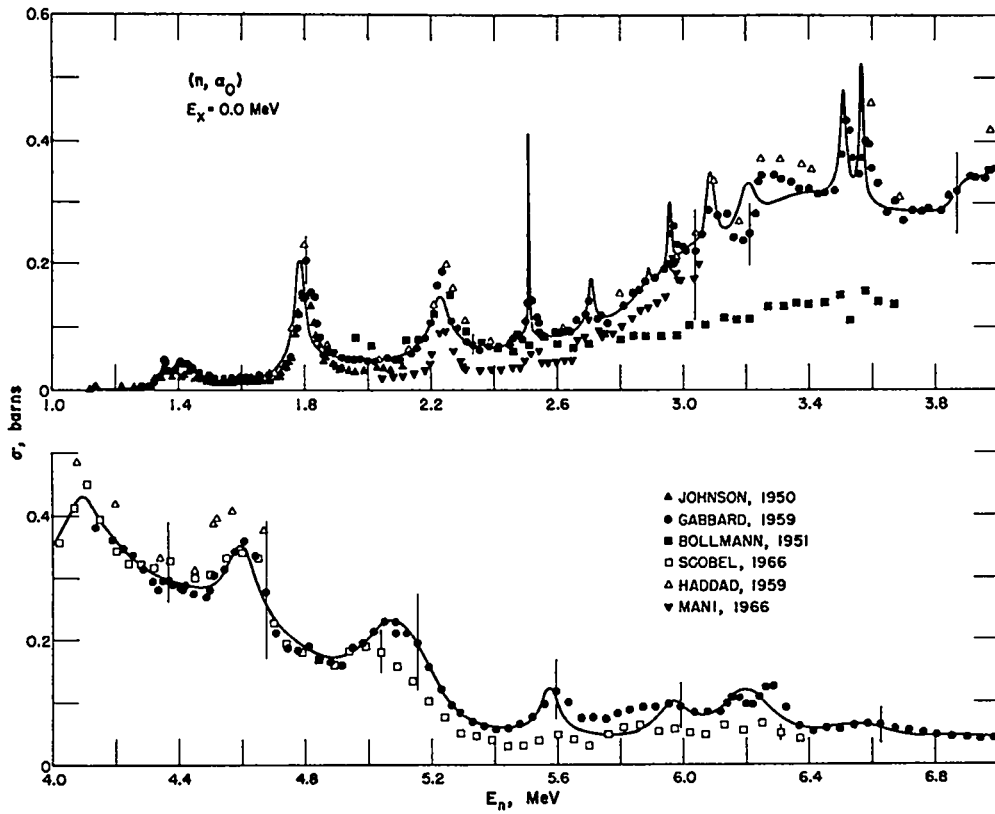
Fig. 56. Measured and evaluated (n,α_o) cross sections from 1 to 7 MeV. The resonance energies and total widths for many of the resonances are taken from the total cross section.
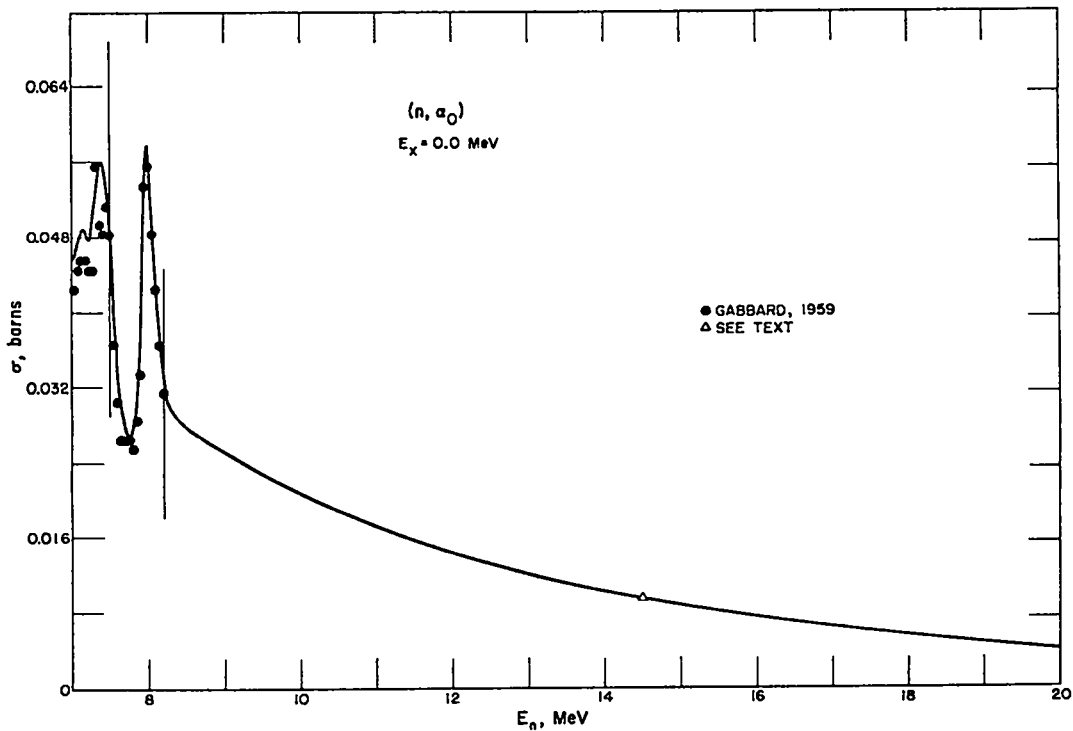
Fig. 57. Measured and evaluated (n,α_o) cross sections from 7 to 20 MeV. The triangle at 14 MeV is a composite of four measurements.

extent the (n,αγ) measurements described below. Lillie cites a value of 100 mb for the integrated (n,α) cross section (Li52), whereas Leroux et al. give 60 mb (Le68). Our evaluated spectrum is normalized to 92.5 mb at 14.5 MeV. There are no available measurements for the (n,α_o) cross section between 8.2 and 14 MeV; we based the shape of the evaluated curve in this region upon the compound-nucleus reaction-theory calculations described in Appendix A. The curve was extrapolated smoothly from 14.5 to 20 MeV.

The decay scheme for ^{11}B, which relates the (n,αγ) measurements to the (n,α) level excitation cross sections, is given in Fig. 58. The level energies, spins, and parities come from the A = 11 to 12 energy-level compilation by Ajzenberg-Selove and Lauritsen (Aj68). The branching ratios that are included in the compilation were obtained mainly from ^{9}Be(^{3}He,pγ)^{11}B and ^{10}B(d,pγ)^{11}B coincidence measurements by Olness et al. (Ol65).
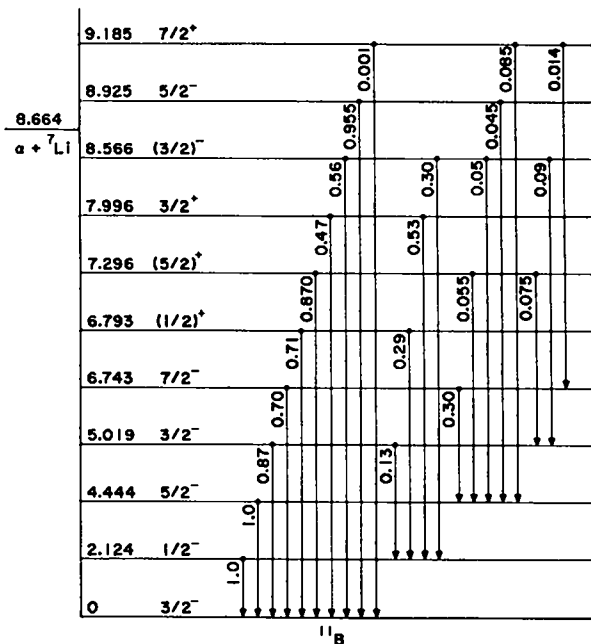
Fig. 58. Decay scheme for ^{11}B used in interpreting the (n,αγ) measurements.

The probabilities for gamma-ray emission from the 8.925-MeV level (100%) and the 9.185-MeV level (10%) are also from the Olness measurements; all known higher levels have total widths in the keV range and do not decay significantly by gamma ray emission. Table VIII summarizes the gamma-ray tran-

sitions that appear in the evaluation; some of the weaker transitions have been combined, as indicated.

TABLE VIII

GAMMA RAYS FROM ^{14}N(n,α)^{11}B REACTIONS

E_γ (MeV)	$E_{initial}$ (MeV)	E_{final} (MeV)
8.925	$\begin{cases}9.185\\8.925\end{cases}$	$\begin{matrix}0\\0\end{matrix}\Big\}$
8.566	8.566	0
7.996	7.996	0
7.296	7.296	0
6.77	$\begin{cases}6.793\\6.743\end{cases}$	$\begin{matrix}0\\0\end{matrix}\Big\}$
6.442	8.566	2.124
5.872	7.996	2.124
5.019	5.019	0
4.65	$\begin{cases}9.185\\6.793\\8.925\end{cases}$	$\begin{matrix}4.444\\2.124\\4.444\end{matrix}\Big\}$
4.444	4.444	0
3.800	$\begin{cases}8.566\\8.566\end{cases}$	$\begin{matrix}4.444\\5.019\end{matrix}\Big\}$
2.895	5.019	2.124
2.852	7.296	4.444
2.30	$\begin{cases}9.185\\6.743\\7.296\end{cases}$	$\begin{matrix}6.743\\4.444\\5.019\end{matrix}\Big\}$
2.124	2.124	0

The evaluated curves for the E_γ = 2.124 MeV (n,αγ) cross section and the ^{14}N(n,α_1)^{11}B* cross section to the 2.124-MeV level are compared to the available measurements for E_n = 4-7 MeV in Fig. 59. Although there is some cascading to the 2.124-MeV level, the (n,αγ) cross section for the ground-state transition is mainly determined by the (n,α_1) excitation cross section. Therefore, the comparison given in Fig. 59 provides a check on two entirely independent sets of experimental data, i.e., the (n,αγ) and the (n,α) measurements. The agreement is reasonable considering the error bars on the measurements and gives us confidence in both sets of data.

The same results are given in Fig. 60 for the 7- to 20-MeV neutron-energy region. The open triangle at 14.5 MeV in the lower half of the figure again results from our evaluation of the (n,α) spectrum and cross section from four measurements (Li52, Le68, Ba68, Ma68). The overall consistency in the two parts of Fig. 60 is reasonable, although Hall and Bonner's (n,αγ) data (Ha59) are lower than the
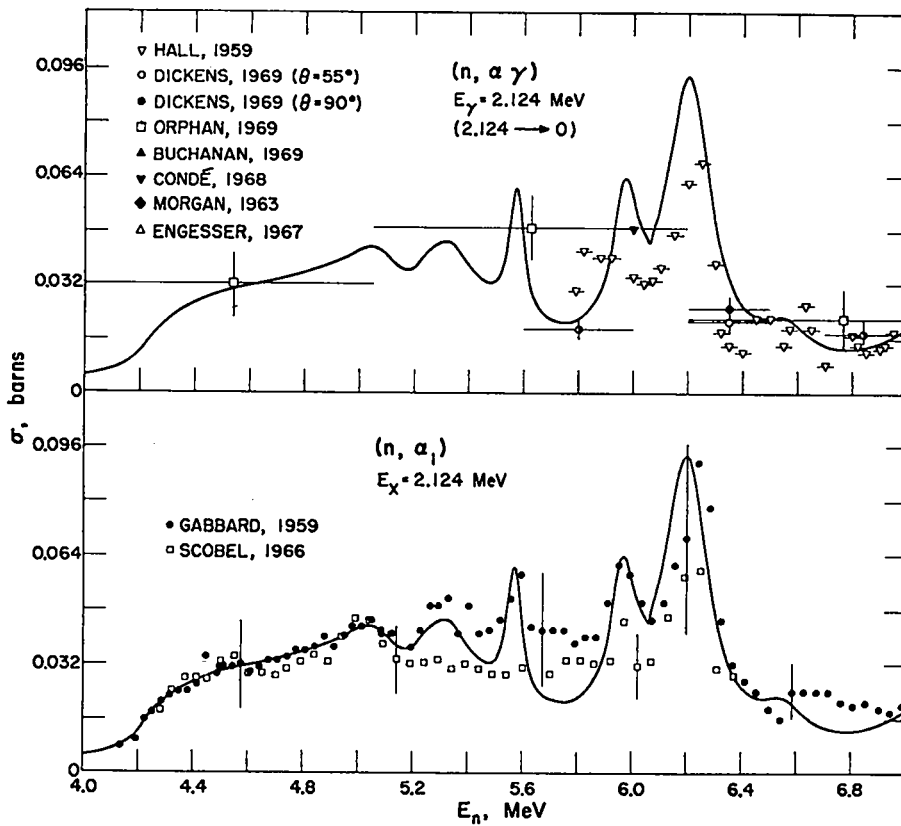
Fig. 59. Measured and evaluated (n,α_1) and $(n,\alpha\gamma)$ cross sections for the 2.124-MeV level and ground-state transition for neutron energies between 4 and 7 MeV.
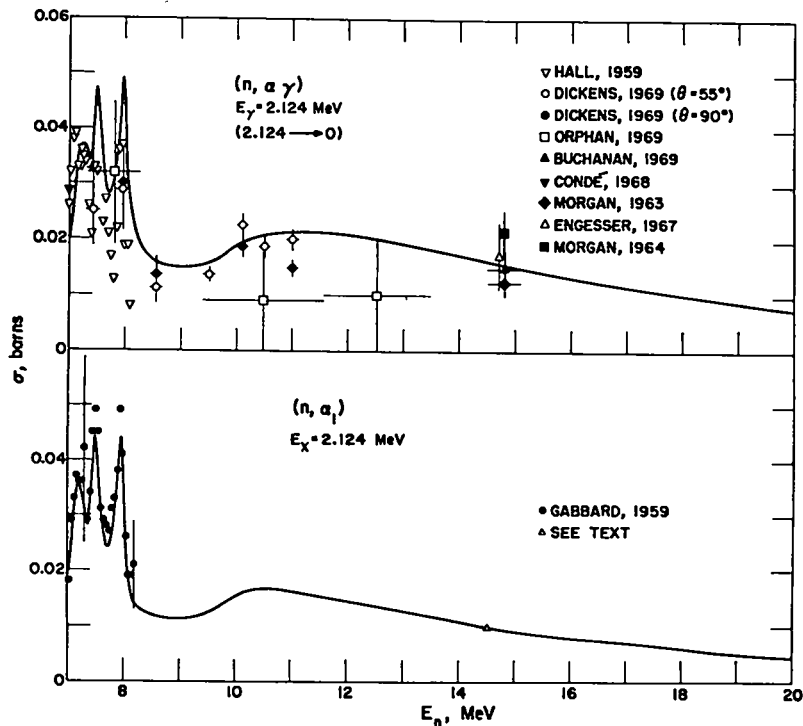
Fig. 60. Measured and evaluated (n,α_1) and $(n,\alpha\gamma)$ cross sections for the 2.124-MeV level and ground-state transition. The 14.5-MeV (n,α_1) datum is a composite of four measurements.

evaluation near 8 MeV. Further, the new TNC compilation (Bu71) gives a value of 30 mb for the (n,αγ) cross section at 14.8 MeV, compared to their old value of 15 mb (Bu69) and our evaluated result of 16 mb. The measurement by Maslov et al. (Ma68a) for the sum of the 2.124- and 2.313-MeV photons gives a value at 14 MeV that agrees well with the evaluated results.

The $^{14}N(n,\alpha_2)^{11}B^*$ cross section for the 4.444-MeV level and the photon production cross section for the 4.444-MeV photon are given in Fig. 61. The dashed curve in the upper half of the figure results if the $^{14}N(n,t\gamma)^{12}C$ cross section for the 4.439-MeV gamma ray is added to the $E_\gamma = 4.444$-MeV cross section. Because these lines differ in energy by only 5 keV, they are undoubtedly unresolved in the NaI gamma-ray measurements and are probably unresolved in the Ge(Li) measurements. The open triangle at 14.5 MeV in the lower half of Fig. 61 results from our evaluated spectrum, as described ear-

lier. The reasonable consistency between the (n,α) and the (n,αγ) measurements in Fig. 61 gives us confidence in the branching ratios involved. The fact that the dashed curve rises above the (n,xγ) measurement of Dickens and Perey (Di69) near 11 MeV probably indicates that either our (n,α_2) cross section or our (n,t_1) cross section to the 4.439-MeV level of ^{12}C is too high in this energy region. We did not discover this inconsistency until the evaluation was completed.

The $^{14}N(n,\alpha_3)^{11}B^*$ cross section to the 5.019-MeV level and the (n,αγ) cross section for the 5.019-MeV photon are given in Fig. 62. We have corrected the (n,α_3) measurements by Gabbard et al. (Ga59) for contributions from the (n,d_o) and (n,p_1) reactions which were not resolved in their experiment. The open triangle at 14.5 MeV in the lower part of Fig. 62 is from our evaluated spectrum. The 5.019-MeV gamma ray has not been observed in measurements with Ge(Li) detectors. This is prob-
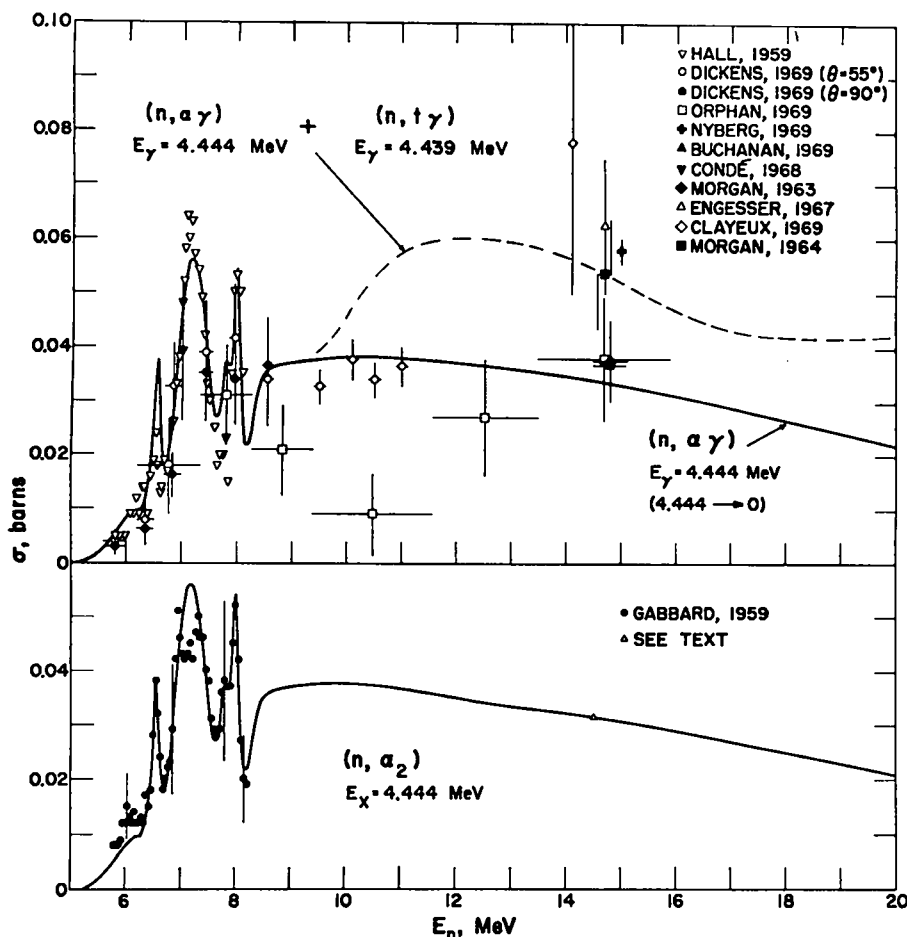
Fig. 61. Measured and evaluated cross sections for the (n,α_2) and (n,αγ) cross sections for the 4.444-MeV level and ground-state transition. The dashed curve includes a contribution from the 4.439-MeV (n,tγ) photon.

ably because of Doppler broadening of the gamma rays from the 5.019- → 0-MeV transition, to the extent that they are not observed as peaks in high-resolution Ge(Li) spectra. This broadening is too small to affect poorer-resolution NaI or CsI measurements seriously, and we have included the (n,xγ) data from these measurements in the upper part of Fig. 62. These results should be compared to the upper evaluated curve, which includes the (n,n'γ) cross section for the 5.106-MeV photon, because the 5.106- and 5.019-MeV photons are not resolved in the poorer-resolution measurements.

Reynolds et al. (Re70) have suggested that the "missing" 200 mb in the nitrogen discrepancy near 8 MeV (see Sec. 3.10) might be partially accounted for by the (n,α_3) channel. The results in Fig. 62 indicate that the (n,α_3) cross section can be increased by no more than 20 to 30 mb and still be consistent with the (n,α_3) and $(n,\alpha\gamma)$ measurements near 8 MeV.

The evaluated curves and the measurements in Fig. 62 agree reasonably well. However, the new

TNC compilation (Bu71) quotes an (n,xγ) cross section at 14.8 MeV which falls near the Engesser and Thompson (En67) point. Because this new result supersedes the older TNC measurements (Mo63, Mo64, Bu69), the evaluated composite (n,xγ) cross section is possibly a little low near 15 MeV. Also, the Maslov et al. (Ma68a) measurement at 14 MeV, which was inadvertently omitted from the graph, supports a higher cross section in this region.

The evaluated (n,α) level-excitation cross sections for the 4th through 10th excited levels of [11]B are given in Fig. 63. We obtained the curves for all levels except those at 8.925 and 9.185 MeV by normalizing the compound-nucleus reaction-theory calculations described in Appendix A to our evaluated spectrum at 14.5 MeV (open triangles). For the cross section to the 8.925- and 9.185-MeV levels, we normalized the calculations by the same factor required for the 8.566-MeV-level cross section, because estimates for the 8.925- and 9.185-MeV contributions were not obtained from the spectrum measurements.
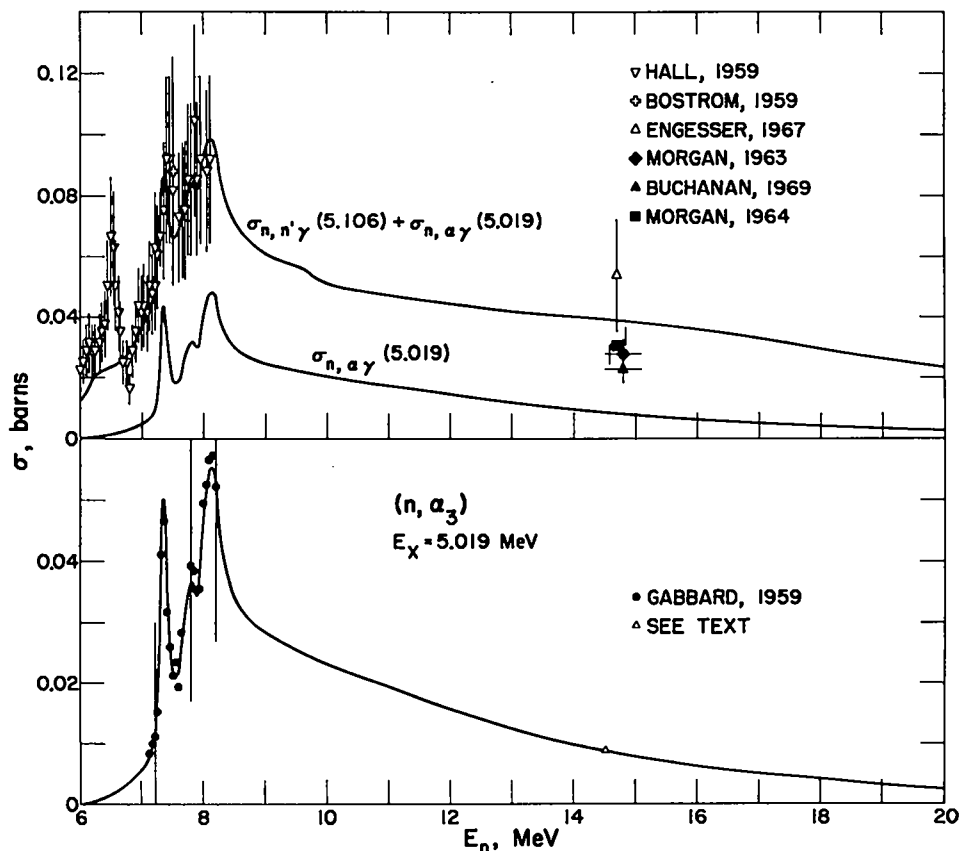
Fig. 62. Measured and evaluated (n,α_3) cross section and the cross section for producing the 5.019-MeV gamma ray from this reaction. The combined photon-production cross section for the 5.019- and 5.106-MeV photons is compared to the available NaI measurements in the upper part of the figure.

The $^{14}N(n,\alpha\gamma)^{11}B$ cross sections that result from excitation of the higher levels in ^{11}B are given in Figs. 64 and 65. We obtained the evaluated curves from the foregoing estimates of the level-excitation cross sections using the ^{11}B decay scheme given in Fig. 58. Although the existence of these gamma rays is implied by alpha-spectrum measurements at 14.5 MeV (Li52, Le68, Ba68, Ma68), the only direct observation[*] of the higher-energy photons given in Fig. 65 occurred in an integral experiment by Reynolds and Sperling (Re71), in which gamma-ray spectra were measured in a large tank of liquid nitrogen pulsed with 14-MeV neutrons. Broad peaks in the unfolded

spectrum from this measurement are probably due to the 6.77-, 7.296-, 7.996-, 8.566-, and 8.925-MeV photons indicated in Fig. 65.

We obtained the evaluated total (n,α) cross section in Fig. 5 (Sec. 2) by summing the level-excitation cross sections for the ground and first 10 excited states of ^{11}B. The excitation cross sections to higher levels in ^{11}B are included in the $(n,2\alpha)$ cross section, because these levels decay mainly by alpha emission.

3.8 The $^{14}N(n,2\alpha)^{7}Li$ Cross Section

The only experimental data available on the $(n,2\alpha)$ cross section are the cloud-chamber measurements by Lillie (Li52) and Mösner et al. (Mo67).

[*]Maslov et al. (Ma68a) report a 9.1-MeV photon at E_n = 14.1 MeV with a cross section of 8±4 mb which might correspond to the 8.925-MeV line in Fig. 65.
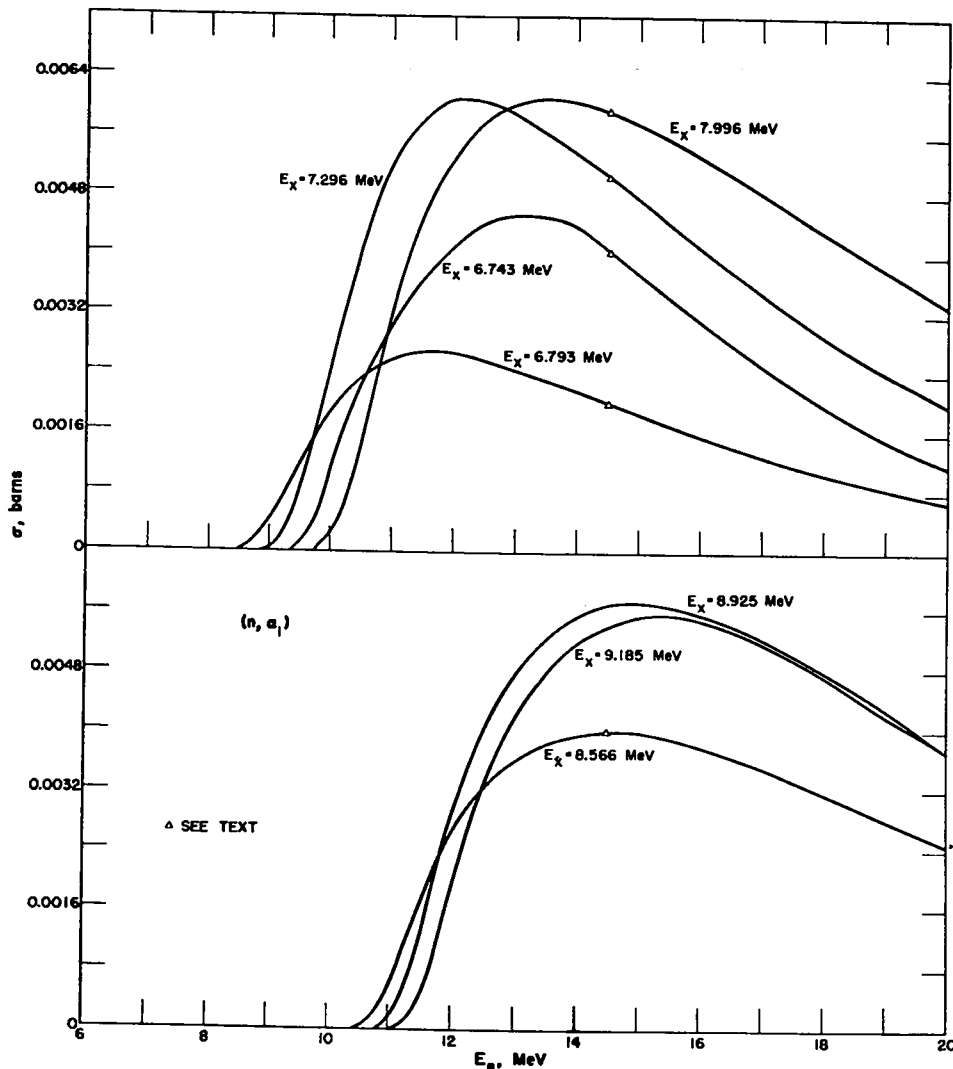
Fig. 63. Evaluated cross sections for the (n,α_4) through (n,α_9) reactions.

The experimental results are compared with our curve in Fig. 66. We crudely estimated the shape of the curve to 16 MeV by calculating (Appendix A) the contribution from (n,α) reactions to known states in ^{11}B above 9.2-MeV excitation energy relative to the contribution from states below 9.2 MeV, and then applied this ratio to our total (n,α) cross section.

The absolute value of the calculated curve agreed better with the Mösner (Mo67) datum than is indicated in Fig. 66. We decided, however, to compromise the evaluated curve between the two measurements. Above 16 MeV, we made a smooth extrapolation of the curve.
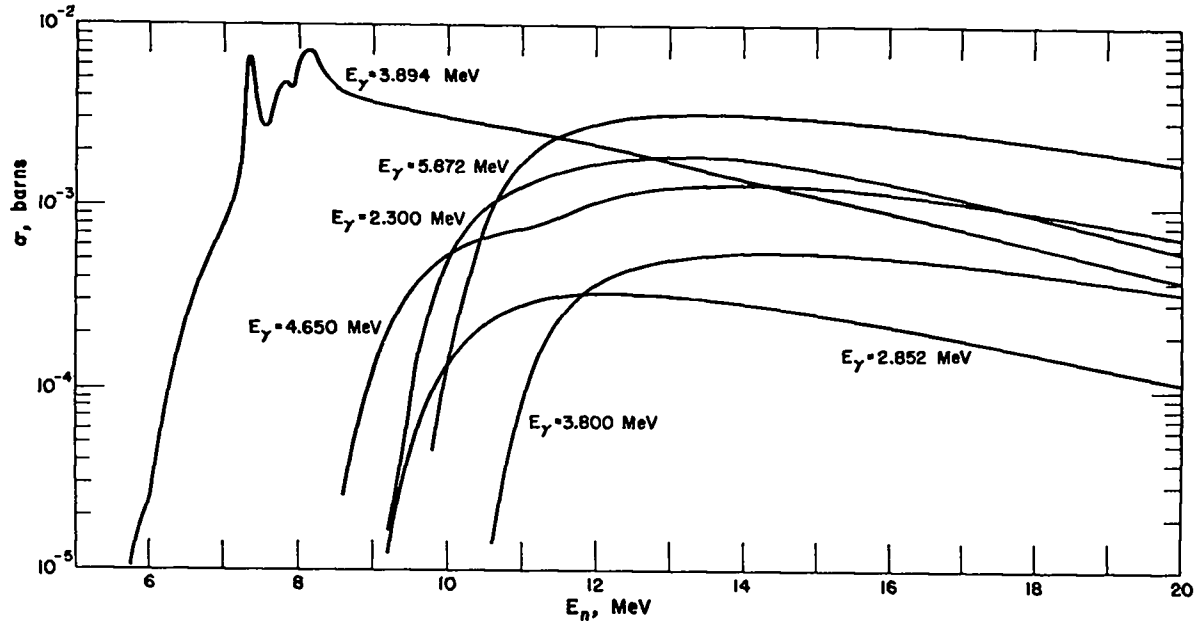
Fig. 64. Evaluated photon-production cross sections for six of the weaker (n,αγ) transitions with photon energies below 6 MeV.
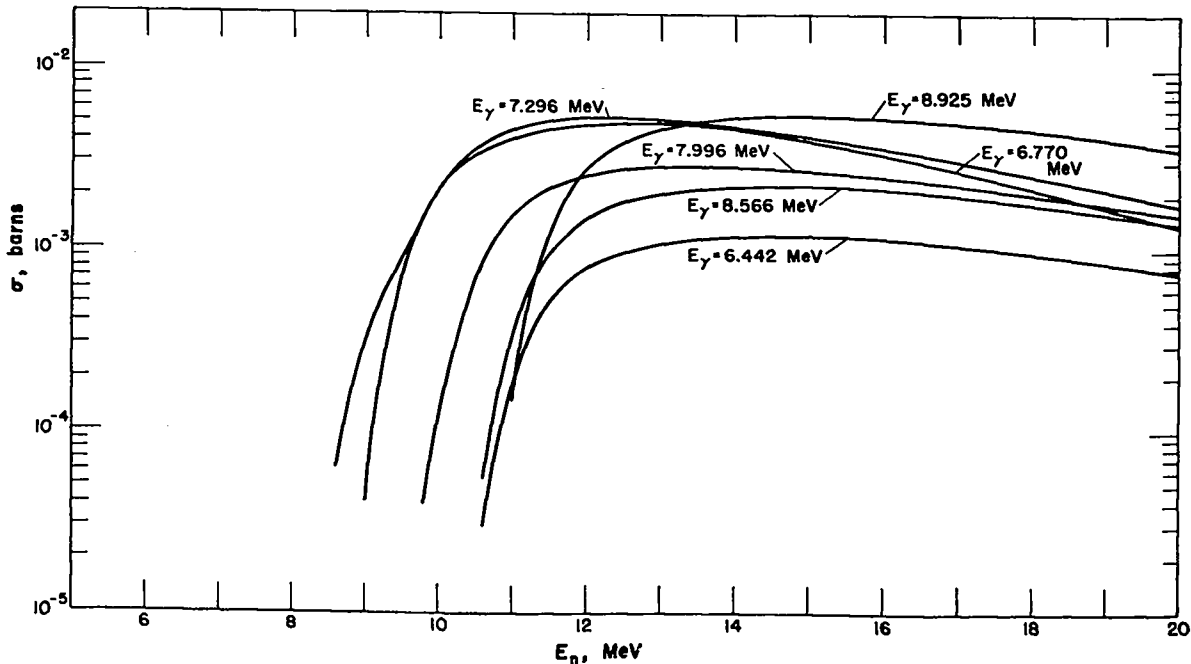
Fig. 65. Evaluated photon-production cross sections for six of the weaker (n,αγ) transitions with photon energies between 6 and 9 MeV.
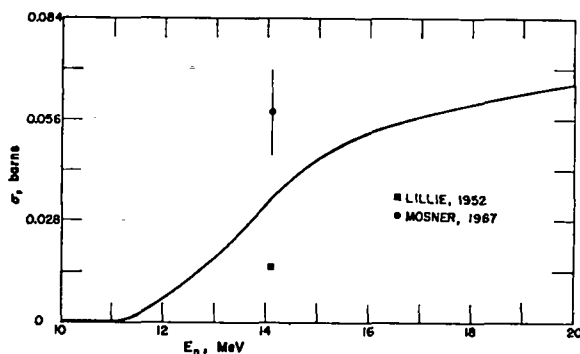
Fig. 66. Measured and evaluated (n,2α) cross
sections.

3.9 The ^{14}N(n,2n)^{13}N Cross Section and Energy Distribution

The threshold for the ^{14}N(n,2n)^{13}N reaction occurs at 11.31 MeV. A number of activation measurements of the (n,2n) cross section have been made using the 10-min half-life positron decay of ^{13}N. The evaluated (n,2n) cross section is compared to many of the available measurements in Fig. 67.[*] The evaluated curve is based mainly on measurements by Ferguson et al. (Fe60), Prud'homme et al. (Pr60), and Bormann et al. (Bo65). The (n,2n) cross section is seen to be less than 12 mb at all neutron energies below 20 MeV.

There are no measurements of the energy distribution of neutrons from the (n,2n) reaction. To estimate the energy distribution, we performed a calculation assuming that the cross section follows a purely phase-space or statistical energy distribution (Oh65); that is,

Fig. 67. Measured and evaluated (n,2n) cross sections. Several one-energy measurements near 14 MeV are not plotted, although they were included in the evaluation.

3.10 The Elastic-Scattering Cross Section

Our evaluation of the elastic-scattering cross section in the eV energy region, which results in a thermal free-atom scattering cross section of 9.957 barns, is described in the discussion of the total cross section (Sec. 3.1). Aside from the eV region, we determined the elastic cross section for neutron energies below 10 MeV by subtracting the sum of the evaluated partial-reaction cross sections from the evaluated total cross section. The results of this analysis for neutron energies up to 6 MeV are compared to the available elastic measurements in Fig. 69. We obtained the elastic results by fitting our

$$\frac{d^2\sigma}{d\Omega_1 dE_1} \propto \left\{ E_1 \left[\frac{14}{15} \left(\frac{14}{15} E_n + Q \right) - E_1 + \frac{2}{15} \sqrt{E_n E_1} \mu_1 - \frac{E_n}{15^2} \right] \right\}^{1/2} \quad ,$$

where E_1 is the laboratory energy of the outgoing neutron, μ_1 is the cosine of the laboratory angle, Ω_1 is the laboratory solid angle, E_n is the incident neutron energy, and Q is the Q-value for the (n,2n) reaction (-10.553 MeV). We integrated this expression over laboratory solid angle to obtain average energy spectra for various incident-neutron energies. Sample results are given in Fig. 68, where the spectra are normalized so that the area under each curve is unity.

evaluated angular-distribution shapes (Sec. 4.1) to the angular distribution measurements. We arbitrarily placed error bars of 10% on the experimental data by Fowler (Fo55, Fo66) and Chase (Ch61); we consider the Bostrom results (Bo57) less accurate and have given them error bars of 20%. The agreement between the evaluated curve and the measurements is quite good below 3 MeV and reasonably good up to 6 MeV.

The relative elastic measurements by Boreli et al. (Bo68) between 4.2 and 6.3 MeV are not included in Fig. 69. These results, obtained using a spherical-shell technique, substantially disagree with our

---

[*] Several 14-MeV measurements (As58, Ce62, Cs66, Du54, Gr65, Pa53, Pa67, Ra61, St65a) are omitted from Fig. 67.
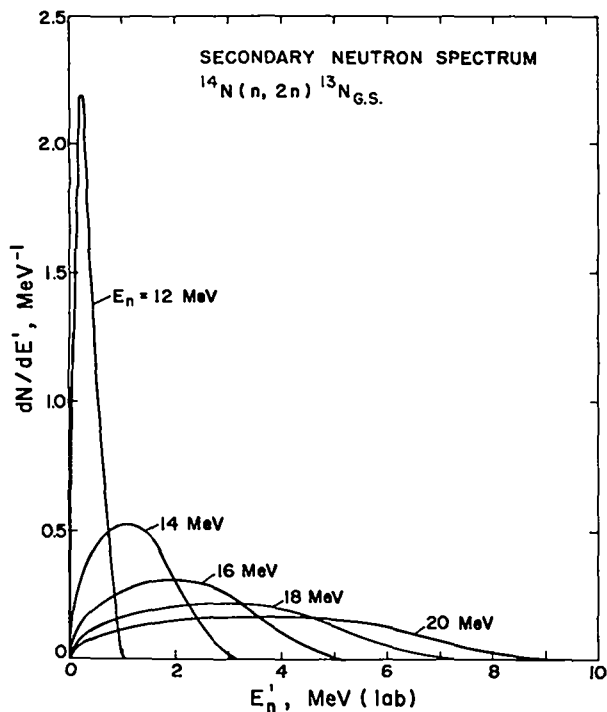
Fig. 68. Evaluated secondary-neutron energy spectra for the (n,2n) reaction for several laboratory energies of the incident neutron.

evaluated curve, as they were normalized to an elastic cross section of 0.7 barns at 6.3 MeV. The shape of their measured curve also does not agree with the evaluated shape above 5.0 MeV, principally because of its overall decrease with increasing energy relative to the evaluated result. Finally, the nonelastic cross section measured in the Boreli experiment also disagrees substantially with the evaluated nonelastic cross section and is therefore inconsistent with the sum of the available (n,n'), (n,p), and (n,α) measurements at these energies.

The elastic cross section for the 6- to 20-MeV energy region is given in Fig. 70. As stated earlier, below 10 MeV we determined the evaluated elastic cross section by subtracting the nonelastic from the total, and above 10 MeV we joined the evaluated curve smoothly to the experimental results.

The energy range covered in Fig. 70 includes the region of the well-known discrepancy in the nitrogen cross sections (St69, Di69) near 8 MeV. The essence of this problem is that the elastic cross
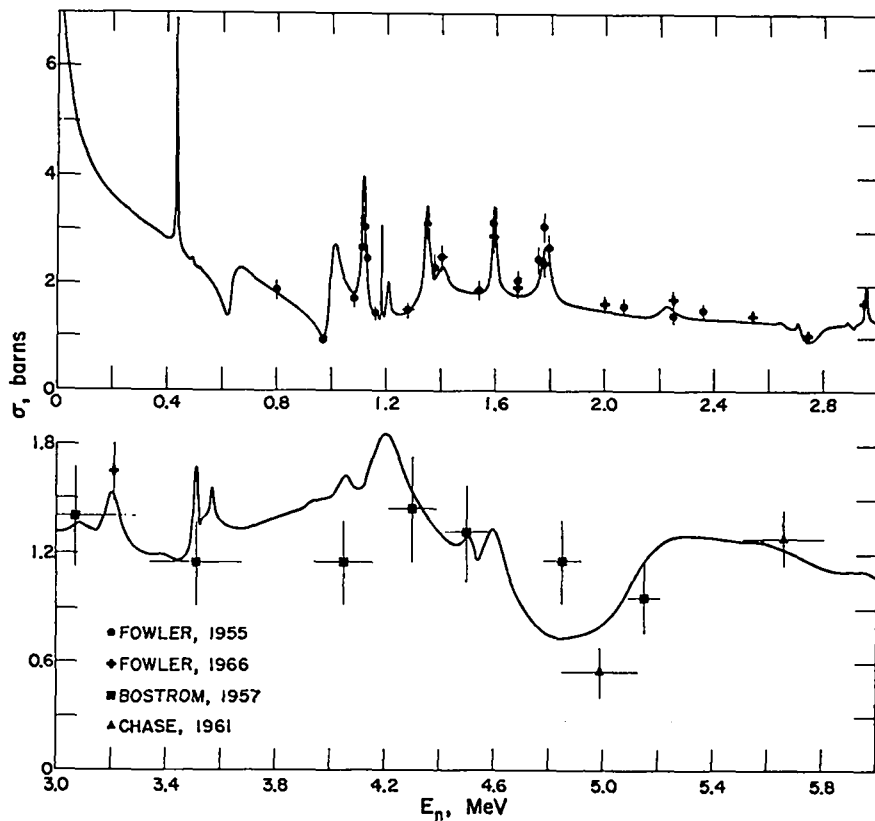
Fig. 69. Measured and evaluated cross sections for elastic scattering between 10 keV and 6 MeV.

section determined by subtracting the nonelastic cross section from the total, which is how we obtained the evaluated curve, lies roughly 200 mb above the elastic measurements by Bauer et al. (Ba67). At the time this evaluation was completed, the Nellis et al. (Ne71)[*] and Perey (Pe71) results shown in Fig. 70 were not available, and there was little evidence from elastic measurements to support the evaluated curve. Our decision to rely upon the evaluated non-elastic and total cross sections rather than the measurements by Bauer et al. (Ba67) was based mainly on two considerations. First, it was difficult to reconcile some of the Bauer results at small angles with Wick's limit (Wi43) for the minimum possible elastic cross section at a scattering angle of 0°. This problem was made more severe by preliminary results from small-angle scattering measurements at Edgewood (Bu71a) which indicated that the zero-degree elastic cross section near 8 MeV was substantially higher than Wick's limit. Second, with our choice of the elastic cross section it was necessary to assume that only one measurement, the Bauer (Ba67) elastic-scattering data, was wrong. If we assumed that the error was in the (n,n') or (n,α) channels,

the cross section from one of these channels would have to be doubled or the contribution from both reactions would have to be increased 50% to account for the "missing" 200 mb. This would require assuming substantial errors in several measurements (see Sec. 3.3.1 and 3.7).

The new results by Perey and Kinney (Pe71) and Nellis et al. (Ne71) given in Fig. 70 support our choice for the elastic cross section. Although there is still a possibility of errors in this energy region, particularly from unknown structure in the cross sections, the situation has been greatly clarified by the new measurements, and the evaluated curve appears a reasonable choice for the elastic cross section at these energies.

We based the elastic cross section near 14 MeV upon a composite of the available elastic measurements, although the measurement by Bauer et al. (Ba63) was weighted heavily in the decision, together with the knowledge that Anderson and McClure's (n,n') measurements (An64) and the nonelastic measurements by Flerov and Talyzin (Fl58) and Degtyarev (De65) suggest a somewhat lower elastic cross section than is indicated by some of the elastic measurements. The extension of the elastic cross section from 14 to 20 MeV is based upon relative[*] measurements

[*] The preliminary values from the Nellis experiment, which were available for the evaluation, were some 15% lower than the final results given in Fig. 70.

[*] These results are given in Fig. 70 with the same normalization used by Boreli et al. (Bo68).

Fig. 70. Measured and evaluated elastic scattering cross sections from 6 to 20 MeV. The data of Perey (Pe71) and the revised results of Nellis (Ne71) became available after our evaluation (shown by the solid line) was completed.

by Boreli et al. (Bo68). The evaluated elastic and
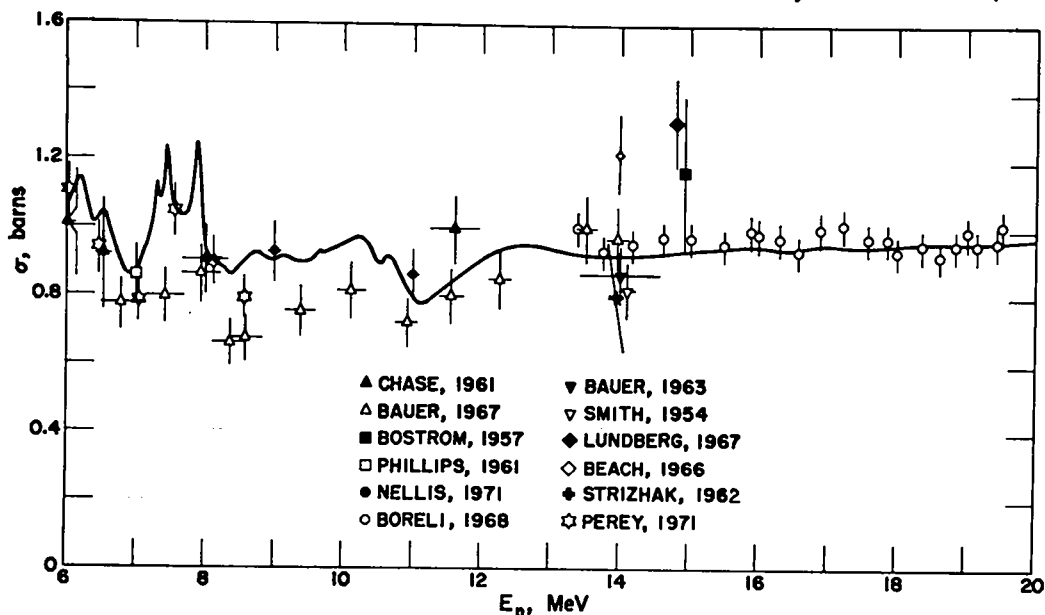total cross sections at 19.8 MeV result in an eval-
uated nonelastic cross section of 0.58 barns, as
compared to Degtyarev's measurement of 0.69 ± 0.05
barns (De65).

4. NEUTRON ANGULAR DISTRIBUTIONS

4.1 Elastic-Scattering Angular Distributions

4.1.1 Elastic Angular Distributions for $E_n < 8$ MeV

We determined the elastic-scattering angular
distributions at neutron energies below 8 MeV from
a resonance-theory analysis that incorporated the
resonance energies and total widths from our analy-
sis of the total cross section and reaction widths
from our analysis of the partial cross sections.
With the resonance parameters fixed, the $\ell = 0$ and
$\ell = 1$ potential phase shifts were obtained by fit-
ting the available angular distribution measurements.
We then constructed the final evaluated angular dis-
tributions from a smooth curve through the fitted
potential phase shifts.

Our resonance-theory parameterization is based
upon the single-level R-matrix treatment by Lane and
Thomas (La58) and is given explicitly in Appendix B.
The expressions used to calculate the differential
cross sections, constructed from the general equa-
tions given by Blatt and Biedenharn (Bl52a), do not
contain terms due to $s \neq s'$ or $\ell \neq \ell'$, where s and
s' are the incoming and outgoing channel spins and
ℓ and ℓ' are the incoming and outgoing orbital angu-
lar momenta. Both these approximations were made
to limit the number of phase shifts. The resulting
expressions, which in general still contain six
phase shifts per ℓ value, adequately describe the
available elastic angular-distribution measurements.

The calculations were carried out on LASL CDC
6600 computers using a locally written least-squares
fitting subroutine (An70). The resonance parameters
were entered as fixed input for each partial wave,
and the s- and p-wave potential phase shifts were
obtained by fitting angular-distribution measure-
ments by Fowler (Fo55, Fo66), Bostrom (Bo57), Chase
(Ch61), and Bauer (Ba67). The d- and f-wave poten-
tial phase shifts were set equal to hard-sphere
values calculated as described in Appendix B. This
approximation was checked by fitting several distri-
butions near 8 MeV with $\ell = 0$, 1, and 2 potential

phase shifts; the resulting d-wave values are small
and in reasonable agreement with the hard-sphere
calculations.

We included a total of 33 resonances in the an-
alysis. The resonance parameters used are given in
Table IX. The quantity E_R is the resonant energy
in the laboratory system, Γ is the total width of
the resonances in the center-of-mass system, and E_x
is the center-of-mass excitation energy in ^{15}N cor-
responding to E_R. We obtained the parameters E_R
and Γ mainly by fitting the resonances in the total
cross section with Breit-Wigner shapes above straight-
line backgrounds. Exceptions are the parameters of
the 0.647- and 0.996-MeV s-wave resonances which we
obtained from Ajzenberg-Selove's compilation (Aj70).
We assumed a radius of 5.1×10^{-13} cm for the s-wave
resonances, and used radii of 3.6×10^{-13} cm for all
higher waves. We selected the larger value for the
s-wave radius so that the calculated hard-sphere
phase shifts at lower energy roughly agreed with
the fitted potential phase shifts.

The ratios of the neutron width to the total
width (Γ_n/Γ) for the various resonances are based
upon several considerations. We estimated this
ratio for many of the resonances by comparing the
areas under the resonance peaks in the (n,p) and
(n,α) cross sections to the areas under the peaks
in the total cross section. We also obtained infor-
mation on Γ_n/Γ from Ajzenberg-Selove's compilation
(Aj70). The change in total cross section ($\Delta\sigma_T$)
over a resonance is also related to Γ_n/Γ through the
expression (Wi63)

$$\Delta\sigma_T = \frac{2\pi \, \lambdabar^2}{3} \quad (2J + 1) \quad \frac{\Gamma_n}{\Gamma} \quad ,$$

where J is the total angular momentum of the reso-
nance and $\lambdabar$ is the reduced wavelength for the inci-
dent neutron beam. Where Γ_n/Γ was uncertain, we
chose the ratio to be consistent with the angular
momentum of the resonance and with the measured
value of $\Delta\sigma_T$. Often, the reverse situation occurred,
and we chose the unknown spin J to be consistent with
the available information on Γ_n/Γ.

We took the spins and parities for many of the
resonances below 3 MeV from an analysis like ours
performed by Fowler and Johnson (Fo55) or from
Ajzenberg-Selove's compilation (Aj70). Sometimes,

TABLE IX

NITROGEN RESONANCE PARAMETERS

E_R (MeV)	E_X (MeV)	J^π	Resonant Phase Shift	Γ (MeV)	Γ_n/Γ
0.4336	11.239	$3/2^-$	$^2P_{3/2}$	0.0051	1.0
0.4926	11.294	$1/2^-$	$^2P_{1/2}$	0.0087	0.29
0.647	11.438	$1/2^+$	$^2S_{1/2}$	0.041	0.70
0.996	11.764	$3/2^+$	$^4S_{3/2}$	0.040	0.95
1.1164	11.876	$5/2^-$	$^4P_{5/2}$	0.0159	0.99
1.1840	11.939	$3/2^+$	$^2D_{3/2}$	0.0019	1.0
1.2090	11.963	$1/2^-$	$^4P_{1/2}$	0.0146	0.99
1.3490	12.093	$5/2^+$	$^4D_{5/2}$	0.0173	0.92
1.406	12.146	$3/2^-$	$^4P_{3/2}$	0.044	0.61
1.5974	12.325	$5/2^-$	$^4P_{5/2}$	0.0172	0.99
1.784	12.499	$5/2^+$	$^2D_{5/2}$	0.041	0.85
2.229	12.914	$1/2^-$	$^2P_{1/2}$	0.070	0.70
2.5105	13.177	$9/2^-$	$^4F_{9/2}$	0.0038	0.15
2.7081	13.361	$1/2^+$	$^4D_{1/2}$	0.0164	0.50
2.75	13.40	$1/2^+$	$^2S_{1/2}$	0.075	0.50
2.9576	13.594	$7/2^+$	$^4D_{7/2}$	0.0116	0.84
3.087	13.714	$3/2^+$	$^4D_{3/2}$	0.032	0.25
3.205	13.824	$3/2^+$	$^2D_{3/2}$	0.064	0.78
3.5101	14.109	$7/2^+$	$^4D_{7/2}$	0.0219	0.74
3.5689	14.164	$7/2^-$	$^4F_{7/2}$	0.0143	0.40
4.055	14.617	$1/2^+$	$^2S_{1/2}$	0.059	0.60
4.195	14.748	$5/2^+$	$^4D_{5/2}$	0.183	0.8
4.515	15.046	$3/2^+$	$^4D_{3/2}$	0.072	0.7
4.599	15.125	$7/2^+$	$^4D_{7/2}$	0.112	0.8
4.85	15.36	$3/2^+$	$^4S_{3/2}$	0.32	1.0
5.10	15.59	$5/2^-$	$^4P_{5/2}$	0.18	0.8
5.572	16.032	$3/2^+$	$^2D_{3/2}$	0.071	0.3
5.965	16.399	$5/2^+$	$^4D_{5/2}$	0.112	0.3
6.198	16.616	$7/2^+$	$^4D_{7/2}$	0.192	0.4
6.550	16.945	$3/2^+$	$^4S_{3/2}$	0.207	0.55
7.295	17.640	$1/2^+$	$^4D_{1/2}$	0.041	0.7
7.437	17.772	$5/2^-$	$^2F_{5/2}$	0.122	0.8
7.883	18.188	$5/2^-$	$^4F_{5/2}$	0.149	0.9

however, we chose values in disagreement with one or both of these sources in order to produce better overall agreement with the estimates of $\Delta\sigma_T$ and with the angular-distribution measurements.

Very little is known about the spins and parities of resonances above 3 MeV in nitrogen, and all such values in Table IX are from our analysis. We made these assignments on the basis of $\Delta\sigma_T$ and the available angular-distribution measurements, requiring that the potential phase shifts vary smoothly with energy. For many resonances, however, there were no angular-distribution data or the resolution of the available measurement was too broad to be useful. Then we were forced to estimate the value of ℓ from the total width of the resonance, so uncertainties in most of the assignments above 3 MeV are fairly large. The actual fits to the experimental angular distributions, however, remain reasonably good out to 8 MeV.

The s- and p-wave potential phase shifts resulting from this analysis are given in Fig. 71. The angular-distribution measurements used in determining the various phase shifts are indicated by the different symbols. The Fowler (Fo55, Fo66) measurements were the only high-resolution data available for nitrogen.[*] From 3.5 to 5.5 MeV we encountered considerable difficulty in obtaining satisfactory <u>simultaneous</u> fits for the $\ell = 0$ and $\ell = 1$ phase shifts. Consequently, in this region we fitted the s-wave phase shifts to the measurements while holding the p-wave phase shifts fixed at the values given by the $\ell = 1$ curve.

The elastic-scattering angular distributions are represented in the evaluation with Legendre coefficients. The coefficients from 0 to 4 MeV are given in Fig. 72.[**] The values shown were calculated from the smooth curves through the fitted s- and

---

[*] Perey and Kinney (Pe71) have recently made new measurements with good resolution near 7 MeV.

[**] Throughout this evaluation the Legendre coefficients are given using the ENDF normalization so that $d\sigma/d\Omega =$

$$\frac{\sigma}{2\pi} \sum_{\ell=0}^{\ell_{max}} \frac{2\ell+1}{2} f_\ell P_\ell(\cos\theta), \text{ with } f_0 \equiv 1 \text{ and } |f_\ell| \leqslant 1.$$

p-wave potential phase shifts of Fig. 71. The ef-
fects of the many resonances in nitrogen below 4 MeV
are evident in the Legendre coefficients. The coef-
ficients from 4 to 8 MeV are included in Fig. 73.
Here, the coefficients vary more smoothly with energy,
although some structure is still present.

In Figs. 74-79 the evaluated elastic angular
distributions are compared to the experimental re-
sults used in obtaining the s- and p-wave potential
phase shifts. The solid curve given with each meas-
urement represents the evaluated shape averaged
over the energy resolution (assumed rectangular) of
the measurement and normalized to the experimental
data; the dashed curve represents the same shape
normalized to the evaluated elastic cross section,
also suitably corrected for the resolution of the
measurements. The arrows on the left-hand scale be-
low each curve indicate Wick's limit (Wi43) for the
minimum differential cross section at 0°. The values

for Wick's limit, which are based on the evaluated
total cross section, have also been averaged over
the quoted resolution of the measurements.

The elastic angular-distribution measurements
of Fowler (Fo55, Fo66) between 0.8 and 1.35 MeV are
compared to the evaluation in Fig. 74. The evaluated
and measured angular distributions agree well except
for the three distributions near the 1.1164-MeV reso-
nance. This disagreement occurs because of the J=5/2
assignment for this resonance, as much better fits
to the angular distribution can be obtained with
J=3/2, which is the assignment given by Fowler and
Johnson (Fo55). The change in Carlson and Cerbone's
total cross section (Ca70) over this resonance, how-
ever, is inconsistent with the J=3/2 assignment and
suggests $J \geqslant 5/2$, which is the basis for our assign-
ment. A possible explanation for the discrepancy
between the evaluated and experimental angular dis-
tributions might be that the energy spread in the
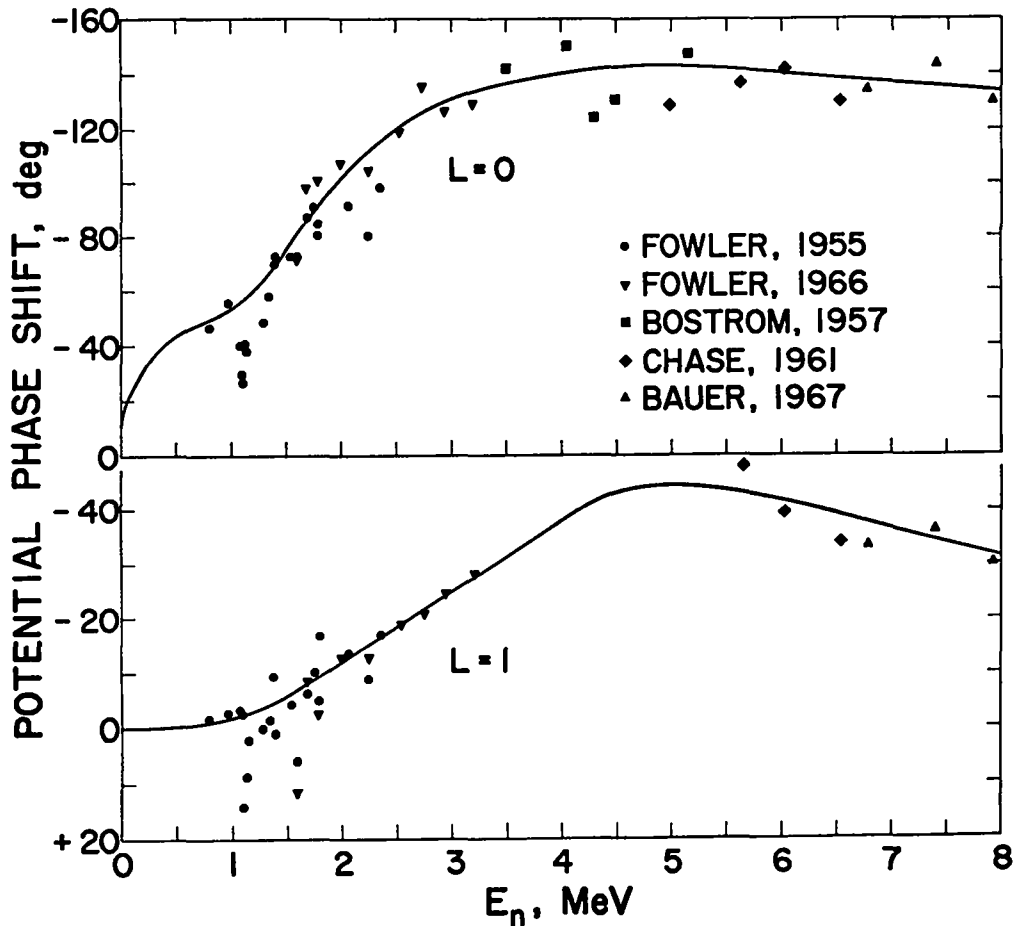
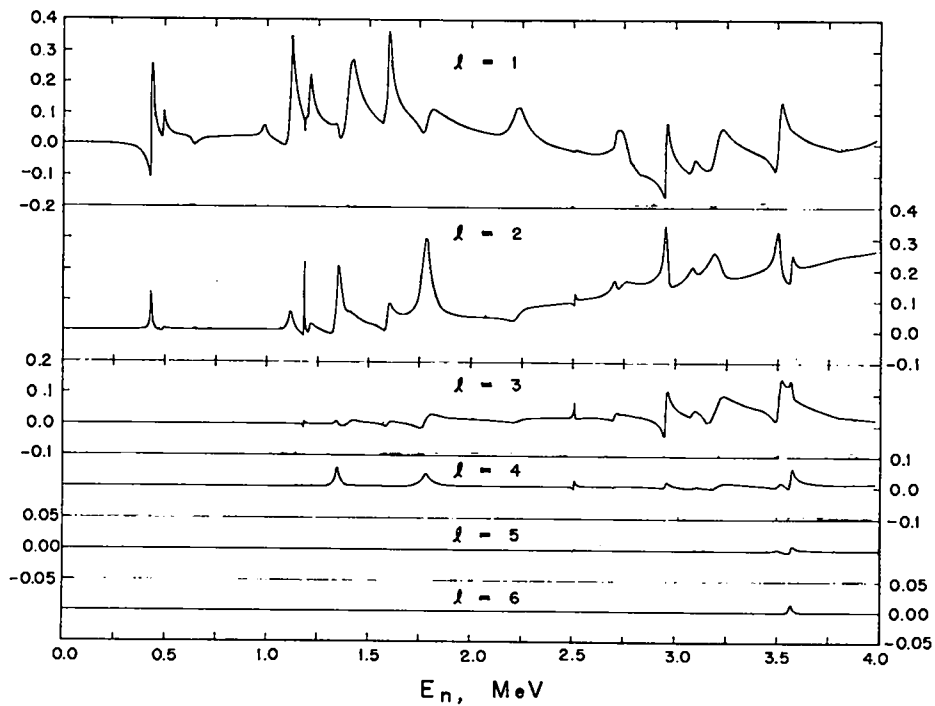Fig. 71. Potential-scattering phase shifts up to 8 MeV deduced from fits to elastic angular distributions.

Fig. 72. Legendre coefficients deduced using the phase shifts of Fig. 71 for elastic scattering below 4 MeV. The coefficients are normalized according to the ENDF/B definition.
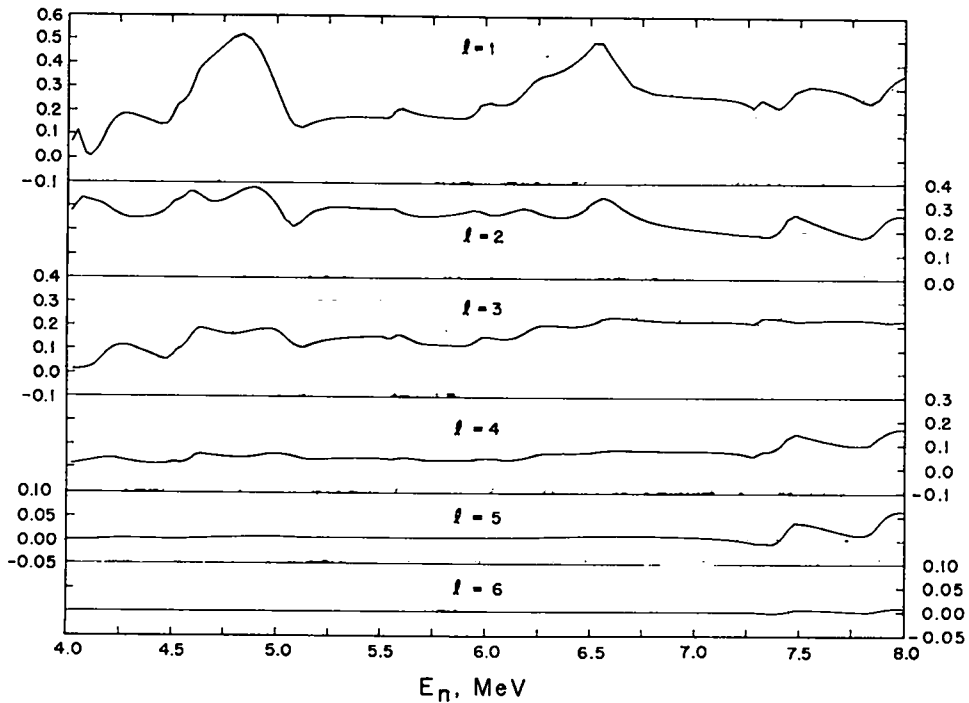

Fig. 73. Legendre coefficients deduced using the phase shifts of Fig. 71 for elastic scattering from 4 to 8 MeV. The coefficients follow the ENDF/B definition.
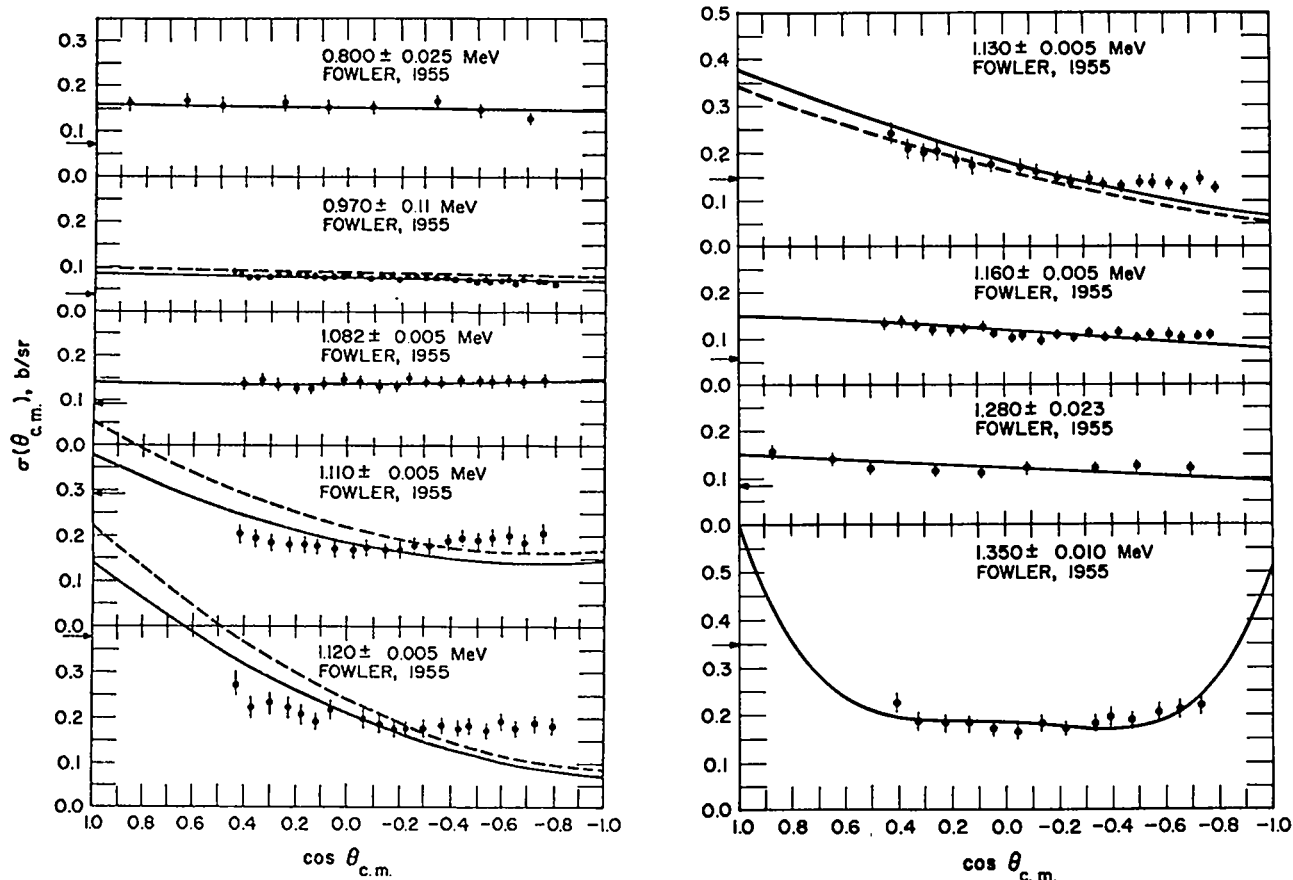
Fig. 74. Measured and evaluated differential cross sections for elastic scattering from nitrogen up to 1.35 MeV.

neutron beam used in the measurement was greater than realized.

The good agreement between the measurements at 0.97 and 1.35 MeV and the evaluated results in Fig. 74 supports the J^π assignments in Table IX for the 0.996- and 1.349-MeV resonances. The measurements in Fig. 74 provide no information on the resonances at 0.4336, 0.4926, 0.647, 1.184, and 1.209 MeV. Except for the 1.184-MeV resonance, we obtained the parameters in Table IX for these resonances from Ajzenberg-Selove's compilation (AJ70). The 1.184-MeV resonance was assumed to be d-wave from its narrow width, and the assignment J=3/2 is consistent with the observed $\Delta\sigma_T$ and $\Gamma_n/\Gamma=1$. However, because this resonance is very sharp (1.9-keV wide), it may have a substantial reaction width not observed in measurements and a higher value of J.

The evaluated results are compared in Fig. 75 to the Fowler measurements (Fo55, Fo66) between 1.377 and 1.756 MeV. The evaluated and measured shapes

agree well in this region and support the J^π assignments in Table IX for the 1.406- and 1.5974-MeV resonances.

The elastic measurements between 1.779 and 2.54 MeV are compared to the evaluated curves in Fig. 76. The comparisons for the 1.779-MeV measurements support the $5/2^+$ assignment for the 1.784-MeV resonance. Our choice of $J^\pi=1/2^-$ for the 2.229-MeV resonance disagrees with the Fowler (Fo55) assignment of $J^\pi=3/2^-$; in fact, there was little to choose between our $J^\pi=1/2^-$ and $J^\pi=3/2^-$ fits for the 2.25-MeV measurement, and the $3/2^-$ assignment is a suitable alternative. No information on the 2.5105-MeV level is provided by the measurements in Fig. 76, and our J^π assignment for this level is based on its narrow width and on the observed $\Delta\sigma_T$ together with our estimate of Γ_n/Γ.

Figure 77 includes the evaluated and experimental results between 2.742 and 4.30 MeV. Our assignments of $7/2^+$ for the 2.9576-MeV resonance and $3/2^+$ for the
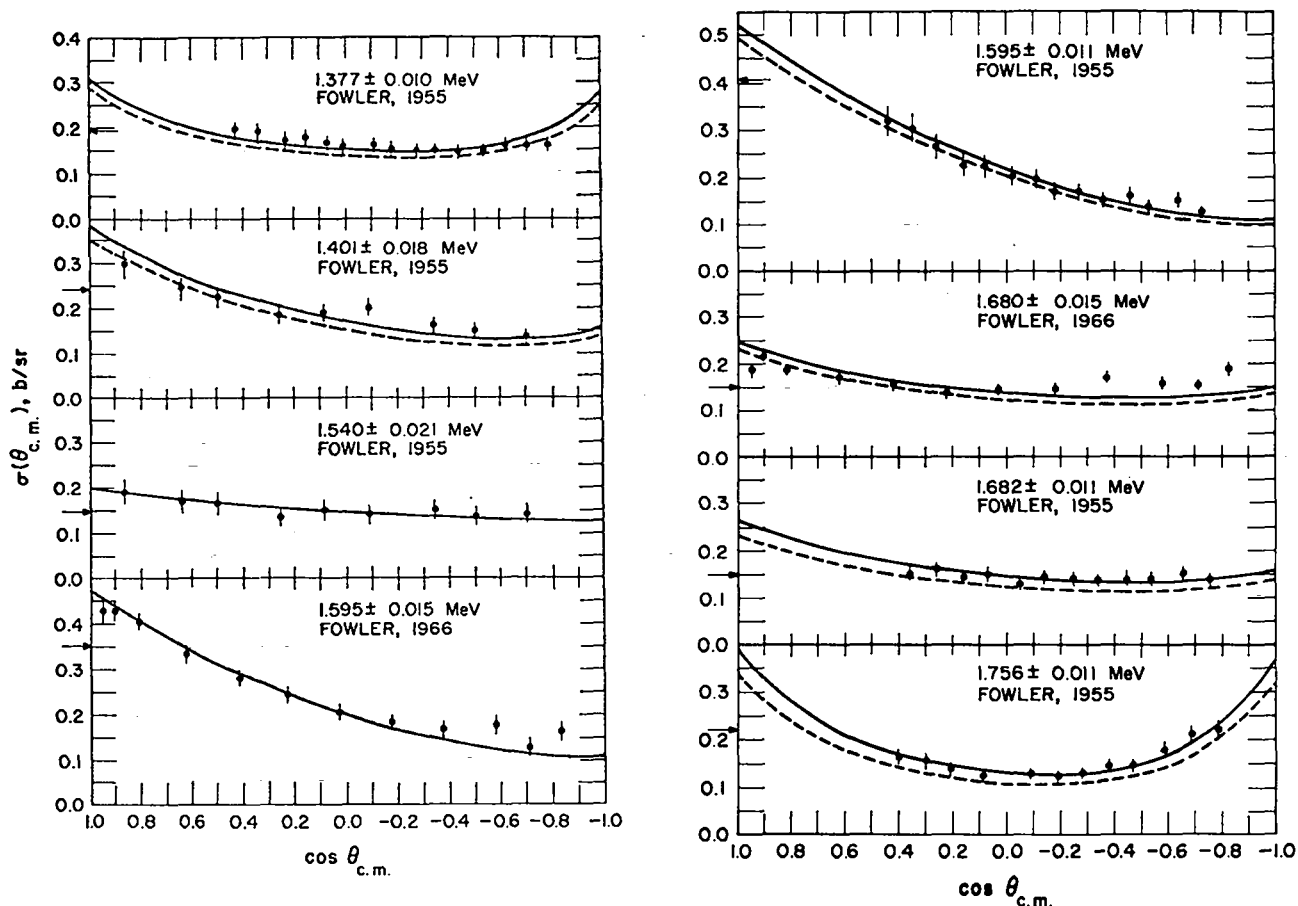
Fig. 75. Measured and evaluated differential cross sections for elastic scattering from 1.37 to 1.76 MeV.

3.205-MeV resonance are supported by the good agreement between the evaluation and the Fowler (Fo66) data at 2.95 and 3.207 MeV. The assignments for other resonances in this energy region are uncertain and are not discussed in detail. They are generally based upon estimates of $\Delta\sigma_T$ and Γ_n/Γ consistent with reasonable fits to the angular-distribution results. The large errors and energy spread in the Bostrom (Bo57) measurements make precise assignments difficult.

The evaluated and experimental results for $E_n =$ 4.5 to 6.78 MeV are given in Fig. 78. Again, the precise J^π assignments in this region are uncertain and are not discussed in detail. The general d-wave character of the resonances here seems to be supported by the measurements, particularly above 5.5 MeV.

Finally, the elastic angular distribution results between 7.11 and 7.93 MeV are given in Fig. 79. Bauer's measurements at 7.41 and 7.93 MeV are a little difficult to reconcile with Wick's limit, and we included artificial points at 0° in fitting potential

phase shifts to these data. The dashed curves in Fig. 79 (and Fig. 78) indicate the significant renormalizations used in the evaluation at these energies.

4.1.2 Elastic Angular Distribution for $E_n > 8$ MeV

We obtained the elastic angular distributions above 8 MeV by fitting the available measurements with Legendre expansions and then drawing smooth curves through the fitted Legendre coefficients. We augmented the experimental data with several fictitious points to anchor the fits at front and back angles. We estimated the supplementary points used near 180° (usually just one point per distribution) from optical-model fits to the measurements. At forward angles, we anchored the fits by a single point at 0° based upon Wick's (Wi43) limit, $\sigma_w(0°)$, which was varied from $(1.4\pm0.2)\sigma_w(0°)$ between 7 and 11 MeV to $(1.05\pm0.05)\sigma_w(0°)$ near 14 MeV. We included the indicated standard deviations with the 0° points so that the fitted 0° cross sections were not dictated by the fictitious points but were strongly influenced by them. Our decision to use values greater
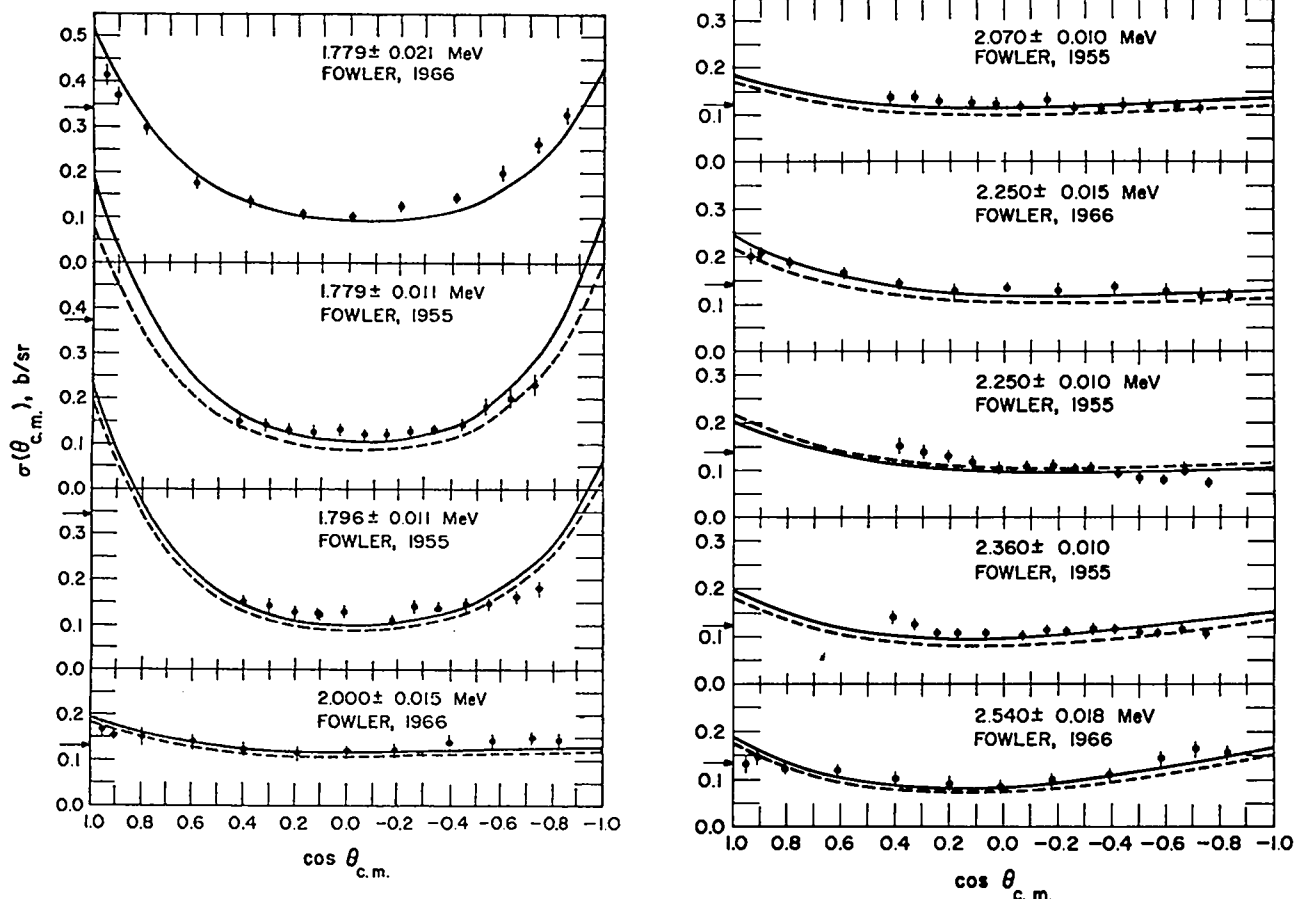
49

Fig. 76. Measured and evaluated differential cross sections for elastic scattering from 1.78 to 2.54 MeV.

than Wick's limit at 0° was based upon preliminary information from Edgewood Arsenal, where measurements of elastic scattering at very small angles (2.5-15°) were in progress. The final results (Bu71a) of this experiment indicate that the 0° cross sections for nitrogen at 7.55±0.06 MeV and 9.50±0.05 MeV are 40 and 20% greater than Wick's limit, respectively. The evaluated cross sections at 0° agree with the final Edgewood results to within about 10%.

The Legendre coefficients from 8 to 20 MeV that resulted from this analysis are smooth functions of energy and are shown in Fig. 80. We based the extrapolation of the curves from 15 to 20 MeV upon optical-model calculations using parameters obtained from the 14-MeV measurements by Bauer et al. (Ba63). We adjusted the coefficients to produce agreement with Wick's limit at all energies.

The elastic angular-distribution measurements between 8.0 and 10.1 MeV are compared to the evaluated curves in Fig. 81. The inclusion of the points at 0° tended to "stretch" the shape obtained from

the Bauer (Ba67) results at small angles. The Nellis results (Ne70) at 9 MeV are preliminary and have since been increased approximately 15% (Ne71) so that now they agree very well with the integrated elastic cross section used in the evaluation (see Fig. 70 of Sec. 3.10).

The elastic angular-distribution results from 10.93 to 13.5 MeV are included in Fig. 82. In this region the shapes of the Bauer (Ba67), Nellis (Ne70), and Chase (Ch61) measurements are quite consistent. The final Nellis results (Ne71) at 11 MeV are again roughly 15% higher than the data (Ne70) in Fig. 82.

Fig. 83 shows the angular-distribution results near 14 MeV. Wick's limit in this and subsequent figures is given by the intersection of the dashed line and the cross-section axis at 0°. At this energy we emphasized the 1963 measurement by Bauer et al. (Ba63) in the evaluation. The resulting shape agrees well with the 1967 Bauer results (Ba67) and the 1966 Beach measurement (Be66) but not with the Strizhak data (St62) or, to a lesser extent, the Lundberg
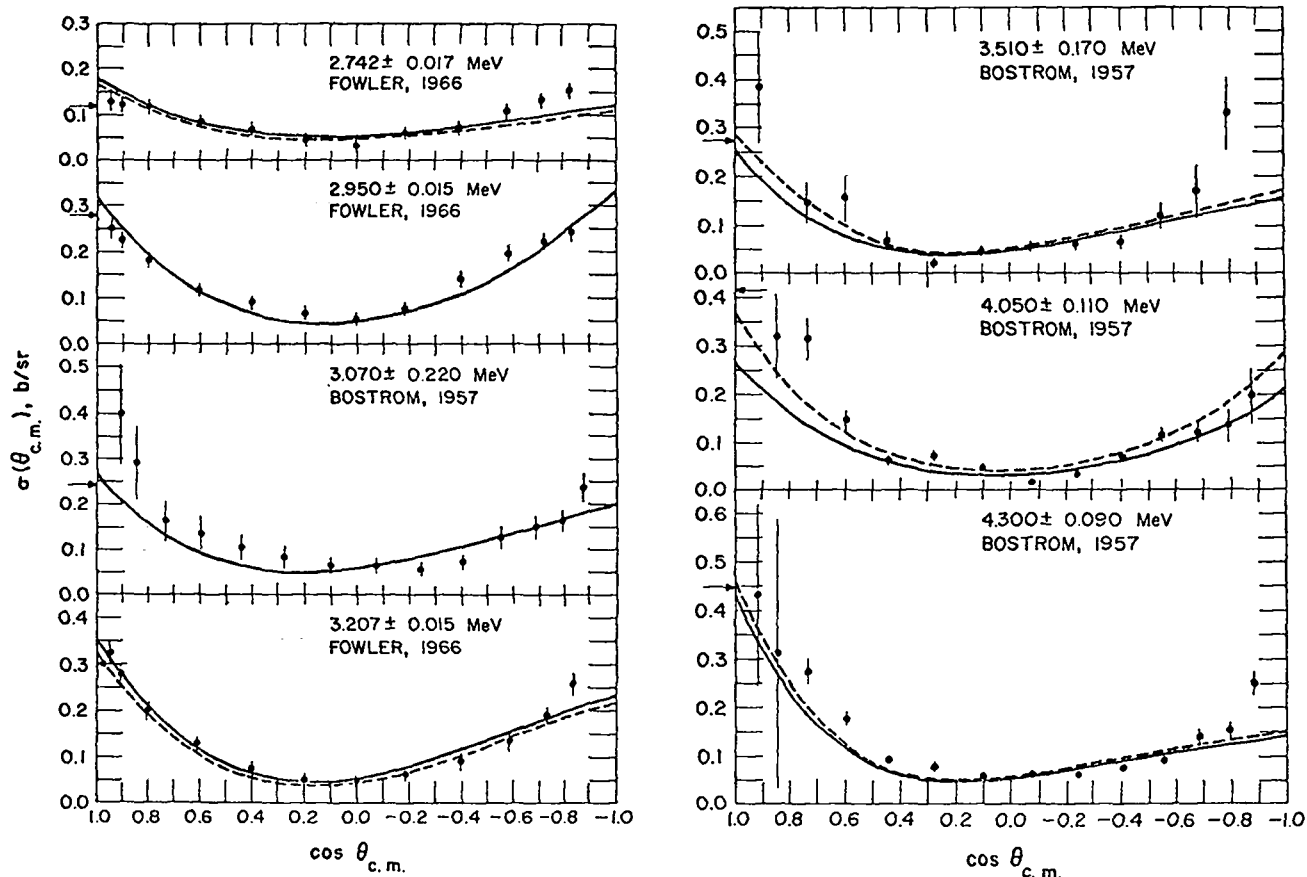
Fig. 77. Measured and evaluated differential cross sections for elastic scattering from 2.74 to 4.30 MeV.

result (Lu67) at 14.8 MeV. Further, a significant normalization difference between the evaluation and the Beach and Lundberg results is evident. The Bostrom measurements (Bo57) at 14.92 and 15.83 MeV given in Fig. 84 exhibit similar differences in shape and normalization; however, these results are not expected to be as accurate as more modern measurements.

Finally, the calculated differential cross sections at 16, 18, and 20 MeV are given in Fig. 85. These curves were extrapolated from the 14-Mev measurements using optical-model parameters, as noted above.

4.2 Inelastic Neutron Angular Distributions

The only direct measurements of ^{14}N (n,n') angular distributions available when this evaluation was completed were the 14-Mev results of Bauer et al. (Ba63) and Bobyr et al. (Bo62). Therefore, at most neutron energies we based our evaluated (n,n') angular distributions upon measured (p,p') angular distributions. The near-equality of (n,n') and (p,p') differential cross sections for charge-conjugate reactions has been pointed out by Lutz and Anderson (Lu66; also see An67) and is based upon the charge symmetry of the nuclear two-body force. This argument is expected to be valid for inelastic reactions to low-lying states, where the outgoing proton energy is high enough that Coulomb penetrability effects are small. The approximation is probably best at higher neutron energies where direct interactions are dominant.

We used the (p,p') measurements by Oda et al. (Od60), Donovan et al. (Do64), Freemantle (Fr54), and Hansen (Ha70) in the analysis. We did not incorporate the extensive (p,p') data by Boreli et al. (Bo68) in the study, but their results are qualitatively very similar to the measurements used. We determined the minimum odd number of coefficients required to produce a statistically acceptable fit to the (p,p') data for all levels below 8.5-MeV excitation in ^{14}N. We then plotted the resulting coefficients as a func-
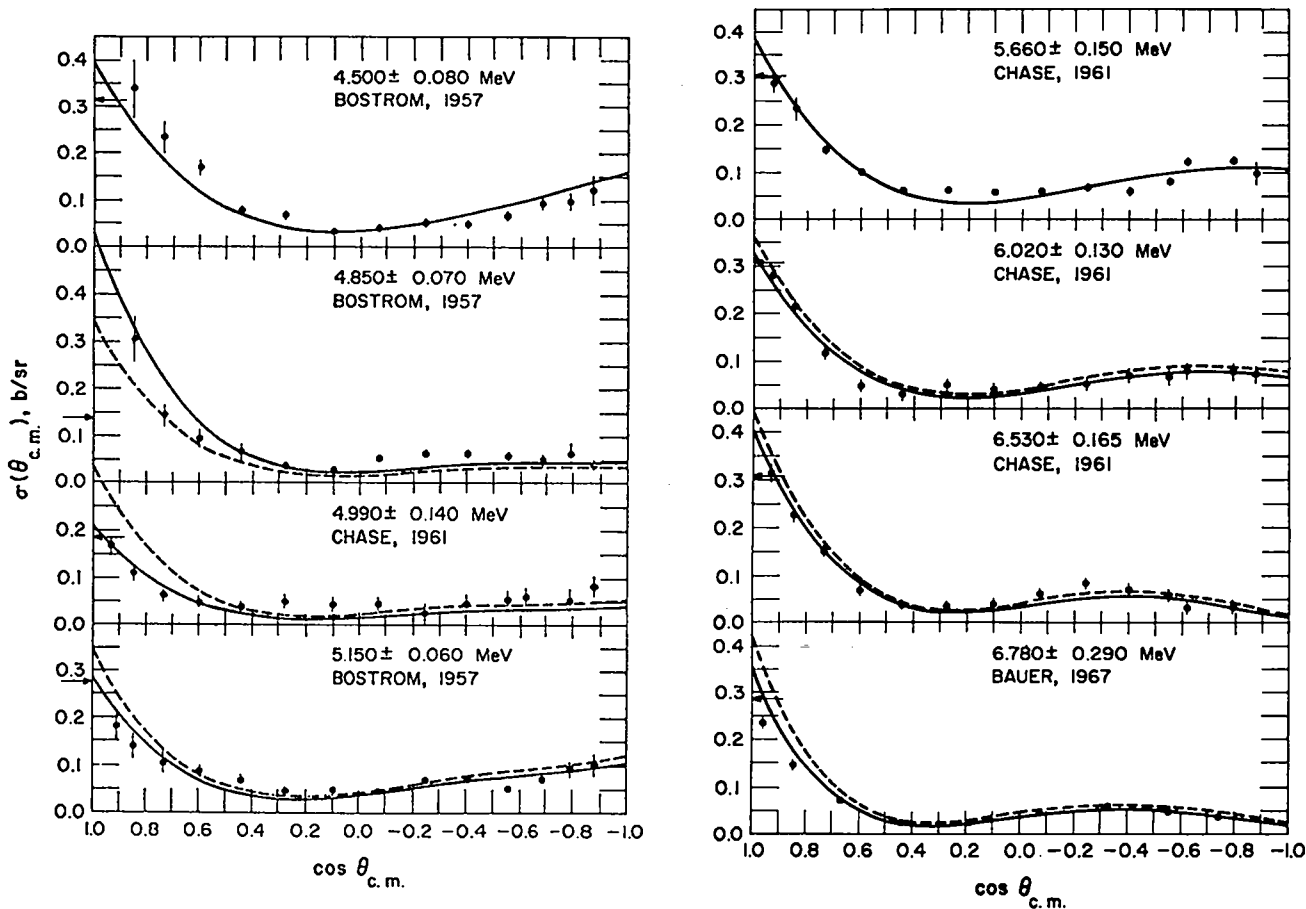
51

Fig. 78. Measured and evaluated differential cross sections for elastic scattering from 4.50 to 6.78 MeV.

tion of incident energy, and drew smooth curves through the points. Because there are no measurements below 7 MeV for any level and because the similarity between (n,n') and (p,p') cross sections is probably least at the lowest energies, we estimated the variation of the coefficients near threshold from Hauser-Feshbach calculations using an energy-dependent local optical model. The extrapolation of the coefficients from 15 to 20 MeV was also based partly on these calculations. The (p,p') data were insufficient to determine the cross section for the 8.061- and 8.589-MeV levels at back angles, so we assumed these angular distributions to be symmetric about 90°. We tested the smoothed coefficients at all incident energies to insure nonnegativity of the resulting angular distributions before adopting them in the evaluation.

The evaluated (n,n') angular distributions for the 2.313-MeV level of ^{14}N are compared in Fig. 86 to the (p,p') measurements upon which they are based. The solid curves are the evaluated shapes normalized

to the measurements; the dashed curves are the evaluated shapes normalized to our (n,n') cross sections and are shown only where the maximum difference occurred. The 14.15-MeV measurement by Bauer et al. (Ba63) is the only (n,n') experiment included in Fig. 86. The shape deduced from the (p,p') data of Oda et al. (Od60) at 14.10 MeV agrees nicely with the Bauer (n,n') measurement.

Similar results are given in Fig. 87 for the inelastic angular distributions to the 3.945-MeV level of [14]N. (The solid and dashed curves are as in Fig. 86.) Again, the shape of the angular distribution obtained from the 14.10-MeV (p,p') data of Oda et al. (Od60) agrees well with the (n,n') measurement by Bauer et al. (Ba63) at 14.15 MeV.

Complete graphs of the evaluated Legendre coefficients as functions of neutron energy are included in Appendix C for all states in ^{14}N below 8.5-MeV excitation energy. Sample angular distributions are also given for each level at various incident neutron energies. The angular distributions
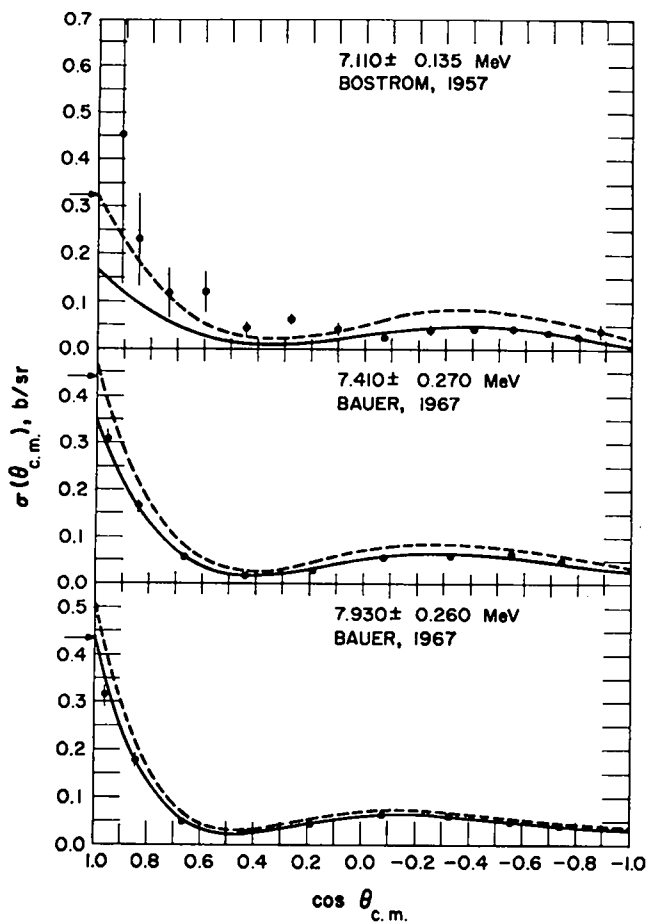
Fig. 79. Measured and evaluated differential cross sections for elastic scattering from 7.11 to 7.93 MeV.

Fig. 80. Legendre coefficients for elastic scattering from 8 to 20 MeV in the ENDF/B form.

Fig. 81. Measured and evaluated differential cross sections for elastic scattering from 8.00 to 10.1 MeV.
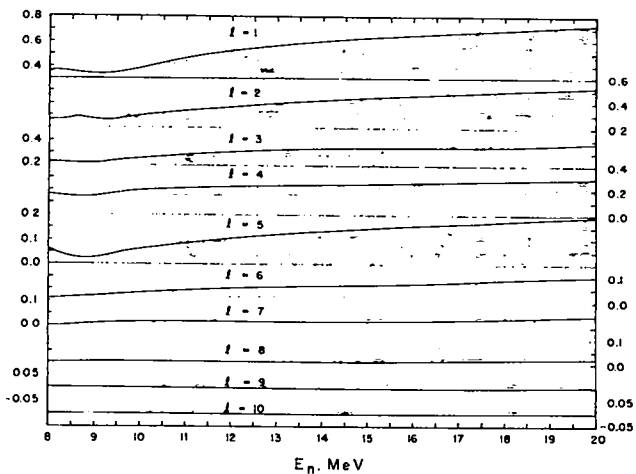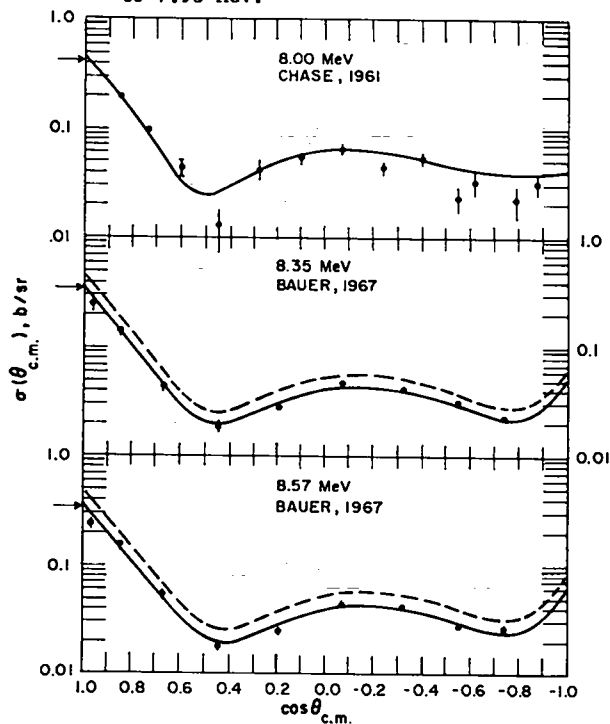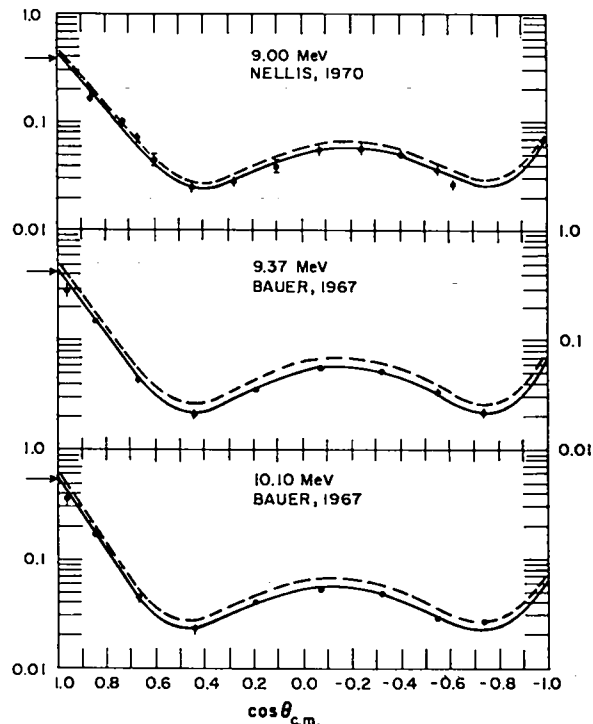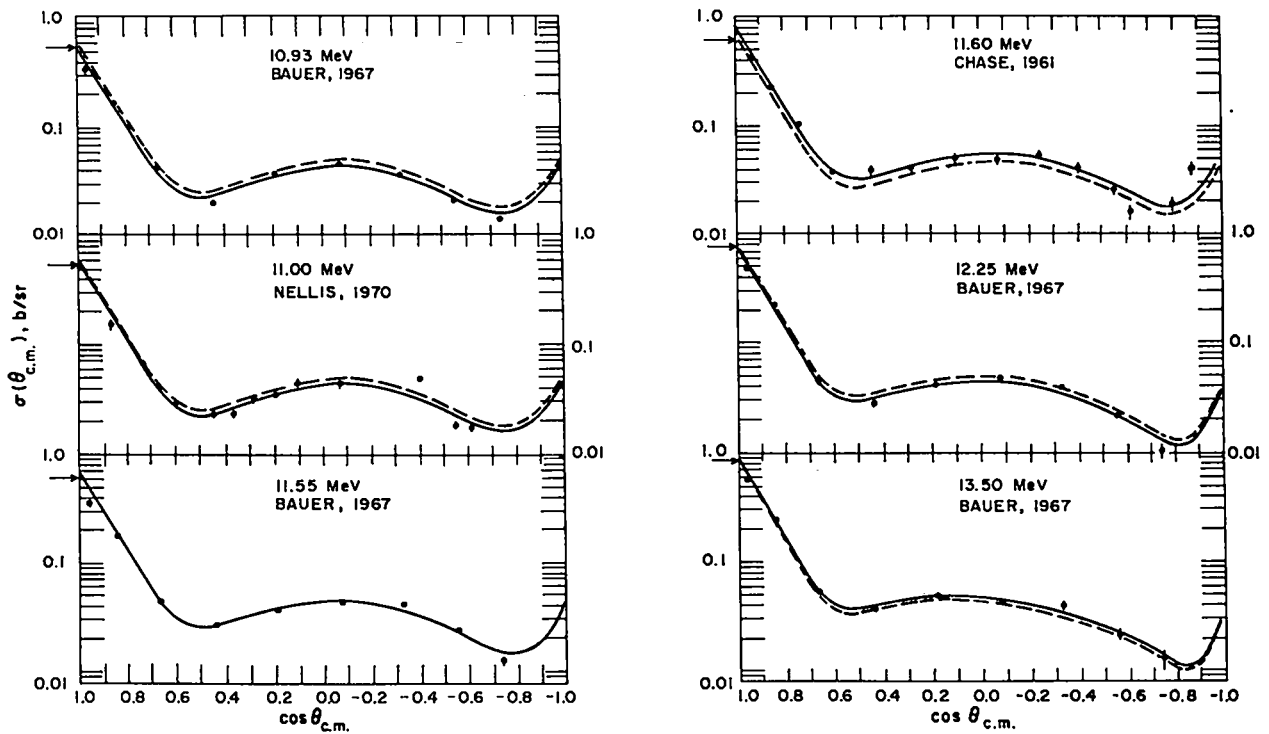
Fig. 82. Measured and evaluated differential cross sections for elastic scattering from 10.9 to 13.5 MeV.
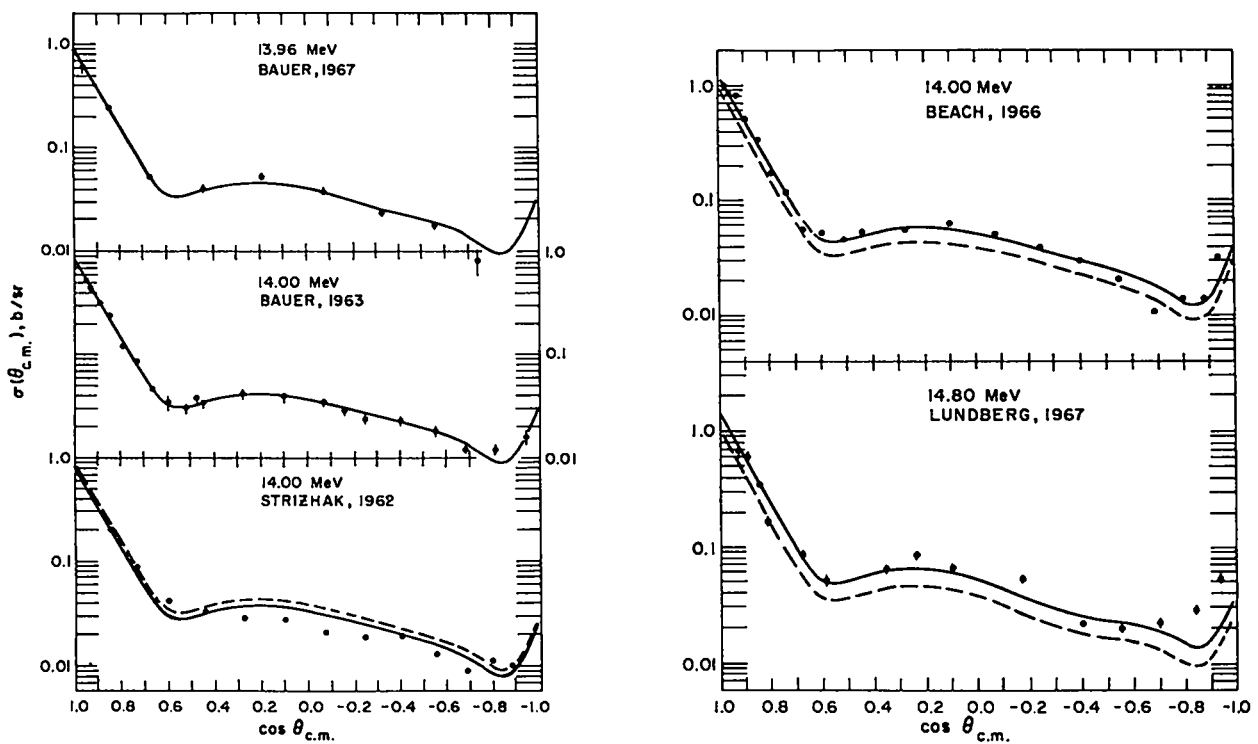

Fig. 83. Measured and evaluated differential cross sections for elastic scattering from 13.9 to 14.8 MeV.
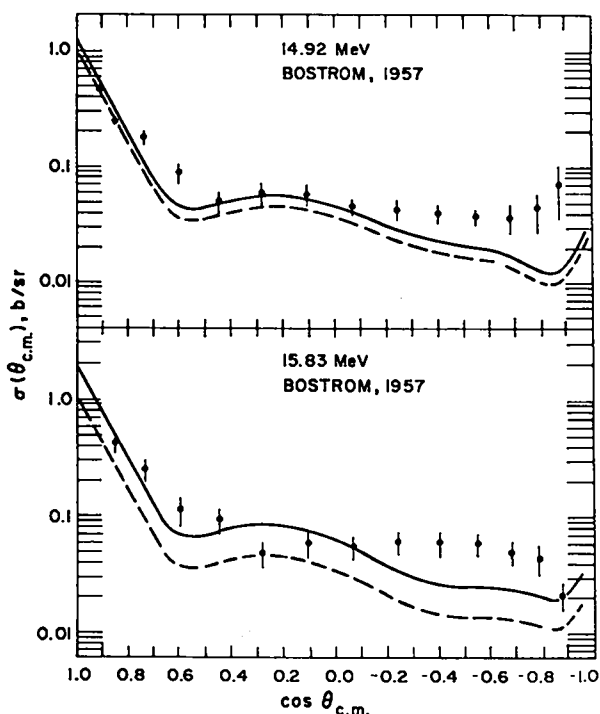
Fig. 84. Measured and evaluated differential cross
sections for elastic scattering at 14.92
and 15.83 MeV.

for all states with excitation energy higher than
8.5 MeV are assumed to be isotropic in the center-of-
mass reference system.

The excellent agreement between the 14-MeV (p,p')
and (n,n') results should not be assumed necessarily
to hold true at lower energies, particularly within a
few MeV of the threshold for particular reactions.
The agreement between the integrated (p,p') cross
sections and the (n,n') cross sections deduced from
(n,n'γ) measurements is no better than semiquantita-
tive. Therefore, although we expect the evaluated
shapes to be reasonably good, calculations that de-
pend critically on the inelastic angular distribu-
tions below, say, 10 MeV should be treated with
some skepticism.

4.3 Angular Distributions for the ^{14}N(n,2n)^{13}N
Reaction

The cross section for the (n,2n) reaction is
small at all neutron energies (<12 mb), so no great
effort was expended in estimating the neutron angular
distribution from this reaction. We obtained the
evaluated angular distributions by simply integrating
the phase-space expression for the differential cross

section used in Sec. 3.9 over outgoing neutron energy.
The resulting average angular distribtuions are shown
in Fig. 88.

5. PHOTON ANGULAR DISTRIBUTIONS

The thermal-capture gamma rays from the ^{14}N
(n,γ)^{15}N reaction are assumed to have isotropic angu-
lar distributions. This should be a good approxima-
tion as the first p-wave resonance does not occur
until 434 keV, and s-wave capture must be dominant
at lower energies. The single ground-state transi-
tion from the ^{14}N(n,γ) reaction in the MeV region is
given the same highly anisotropic angular distribu-
tion observed by Kuan et al. (Ku70) for the ^{14}N(p,γ)
reaction, with an appropriate adjustment of the en-
ergy scale as described in Sec. 3.2.

The only available measurements of gamma-ray
angular distributions from (n,xγ) reactions at more
than two angles are the results of Morgan et al.
(Mo64) at 14.8 MeV. These measurements indicate
that most of the angular distributions are essen-
tially isotropic, and the only anisotropic distri-
butions entered into the evaluated files were for
the 1.632- and 4.913-MeV gamma rays from the (n,n'γ)
reaction and for the 3.854-MeV gamma ray from the
(n,dγ) reaction. We obtained the evaluated angular
distributions by fitting the 14.8-MeV measurements
with even-order Legendre coefficients and then allow-
ing the evaluated coefficients to vary linearly from
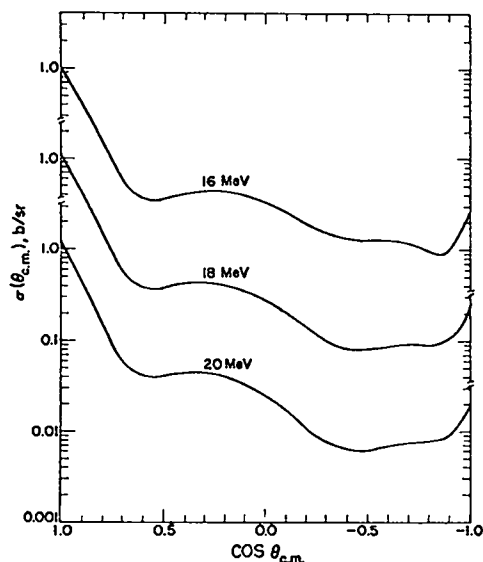
Fig. 85. Differential cross sections for elastic
scattering between 16 and 20 MeV, calcu-
lated from an optical model fitted to the
14-MeV data.
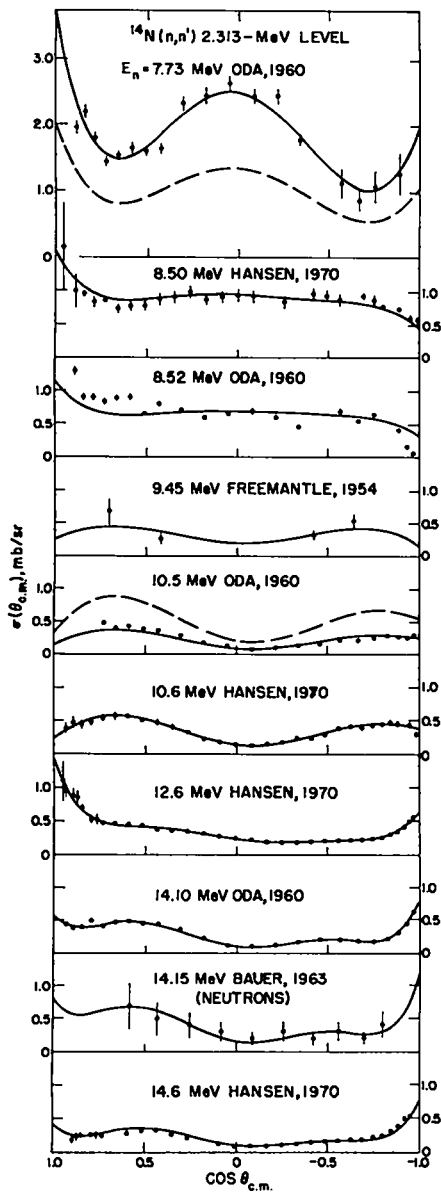
Fig. 86. Comparison of the evaluated (n,n') angular
distributions for the 2.313-MeV level in
^{14}N to the (p,p') measurements on which
they are based. A single (n,n') measure-
ment at 14.15 MeV is included.
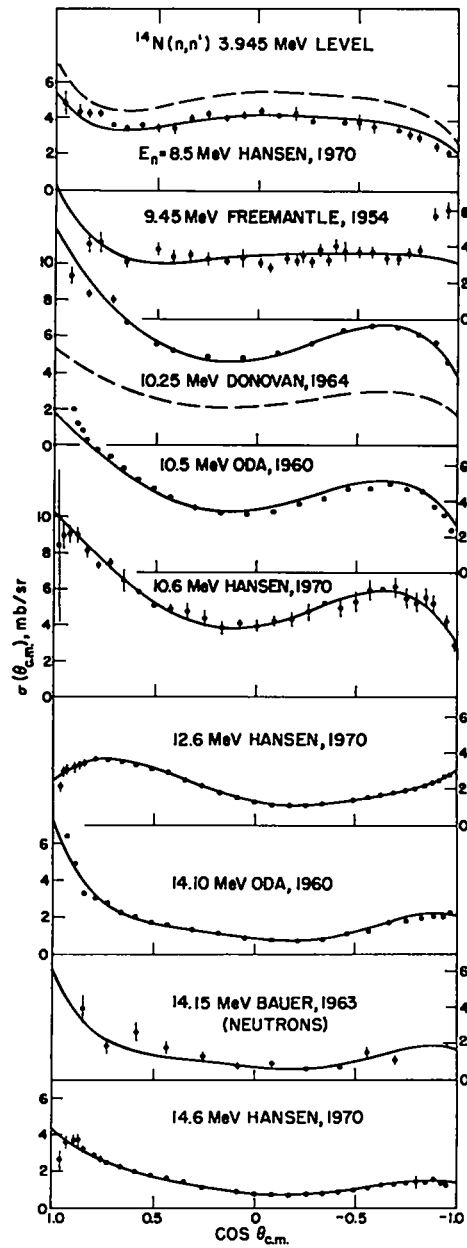
Fig. 87. Evaluated angular distributions for in-
elastic scattering to the 3.945-MeV level
in ^{14}N, compared to the (p,p') measure-
ments on which they are based. A single
(n,n') measurement at 14.15 MeV is in-
cluded.

ANGULAR DISTRIBUTION
$^{14}N(n,2n)^{13}N_{G.S.}$
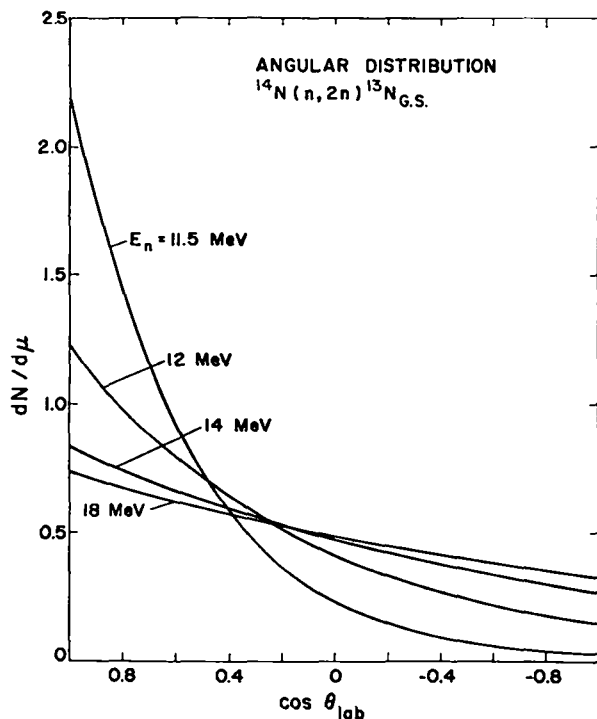
Fig. 88. Evaluated laboratory angular distributions for the (n,2n) reaction. The curves are normalized to unit area and averaged over outgoing neutron energy, as described in the text.

zero at threshold up to the measured value at 14.8 MeV. At higher energies the coefficients are held constant at the 14.8-MeV values. The ratio of $\sigma(0°)/\sigma(90°)$ for the three anisotropic photons is approximately 1.3 at 14.8 MeV. The new TNC compilation (Bu71), which supersedes the Morgan et al. (Mo64) results, states that all gamma rays at 14.8 MeV are isotropic to within 10%.

The (n,xγ) measurements made by Dickens and Perey (Di69), which include data at 55° and 90°, provide further information on the anisotropies in the photon angular distributions. These results are generally consistent with the assumption that the anisotropy in the angular distributions is small, although there are occasional exceptions. A better set of evaluated angular distributions could probably be obtained by a theoretical analysis, but we did not attempt such a study in this evaluation.

6. DISCUSSION

While preparing this report, we have found several areas where the evaluation might be improved. The most obvious possibilities for improvement come from the new measurements (Bu71a, Ne71, Pe71, Yo69)

that were unavailable for the evaluation. Although these measurements generally agree with our results, some improvement could be made by their inclusion. A second area that might be improved is the theoretical calculations used in the evaluation. Specifically, all the partial cross sections above 15 MeV and perhaps some at lower energies could be estimated better with recently improved nuclear-theory codes. Similarly, our estimates of the (n,n'pγ) and (n,n'dγ) cross sections could be improved by better calculations, and a more-complete resonance-theory analysis might be made, although significant improvement in the elastic angular distributions would probably require additional information on states in ^{15}N. Finally, the angular distributions of photons from (n,xγ) reactions could be estimated better using existing theories.

It is useful in many practical applications to be able to estimate the effects of uncertainty in nuclear data on measurements or calculations of various quantities. As an aid to such estimates, we have summarized in Table X the uncertainties associated with most of the cross sections evaluated for nitrogen at several selected neutron energies. Note that these are semiquantitative estimates that are not expected to hold true in great detail. Further, the errors are averaged over the structure in the cross section, and no allowance for the effect of unknown structure is included. Where possible, the uncertainties are based on quoted errors in the experimental measurements, although in several instances we have modified the original estimates. The errors near threshold for the negative-Q reactions are much larger than those given in Table X.

The evaluated elastic angular distributions are expected to have relative errors of the order of 10%. The inelastic angular distributions are substantially less well known, and their accuracy is difficult to estimate. Above 10 MeV the distributions probably have relative errors of about 20%, and at lower energies the accuracy is undoubtedly worse. For the thermal (n,γ) photon spectrum, we estimate the relative error for the strong lines to be about 5%, rising to ~ 20% for moderately weak lines and a factor of 2 for the very weak lines.

TABLE X

ESTIMATED ERRORS IN THE EVALUATED NITROGEN CROSS SECTIONS

Cross Section	ENDF/B Designation	10^{-5} eV	Thermal	0.1 MeV	1 MeV	2 MeV	5 MeV	8 MeV	11 MeV	14 MeV	20 MeV
Total	MF=3,MT=1	±8%	±3%	±3%	±1%	±1%	±1%	±1%	±1%	±1%	±1%
Elastic	MF=3,MT=2	3%	3%	3%	1%	1%	10%	10%	15%	10%	12%
Nonelastic	MF=3,MT=3	5%	5%	30%	30%	30%	30%	20%	20%	15%	20%
Total (n,n')	MF=3,MT=4	-	-	-	-	-	30%	20%	20%	20%	25%
Discrete (n,n') $E_x(^{14}N)<8.5$ MeV	MF=3 MT=51-62	-	-	-	-	-	30%	Strong levels 15% Weak levels 30%	Strong levels 15% Weak levels 30%	Strong levels 15% Weak levels 30%	Factor of 2
Discrete (n,n') $E_x(^{14}N)>8.5$ MeV	MF=3 MT=63-82	-	-	-	-	-	-	-	50%	50%	50%
(n,γ)	MF=3,MT=102	10%	10%	Factor of 4	Factor of 4	Factor of 4	Factor of 2	Factor of 2	Factor of 2	Factor of 2	Factor of 2
Total (n,p), (n,d) and (n,t)	MF=3 MT-103,104,105	5%	5%	30%	30%	30%	30%	40%	40%	30%	Factor of 2
Total (n,α)	MF=3,MT=107	-	-	-	-	40%	30%	30%	30%	30%	Factor of 2
(n,2α)	MT=3,MT=108	-	-	-	-	-	-	-	-	50%	50%
(n,2n)	MF=3,MT=16	-	-	-	-	-	-	-	-	20%	20%
Total (n,xγ)	MF=13 Sum of MT=4, 103-107	-	-	-	-	-	30%	20%	20%	20%	25%
Individual (n,xγ) lines	MF=13 MT=4, 103-107	-	-	-	-	-	30%	Strong levels 15% Weak levels 30%	Strong levels 15% Weak levels 30%	Strong levels 15% Weak levels 30%	Factor of 2

REFERENCES

AJ68   F. Ajzenberg-Selove and T. Lauritsen, "Energy Levels of Light Nuclei (VII). A=11-12," Nucl. Phys. A114, 1 (1968).

AJ70   F. Ajzenberg-Selove, "Energy Levels of Light Nuclei A=13-15," Nucl. Phys. A152, 1 (1970).

Al66   D. E. Alburger, A. Gallmann, J. B. Nelson, J. T. Sample, and E. K. Warburton, "Properties of Excited States in C^{14}," Phys. Rev. 148, 1050 (1966).

An64   J. D. Anderson and J. W. McClure, "Inelastic Scattering of 14 MeV Neutrons from Nitrogen," WASH-1048, p. 48 (1964).

An67   J. D. Anderson, C. Wong, and V. A. Madsen, "Application of Charge Independence to Neutron Inelastic Scattering," Lawrence Livermore Laboratory report UCRL-50197 (1967).

An70   W. Anderson, private communication (1970).

As58   V. J. Ashby, H. C. Catron, L. L. Newkirk, and C. J. Taylor, "Absolute Measurement of (n,2n) Cross Sections at 14.1 MeV," Phys. Rev. 111, 616 (1958).

Au62   E. H. Auerbach, "Abacus-2 (Revised Version)," Brookhaven National Laboratory report BNL-6562 (1962).

Ba49   R. Batchelor and B. H. Flowers, "Thermal Neutron Capture in Nitrogen," Harwell Laboratory report AERE-N/R-370 (1949).

Ba57   G. A. Bartholomew and P. J. Campion, "Neutron Capture Gamma Rays from Lithium, Boron, and Nitrogen," Can. J. Phys. 35, 1347 (1957).

Ba63   R. W. Bauer, J. D. Anderson, and L. J. Christensen, "Scattering of 14 MeV Neutrons from Nitrogen and Oxygen," Nucl. Phys. 47, 241 (1963).

Ba67 R. W. Bauer, J. D. Anderson, H. F. Lutz, C. Wong, J. W. McClure, and B. A. Pohl, "Elastic Scattering for 7 to 14 MeV Neutrons from Nitrogen," Nucl. Phys. $\underline{A93}$, 673 (1967).

Ba68 R. Bachinger and M. Uhl, "Die Reaktion ^{14}N $(n,\alpha)^{11}B$ mit 14.1 MeV Neutronen," Nucl. Phys. $\underline{A116}$, 673 (1968).

Be56 R. L. Becker and H. H. Barschall, "Total Cross Sections of Light Elements for (α,n) Neutrons," Phys. Rev. $\underline{102}$, 1384 (1956).

Be63 R. E. Benenson and B. Yaramis, "$C^{13}(d,n)N^{14}$ and $O^{18}(d,n)F^{19}$ Differential Cross Sections at 3.9 MeV Bombarding Energy," Phys. Rev. $\underline{129}$, 720 (1963).

Be66 P. L. Beach, R. W. Finlay, R. D. Koshel, and R. L. Cassola, "Elastic Neutron Scattering from N, O, and Ar at 14.1 MeV," Bull. Am. Phys. Soc. $\underline{11}$, 471 (1966).

Be68 R. A. I. Bell, R. D. Gill, B. C. Robertson, J. S. Lopes, and H. J. Rose, "Electromagnetic Transitions in ^{11}B and ^{14}C," Nucl. Phys. $\underline{A118}$, 481 (1968).

Bi59 E. G. Bilpuch, L. W. Weston, C. D. Bowman, and H. W. Newson, "Recent Total Neutron Cross Sections for Li, N, C, Cl, Co, Sr, and Pb," Bull. Am. Phys. Soc. $\underline{4}$, 42 (1959).

Bi62 E. G. Bilpuch, J. A. Farrell, G. C. Kyker, P. B. Parks, and H. W. Newson, private communication to R. J. Howerton (1962).

Bl52 J. M. Blatt and V. F. Weisskopf, Theoretical Nuclear Physics, John Wiley and Sons, N. Y. (1952).

Bl52a J. M. Blatt and L. C. Biedenharn, "The Angular Distribution of Scattering and Reaction Cross Sections," Rev. Mod. Phys. $\underline{24}$, 258 (1952).

Bo51 W. Bollman and W. Zünti, "Wirkungsquerschnitt-messungen des $N^{14}(n,\alpha)B^{11}$- und des $N^{14}(n,p)C^{14}$- Prozesses mit monochromatischen D-D-Neutronen," Helv. Phys. Acta $\underline{24}$, 517 (1951).

Bo57 N. A. Bostrom, I. L. Morgan, J. T. Prud'homme, and A. R. Sattar, "The Elastic Scattering of Fast Neutrons from Oxygen and Nitrogen," Wright Air Development Center report WADC-TR-57-446 (1957).

Bo59 N. A. Bostrom, I. L. Morgan, J. T. Prud'homme, P. L. Okhuysen, and O. M. Hudson, Jr., "Interaction of Fast Neutrons in Iron, Lead, Oxygen, and Nitrogen," Wright Air Development Center report WADC-TR-59-31 (1959).

Bo62 V. V. Bobyr, L. Ya. Grona, and V. I. Strizhak, "Angular Distribution of 14-MeV Neutrons Inelastically Scattered on Carbon, Nitrogen, and Sulfur," Soviet Phys.-JETP $\underline{14}$, 18 (1962).

Bo65 M. Bormann, E. Fretwurst, P. Schehka, G. Wrege, H. Büttner, A. Lindner, and H. Meldner, "Some Excitation Functions of Neutron Induced Reactions in the Energy Range 12.6-19.6 MeV," Nucl. Phys. $\underline{63}$, 438 (1965).

Bo68 F. Boreli, P. N. Shrivastava, B. B. Kinsey, and V. D. Mistry, "Proton and Neutron Resonances in Nitrogen," Phys. Rev. $\underline{174}$, 1221 (1968); University of Texas report ORO-2972-47 (1967).

Br61 O. D. Brill, N. A. Vlasov, S. P. Kalinin, and L. S. Sokolov, "Cross Section of the (n,2n) Reaction in C^{12}, N^{14}, O^{16}, and F^{19} in the Energy Interval 10-37 MeV," Soviet Phys.-Doklady $\underline{6}$, 24 (1961).

Br64 G. Breit, "Definitions of Compound States," Rev. Mod. Phys. $\underline{36}$, 1072 (1964).

Bu69 P. S. Buchanan, "A Compilation of Cross Sections and Angular Distributions of Gamma Rays Produced by Neutron Bombardment of Various Nuclei," Texas Nuclear Corporation report ORO-2791-28 (1969).

Bu71 P. S. Buchanan, D. O. Nellis, and W. E. Tucker, "A Compilation of Cross Sections and Angular Distributions of Gamma Rays Produced by Neutron Bombardment of Various Nuclei," Texas Nuclear Corporation report ORO-2791-32 (1971).

Bu71a W. P. Bucher, C. E. Hollandsworth, R. D. Lamoreaux, A. Niiler, R. R. Sankey, and D. Eccleshall, "Small-Angle Elastic Scattering of 7.55 and 9.50 MeV Neutrons from C, N, and O," Ballistic Research Laboratory report BRL R 1562 (1971).

Ca57 R. R. Carlson, "Cross Sections for Pickup Reactions of 14-MeV Neutrons with N^{14}," Phys. Rev. $\underline{107}$, 1094 (1957).

Ca66 R. R. Carlson, "Branching Rations in C^{14} and N^{14}," Phys. Rev. $\underline{148}$, 991 (1966).

Ca70 A. D. Carlson and R. J. Cerbone, "High Resolution Measurements of the Total Neutron Cross Sections of Nitrogen and Iron," Nucl. Sci. Eng. $\underline{42}$, 28 (1970).

Ce62 M. Cevolani and S. Petralia, "Cross Section Measurement of (n,2n) Reactions on 14.1-MeV Neutrons," Nuovo Cimento $\underline{26}$, 1328 (1962).

Ch61 L. F. Chase, Jr., R. V. Smith, R. G. Johnson, F. J. Vaughn, and M. Walt, "Fast Neutron Cross Sections of Oxygen and Nitrogen," Air Force Special Weapons Center report AFSWC-TR-61-15 (1961).

Cl69 G. Clayeux and G. Grenier, "Spectres de renvoi des gammas produits par des neutrons de 14.1 MeV," Centre d'Etudes de Limeil report CEA-R-3807 (1969).

Co49 J. H. Coon and R. A. Nobles, "Disintegration of He^3 and N^{14} by Thermal Neutrons," Phys. Rev. $\underline{75}$, 1358 (1949).

Co49a L. J. Cook, E. M. McMillan, J. M. Peterson, and D. C. Sewell, "Total Cross Sections of Nuclei for 90-MeV Neutrons," Phys. Rev. $\underline{75}$, 7 (1949).

Co52 J. H. Coon, E. R. Graves, and H. H. Barschall, "Total Cross Sections for 14 MeV Neutrons," Phys. Rev. $\underline{88}$, 562 (1952).

Co68 H. Condé, I. Bergqvist, and G. Nyström, "Gamma-Rays from Inelastic Neutron Scattering in Nitrogen," Neut. Cross Sect. and Tech. Conf. Wash., D. C., (1968), p. 763.

Cs66 J. Csikai, "Fluctuations in the Total Cross Sections of (n,2n) Reactions," Conference on the Study of Nucl. Structure with Neutrons, Antwerp, 1965 (North-Holland Publishing Co., Amsterdam, 1966) p. 537.

Cs67 J. Csikai and S. Nagy, "Some (n,p) Reaction Cross Sections for 14.7 MeV Neutrons," Nucl. Phys. $A91$, 222 (1967).

Cs67a J. Csikai and G. Peto, "Influence of Direct Inelastic Scattering on (n,2n) Cross Sections," Acta Phys. Acad. Sci. Hung. 23, 87 (1967).

Cu51 P. Cüer, J.-P. Lonchamp, and S. Gorodetzky, "Determination de la section de desintegration de l'azote sous l'action des neutrons thermiques," J. Phys. Radium 12, 6 S (1951).

De50 J. DeJuren and N. Knable, "Nuclear Cross Sections for 95-MeV Neutrons," Phys. Rev. 77, 606 (1950).

De65 Yu. G. Degtyarev, "Cross Sections for the Inelastic Interaction of Neutrons with Nuclei of Li^7, C^{12}, N^{14}, Al^{27}, Fe^{56}, Cu, Pb, U^{235}, U^{238}, and Pu^{239}," Soviet J. At. Energy 19, 1426 (1965).

Di69 J. K. Dickens and F. G. Perey, "The $^{14}N(n,x\gamma)$ Reaction for $5.8 \leq E_n \leq 8.6$ MeV," Nucl. Sci. Eng. 36, 280 (1969).

Do64 P. F. Donovan, J. F. Mollenauer, and E. K. Warburton, "Inelastic Scattering of 10.2-MeV Protons by N^{14}," Phys. Rev. 133, B113 (1964).

Du54 J. D. Dudley and C. M. Class, "$^{14}N(n,2n)^{13}N$ Cross-Section Measurement with 14 MeV Neutrons," Phys. Rev. 94, 807 (1954).

En67 F. C. Engesser and W. E. Thompson, "Gamma Rays Resulting from Interactions of 14.7 MeV Neutrons with Various Elements," J. Nucl. Energy 21, 487 (1967).

Fe60 J. M. Ferguson and W. E. Thompson, "Cross Sections for the (n,2n) Reaction in N^{14}, P^{31}, Cu^{63}, and Pr^{141}," Phys. Rev. 118, 228 (1960).

Fe67 P. Fessenden and D. R. Maxson, "$N^{14}(n,d)C^{13}$, $N^{14}(n,t)C^{12}$, and $N^{15}(n,d)C^{14}$ near $E_n = 14$ MeV," Phys. Rev. 158, 948 (1967).

Fe68 J. M. Ferguson, "A Code for Calculating Neutron Compound-Nucleus Cross Sections and Angular Distributions: JANE," Naval Radiological Defense Laboratory report NRDL-CP-68-4 (1968).

Fl58 N. N. Flerov and V. M. Talyzin, "Cross Section for Inelastic Interactions of 14.5 MeV Neutrons with Various Elements," Soviet J. At. Energy 1, 617 (1958).

Fo55 J. L. Fowler and C. H. Johnson, "Differential Elastic Scattering Cross Section for Neutrons on Nitrogen," Phys. Rev. 98, 728 (1955).

Fo66 J. L. Fowler, C. H. Johnson, and R. L. Kernell, "Differential Elastic Scattering of Neutrons from Nitrogen," Neut. Cross Sect. and Tech. Conf. Wash., D. C. (1968), p. 653.

Fo71 D. G. Foster, Jr., and D. W. Glasgow, "Neutron Total Cross Sections 2.5-15 MeV. I. Experimental," Phys. Rev. C 3, 576 (1971).

Fr54 R. G. Freemantle, D. J. Prowse, and J. Rotblat, "Scattering of 9.5-MeV Protons by Nitrogen," Phys. Rev. 96, 1268 (1954).

Ga59 F. Gabbard, H. Bichsel, and T. W. Bonner, "The Disintegration of Nitrogen by Fast Neutrons," Nucl. Phys. 14, 277 (1959).

Ga63 F. Gabbard, private communication to the Sigma Center at the Brookhaven National Laboratory (1963).

Ga66 A. Gallmann, P. Fintz, J. B. Nelson, and D. E. Alburger, "Study of Excited States in N^{15} and N^{16}," Phys. Rev. 147, 753 (1966).

Ga67 A. Gallmann, F. Haas, and B. Heusch, "Study of Unbound Levels in N^{14} by the $C^{12}(He^3,p\gamma)N^{14}$ Reaction," Phys. Rev. 164, 1257 (1967).

Gi59 J. H. Gibbons and R. L. Macklin, "Total Neutron Yields from Light Nuclei under Proton and Alpha Bombardment," Phys. Rev. 114, 571 (1959).

Go65 N. W. Golchert, D. G. Gardner, and J. Sedlet, "Cross Section of Some Reactions of 99_{Tc} with 14.1 MeV Neutrons," Nucl. Phys. 73, 349 (1965).

Go66 S. Gorodetzky, R. M. Freeman, A. Gallmann, and F. Haas, "Angular-Correlation Studies of the Reactions $O^{16}(He^3,\alpha\gamma)O^{15}$, $C^{12}(He^3,p\gamma)N^{14}$, and $C^{12}(d,p\gamma)C^{13}$," Phys. Rev. 149, 801 (1966).

Gr65 B. Grimeland, E. Kjellsby, and J. Vines, "Cross Sections of Some Reactions Induced in Nitrogen, Phosphorus, Copper, and Bromine with Neutrons of Energy 14.8 MeV," Phys. Rev. 137, B878 (1965).

Gr68 R. C. Greenwood, "Observation of a 9.15 MeV Doublet Level in ^{15}N from a Study of the ^{14}N $(n,\gamma)^{15}N$ Reaction," Phys. Letters $27B$, 274 (1968).

Ha52 W. Hauser and H. Feshbach, "The Inelastic Scattering of Neutrons," Phys. Rev. 87, 366 (1952).

Ha59 H. E. Hall and T. W. Bonner, "Gamma Radiations from Inelastic Scattering of Fast Neutrons in C^{12}, N^{14}, and O^{16}," Nucl. Phys. 14, 295 (1959).

Ha59a E. Haddad, quoted as private communication by Ga59.

Ha61 G. C. Hanna, D. B. Primeau, and P. R. Tunnicliffe, "Thermal Neutron Cross Sections and Resonance Integrals of the Reactions $O^{17}(n,\alpha)$ C^{14}, $Ar^{36}(n,\alpha)S^{33}$, and $N^{14}(n,p)C^{14}$," Can. J. Phys. 39, 1784 (1961).

Ha70 L. F. Hansen, private communication (1970).

He60 D. F. Hebbard and J. L. Vogl, "Elastic Scattering and Radiative Capture of Protons by C^{13}," Nucl. Phys. 21, 652 (1960).

He70 H. T. Heaton, II, R. B. Schwartz, and R. A. Schrack, "Total Cross Section of Nitrogen in the MeV Region," Bull. Am. Phys. Soc. 15, 568 (1970).

Hi50 R. H. Hildebrand and C. E. Leith, "Total Cross Sections of Nuclei for 42-MeV Neutrons," Phys. Rev. 80, 842 (1950).

Hi52 J. J. Hinchey, P. H. Stelson, and W. M. Preston, "The Total Neutron Cross Section of Nitrogen," Phys. Rev. 86, 483 (1952).

Hi54 P. Hillman, R. H. Stahl, and N. F. Ramsey, "Total Cross Sections of Liquefied Gases for High-Energy Neutrons," Phys. Rev. 96, 115 (1954).

Hu61 C. M. Huddleston and F. P. Mooring, "Total Neutron Cross Section of Nitrogen and Oxygen from 1 keV to 450 keV," Argonne National Laboratory report ANL-6376, 13 (1961).

Jo50 C. H. Johnson and H. H. Barschall, "Interaction of Fast Neutrons with Nitrogen," Phys. Rev. 80, 818 (1950).

Jo51 C. H. Johnson, B. Petree, and R. K. Adair, "Total Cross Section of Nitrogen for Fast Neutrons," Phys. Rev. 84, 775 (1951).

Jo52 C. H. Johnson, H. B. Willard, J. K. Bair, and J. D. Kington, "Total Neutron Cross Sections of N^{14}, Ge, Se, Cd, and Hg," Oak Ridge National Laboratory report ORNL-1365, p. 1 (1952).

Jo68 C. H. Johnson, F. X. Haas, J. L. Fowler, F. D. Martin, R. L. Kernell, and H. O. Cohn, "Total Neutron Cross Sections of ^{9}Be, ^{14}N, and ^{16}O," Neutron Cross Sections and Technology Conf. Wash., D. C., (1968) p. 851.

Jo69 L. Jonsson and R. Hardell, "Energies and Intensities of Gamma Rays from Slow Neutron Capture in Nitrogen," International Symposium on Neutron Capture Gamma-Ray Spectroscopy, Studsvik, 1969 (to be published).

Ju63 E. T. Jurney and H. T. Motz, "Thermal Neutron Capture in D and O^{16}," Argonne National Laboratory report ANL-6797, p. 236 (1963).

Ka60 J. V. Kane, R. E. Pixley, and D. H. Wilkinson, "Isotopic Spin Selection Rules XIV: Transitions between Mirror States in ^{13}C and ^{13}N," Phil. Mag. 5, 365 (1960).

Ku70 H. M. Kuan, M. Hasinoff, W. J. O'Connell, and S. S. Hanna, "The Giant Dipole Resonances in ^{11}C and ^{15}O Observed with the Reactions ^{10}B (p,γ)^{11}C and ^{14}N(p,γ)^{15}O," Nucl. Phys. A151, 129 (1970).

La58 A. M. Lane and R. G. Thomas, "R-Matrix Theory of Nuclear Reactions," Rev. Mod. Phys. 30, 257 (1958).

Le68 B. Leroux, K. El-Hammami, J. Dalmas, R. Chastel, G. Lamot, C. Fayard, and J. Hajjboutros, "Etudes des reactions (n,α) sur les noyaux ^{16}O et ^{14}N a 14.9 MeV," Nucl. Phys. A116, 196 (1968).

Li52 A. B. Lillie, "The Disintegration of Oxygen and Nitrogen by 14.1-MeV Neutrons," Phys. Rev. 87, 716 (1952).

Li67 R. H. Lindsay and J. J. Veit, "N^{14}(n,t) and N^{14}(n,d) Angular Distributions at 14.7 MeV," Phys. Rev. 157, 933 (1967).

Lu66 H. F. Lutz and J. D. Anderson, "Neutron Cross Sections Inferred from Charged Particle Data," Lawrence Livermore Laboratory report UCRL-14568 (1966).

Lu67 B. Lundberg, S. Schwarz, and H. O. Zetterstrom, "Elastic Scattering of 14.8 MeV Neutrons from ^{14}N and ^{16}O," Arkiv Fysik 34, 247 (1967).

Ma56 R. J. Mackin, Jr., W. R. Mills, Jr., and J. Thirion, "Radiation from Excited States of Carbon-13," Phys. Rev. 102, 802 (1956).

Ma65 J. H. E. Mattauch, W. Thiele, and A. H. Wapstra, "1964 Atomic Mass Table," Nucl. Phys. 67, 1 (1965).

Ma66 G. S. Mani and G. C. Dutt, "Reaction Mechanism for the ^{11}B(α,n)^{14}N Reaction," Nucl. Phys. 78, 613 (1966).

Ma68 D. R. Maxson and R. D. Murphy, "^{16}O(n,α)^{13}C Reaction at 14.1 MeV," Nucl. Phys. A110, 555 (1968).

Ma68a G. N. Maslov, F. Nasyrov, and N. F. Pashkin, "γ-Radiation in the Interaction of 14 MeV Neutrons with the Nuclei of B, C, N, I, F, and Al Atoms," Soviet J. At. Energy 24, 704 (1968).

Ma69 R. E. Maerker and F. J. Muckenthaler, "Gamma-Ray Spectra Arising from Thermal-Neutron Capture in Elements Found in Soils, Concretes, and Structural Materials," Oak Ridge National Laboratory report ORNL-4382 (1969).

Mc66 L. McFadden and G. R. Satchler, "Optical-Model Analysis of the Scattering of 24.7 MeV Alpha Particles," Nucl. Phys. 84, 177 (1966).

Me49 E. Melkonian, "Slow Neutron Velocity Spectrometer Studies of O_2, N_2, A, H_2, H_2O, and Seven Hydrocarbons," Phys. Rev. 76, 1750 (1949).

Me53 R. Meier, R. Ricamo, P. Scherrer, and W. Zünti, "Totale Wirkungsquerschnitte der Elemente N, Na, Al und Si für Neutronen von 1.9-3.8 MeV," Helv. Phys. Acta 26, 451 (1953).

Me66 D. F. Measday and J. N. Palmieri, "Neutron Total Cross Sections in the Energy Range 80 to 150 MeV," Nucl. Phys. 85, 129 (1966).

Mi68 D. Miljanic, G. Paic, B. Antolkovic, and P. Tomas, "(n,d) Reactions on ^{14}N, ^{35}Cl, ^{39}K, ^{40}Ca, and ^{75}As at 14.4 MeV," Nucl. Phys. A106, 401 (1968).

Mo62 H. T. Motz, R. E. Carter, and W. D. Barfield, "Thermal-Neutron Capture Gamma-Rays from Beryllium and Nitrogen," Pile Neutron Research in Physics (International Atomic Energy Agency, Vienna, 1962), p. 225.

Mo63 I. L. Morgan, J. B. Ashe, R. W. Benjamin, O. M. Hudson, Jr., S. C. Mathur, D. O. Nellis, C. V. Parker, and W. E. Tucker, Annual Progress Report, (Texas Nuclear Corp., Austin, 1963), p. 68.

Mo64 I. L. Morgan, J. B. Ashe, and D. O. Nellis, "Angular Distributions of Gamma Rays from C, O, and N at E_n=14.8 MeV," Nuclear Physics Division Annual Progress Report (Texas Nuclear Corp., Austin, 1964), p. 156.

Mo64a P. A. Moldauer, "Statistical Theory of Nuclear Collision Cross Sections," Phys. Rev. 135, B642 (1964).

Mo67 J. Mösner, G. Schmidt, and J. Schintlmeister, "Four-Particle Disintegration of Nitrogen by Fast Neutrons," Nucl. Phys. A103, 238 (1967).

Ne54 N. E. Nereson and S. Darden, "Average Neutron Total Cross Sections in the 3- to 12-MeV Region," Phys. Rev. 94, 1678 (1954).

Ne70 D. O. Nellis, private communication (1970).

Ne71 D. O. Nellis, P. S. Buchanan, T. C. Martin, W. E. Tucker, G. H. Williams, and A. J. Wolfram, "Neutron Scattering and Gamma-Ray Production Cross Sections for N, O, Al, Si, Ca, and Fe," private communication (1971).

Ny69 K. Nyberg, private communication to L. Stewart (1969).

Od60 Y. Oda, M. Takeda, N. Takano, T. Yamizaki, C. Hu, K. Kikuchi, S. Kobayashi, K. Matsuda, and Y. Nagahara, "Elastic and Inelastic Scattering of Protons from N, Ne, Mg, Si, S, and A in the Energy Range from 7.6 MeV to 14.2 MeV," J. Phys. Soc. Japan 15, 760 (1960).

Oh65 G. G. Ohlsen, "Kinematic Relations in Reactions of the Form A + B → C + D + E," Nucl. Instr. Methods 37, 240 (1965).

Ol65 J. W. Olness, E. K. Warburton, D. E. Alburger, and J. A. Becker, "Studies of Electromagnetic Transitions in B^{11} and C^{11}," Phys. Rev. 139, B512 (1965).

Or69 V. J. Orphan and C. G. Hoot, "Neutron Cross Section Data for Radiation Transport Calculations," Gulf General Atomic report GA-8006 (1969).

Or70 V. J. Orphan, N. C. Rasmussen, and T. L. Harper, "Line and Continuum Gamma-Ray Yields from Thermal-Neutron Capture in 74 Elements," Gulf General Atomic report GA-10248 (1970).

Pa53 E. B. Paul and R. L. Clarke, "Cross-Section Measurements of Reactions Induced by Neutrons of 14.5-MeV Energy," Can. J. Phys. 31, 267 (1953).

Pa67 A. Pasquarelli, "Measurements of Cross Sections for (n,2n), (n,p), and (n,α) Reactions at 14.7 MeV," Nucl. Phys. A93, 218 (1967).

Pe60 J. M. Peterson, A. Bratenahl, and J. P. Stoering, "Neutron Total Cross Sections in the 17- to 29-MeV Region," Phys. Rev. 120, 521 (1960).

Pe71 F. G. Perey and W. E. Kinney, private communication (1971).

Ph61 D. D. Phillips, private communication to R. J. Howerton (1961).

Ph67 G. W. Phillips, F. C. Young, and J. B. Marion, "Energy Levels and Electromagnetic Transitions in N^{15} from the $C^{13}(He^3,p\gamma)N^{15}$ Reaction," Phys. Rev. 159, 891 (1967).

Pi60 R. E. Pixley, J. V. Kane, and D. H. Wilkinson, "Rare E2 Transition in C^{13}," Phys. Rev. 120, 943 (1960).

Po52 H. L. Poss, E. O. Salant, G. A. Snow, and L. C. L. Yuan, "Total Cross Sections for 14-Mev Neutrons," Phys. Rev. 87, 11 (1952).

Pr60 J. T. Prud'homme, I. L. Morgan, J. H. McCrary, J. B. Ashe, and O. M. Hudson, Jr., "A Study of Neutrons and Gamma Rays from Neutron Induced Reactions in Several Elements," Air Force Special Weapons Center report AFSWC-TR-60-30 (1960).

Ra61 L. A. Rayburn, "14.4-MeV (n,2n) Cross Sections," Phys. Rev. 122, 168 (1961).

Re67 D. Rendic, "The Reaction $^{14}N(n,t)^{12}C$ at E_n = 14.4 MeV," Nucl. Phys. A91, 604 (1967).

Re70 G. M. Reynolds, S. M. Sperling, and W. E. Selph, "Secondary Gamma-Ray Production and Transport in Liquid Nitrogen," Nucl. Sci. Eng. 42, 324 (1970).

Re71 G. M. Reynolds and S. M. Sperling, "A Re-analysis of Secondary Gamma-Ray Spectra Produced in Liquid Nitrogen by 14 MeV Neutrons," Science Applications Inc. report SAI-71-550-LJ (1971).

Ro65 L. Rosen, J. G. Beery, A. S. Goldhaber, and E. H. Auerbach, "Elastic Scattering of 10.5- and 14.5-MeV Polarized Protons from Nuclei and the Optical Model Potential at Intermediate Energies," Ann. Phys. (N.Y.) 34, 96 (1965).

Sc66 W. Scobel, R. W. Fink, and M. Bormann, "The Reactions $N^{14}(n,\alpha)B^{11}$ and $N^{14}(n,t)C^{12}$ Observed with a Gridded Ionization Chamber," Z. Physik 197, 124 (1966).

Si69 H. E. Siefken, P. M. Cockburn, and R. W. Krone, "Levels in ^{15}N Resulting from the Proton Capture of ^{14}C," Nucl. Phys. A128, 162 (1969).

Sm54 J. R. Smith, "Scattering of 14.1-MeV Neutrons in Helium, Hydrogen, and Nitrogen," Phys. Rev. 95, 730 (1954).

St62 V. I. Strizhak, V. V. Bobyr, and L. Ya. Grona, "Angular Distributions for Elastic Scattering of 14-MeV Neutrons," Soviet Phys. - JETP $\underline{14}$, 225 (1962).

St65 L. Stewart, private communication from J. D. Anderson (1965).

St65a J. F. Strain and W. J. Ross, "14-MeV Neutron Reactions," Oak Ridge National Laboratory report ORNL-3672 (1965).

St69 L. Stewart, private communication (1969).

Th67 G. E. Thomas, D. E. Blatchley, and L. M. Bollinger, "High-Sensitivity Neutron-Capture Gamma-Ray Facility," Nucl. Instr. Methods $\underline{56}$, 325 (1967).

Wa64 E. K. Warburton, J. W. Olness, D. E. Alburger, D. J. Bredin, and L. F. Chase, Jr., "Studies of Electromagnetic Transitions in N^{14} by Means of the $C^{12}(He^3,p)N^{14}$ Reaction," Phys. Rev. $\underline{134}$, B338 (1964).

Wa65 E. K. Warburton, J. S. Lopes, R. W. Ollerhead, A. R. Poletti, and M. F. Thomas, "Angular-Correlation Studies for the $C^{12}(He^3,\alpha\gamma)C^{11}$, $C^{12}(He^3,p\gamma)N^{14}$ and $O^{18}(p,\alpha\gamma)N^{15}$ Reactions," Phys. Rev. $\underline{138}$, B104 (1965).

Wa65a E. K. Warburton, J. W. Olness, and D. E. Alburger, "Studies of Electromagnetic Transitions in N^{15} and O^{15}," Phys. Rev. $\underline{140}$, B1202 (1965).

Wa66 E. K. Warburton and J. W. Olness, "Angular Correlations in the $C^{13}(He^3,p\gamma)N^{15}$ Reaction: Levels of N^{15}," Phys. Rev. $\underline{147}$, 698 (1966).

Wa71 A. H. Wapstra and N. B. Gove, "The 1971 Atomic Mass Evaluation," Nucl. Data Tables $\underline{9}$, 267 (1971).

Wi43 G. C. Wick, Atti reale accad. Italia, Mem. classes sci. fis., mat. e nat. $\underline{13}$, 1203, (1943); see also J. H. Coon, R. W. Davis, H. E. Felthauser, and D. B. Nicodemus, "Scattering of 14.5-MeV Neutrons by Complex Nuclei," Phys. Rev. $\underline{111}$, 250 (1958), and L. Stewart, "Evaluated Neutron Cross Sections for Tritium," Los Alamos Scientific Laboratory report LA-3270 (1965).

Wi63 H. B. Willard, L. C. Biedenharn, P. Huber, and E. Baumgartner, "Resonance Processes with Fast Neutrons," in Fast Neutron Physics, Part II: Experiments and Theory edited by J. B. Marion and J. L. Fowler, (John Wiley and Sons, Inc., New York, 1963), p. 1284.

Wo67 C. Wong, J. D. Anderson, J. McClure, B. Pohl, V. A. Madsen, and F. Schmittroth, "$C^{14}(p,n)N^{14}$ Reaction and the Two-Body Force," Phys. Rev. $\underline{160}$, 769 (1967).

Yo69 F. C. Young, G. W. Phillips, and J. B. Marion, private communication to F. Ajzenberg-Selove (1969); see Aj70.

Za63 M. R. Zatzick and D. R. Maxson, "Angular Distributions of (n,d) Pickup Reactions in N^{14}, P^{31}, and S^{32} at 14 MeV," Phys. Rev. $\underline{129}$, 1728 (1963).

Zi39 W. H. Zinn, S. Seely and V. W. Cohen, "Collision Cross Sections for D-D Neutrons," Phys. Rev. $\underline{56}$, 260 (1939).

APPENDIX A

COMPOUND-NUCLEUS REACTION-THEORY CALCULATIONS

We used the computer code JANE (^{F}e68) to calculate the (n,n'), (n,p), and (n,α) level-excitation cross sections used to supplement experimental data as described in Sec. 3. This code, which is based on the optical model of the nucleus and on the compound-nucleus theory of reactions, computes partial-reaction cross sections using transmission coefficients generated from the optical model as input for the Hauser-Feshbach (Ha52) calculations, which include refinements by Moldauer (Mo64a, Br64). Before using the code, we made several minor corrections and checked the cross-section calculations against calculations made with ABACUS (Au62) for several different neutron energies. In addition, the code was modified to handle up to 50 levels for (n,n') reactions and 25 levels for (n,p) and (n,α) reactions.

This was sufficient for the n + ^{14}N calculations up to a laboratory neutron energy of ~ 14 MeV.

The form of the optical potential used in the JANE code is

$$-V_r = V\,f(r) + iWg(r) + V_{so}\,(\vec{\ell}\cdot\vec{s})h(r) + Zw(r),$$

where the usual real, imaginary, spin-orbit, and Coulomb terms are included.

The real part is the usual Saxon potential,

$$f(r) = \{1 + \exp[(r-R)/a]\}^{-1}\quad.$$

The imaginary part is a mixture of a volume potential and a Saxon-derivative potential,

$$g(r) = vf(r) + (1-v)(-4b)\frac{d}{dr}\{1 + \exp[(r-R)/b]\}^{-1},$$

where v is a mixing parameter and, normally, $0 \leqslant v \leqslant 1$.

The usual spin-orbit term,

$$h(r) = -\frac{2}{r}\frac{d}{dr}\{1 + \exp[(r-R_{so})/a]\}^{-1} \ ,$$

is included.

We usually renormalized the calculated cross sections to fit experimental measurements, so we made no particular effort to optimize the optical parameters used in the calculations. The optical-model parameters, which are summarized in Table AI, were obtained from the work of Bauer et al. (Ba67) for the n + ^{14}N channel, Rosen et al. (Ro65) for the p + ^{14}C channel, and McFadden and Satchler (Mc66) for the α + ^{11}B channel. The Bauer parameters were obtained from an optical-model study of n + ^{14}N elastic scattering, the Rosen parameters are from an analysis of many proton scattering and polarization measurements, and the McFadden parameters were obtained from a study of α + ^{27}Al elastic scattering.

TABLE AI

OPTICAL-MODEL PARAMETERS USED IN
THE CROSS-SECTION CALCULATIONS

Parameter	n+^{14}N Channel	p+^{14}C Channel	α+^{11}B Channel
V (MeV)	52.7-0.28E	53.8-0.33E	49.1
W (MeV)	5.0	7.5	7.34
v	0.	0.	1
R (F)	2.89	3.01	4.10
a (F)	0.65	0.65	0.57
b (F)	0.47	0.70	0.57
V_{so} (MeV)	7.0	5.5	0
R_{so} (F)	2.89	3.01	4.10

The energy levels of ^{14}N used in the (n,n') calculations are described in Table AII. We obtained the level parameters from the A = 13-15 compilation by Ajzenberg-Selove (Aj70). The parentheses in Table AII indicate limited uncertainty in the parameters, whereas a bracket means that no information was available, and the value in the table was arbitrarily chosen. To account for the different isotopic spins of the states, we multiplied the (n,n') cross sections computed with JANE by $(2T + 1)^{-1}$.

The energy levels of ^{14}C used in the (n,p) calculations are described in Table AIII. These we also obtained from Ajzenberg-Selove's compilation (Aj70). The levels of ^{11}B used in the (n,α) calculations are given in Table AIV. We obtained these values from the earlier A = 11-12 compilation of Ajzenberg-Selove and Lauritsen (Aj68).

TABLE AII

^{14}N LEVEL PARAMETERS USED IN THE COMPOUND-
NUCLEUS REACTION-THEORY CALCULATIONS

E_x	J^π	T	E_x	J^π	T
0	1+	0	10.10	(2)+	[0]
2.313	0+	1	10.228	1(-)	0
3.945	1+	0	10.434	2+	1
4.913	(0)-	0	10.56	1-	[0]
5.106	2-	0	10.809	4+	0
5.691	1-	0	11.04	1+	0
5.833	3-	0	11.051	[5+]	[0]
6.198	1+	0	11.246	3-	1
6.444	3+	0	11.374	1+	0
7.028	2+	0	11.516	3+	[0]
7.966	2(-)	0	11.66	(2-)	[0]
8.061	1-	1	11.75	1+	[0]
8.489	(4-)	0	11.81	(2+)	[0]
8.617	0+	1	11.95	2+	[0]
8.800	0-	1	12.23	3-	[0]
8.907	3-	1	12.29	[2+]	[0]
8.963	5+	0	12.414	4-	[0]
8.979	2+	(0)	12.47	[5+]	[0]
9.129	2-	0	12.504	[4+]	[0]
9.172	2+	1	12.608	3+	[0]
9.388	2-	0	12.689	3-	[0]
9.508	2-	1	12.793	4+	[0]
9.702	1+	[0]	12.825	4-	[0]
10.063	[3+]	0	12.853	[5+]	[0]
			12.942	4[-]	[0]

TABLE AIII

^{14}C LEVEL PARAMETERS USED IN THE COMPOUND-
NUCLEUS REACTION-THEORY CALCULATIONS

E_x (MeV)	J^π	E_x (MeV)	J^π
0	0$^+$	10.433	(2)$^{[-]}$
6.094	1$^-$	10.453	[3$^-$]
6.583	0$^+$	10.740	[3$^+$]
6.728	3$^-$	11.350	[2$^-$]
6.894	0$^-$	11.660	[2$^+$]
7.012	2$^+$	11.900	[1$^-$]
7.337	2$^-$	12.601	[3$^+$]
8.318	(1)$^+$	12.854	[4$^-$]
9.801	(1)$^{[-]}$	12.958	[3$^+$]

TABLE AIV

^{11}B LEVEL PARAMETERS USED IN THE COMPOUND-
NUCLEUS REACTION-THEORY CALCULATIONS

E_x (MeV)	J^π	E_x (MeV)	J^π
0	3/2$^-$	10.25	(3/2$^-$)
2.124	1/2$^-$	10.33	5/2$^-$
4.444	5/2$^-$	10.595	7/2$^+$
5.019	3/2$^-$	11.00	5/2$^-$
6.743	7/2$^-$	11.266	(9/2)$^+$
6.793	(1/2)$^+$	11.462	[7/2$^+$]
7.296	(5/2)$^+$	11.60	[5/2$^-$]
7.996	3/2$^+$	11.884	(5/2$^+$)
8.566	(3/2)$^-$	12.00	[3/2$^+$]
8.925	5/2$^-$	12.565	[3/2$^-$]
9.185	7/2$^+$	13.00	1/2$^-$
9.274	5/2$^+$	13.15	(11/2)$^+$
9.87	3/2$^+$		

APPENDIX B

RESONANCE-THEORY PARAMETERIZATION

The resonance treatment used to derive the elastic-scattering angular distributions (Sec. 4.1.1) is based on the single-level approximation to R-matrix theory, as described by Lane and Thomas (La58). We took the nuclear-scattering phase shifts, δ', as complex to account for the reaction channels, so that a general element of the collision matrix is given by

$$U_{nn} = \exp(2i\delta') = \tau \exp(2i\delta),$$

where δ is the real part of δ' and τ is related to the imaginary part, ν, of δ' by $\tau = \exp(-2\nu)$ and must lie in the range $0 \leq \tau \leq 1$. The real part of the phase shift was divided into resonant (β) and potential scattering (ϕ) components, as

$$\delta_\lambda = \phi_\ell + \beta_\lambda,$$

where λ designates the quantum numbers associated with particular partial waves and ℓ is the orbital angular momentum of the incoming neutron. We assumed the potential scattering phase shifts to be functions of ℓ and incident neutron energy only.

The parameters τ_λ and β_λ can be related to the usual resonance parameters through the expression (La58):

$$U^\lambda_{nn} = \tau_\lambda \exp(2i\beta_\lambda)\exp(2i\phi_\ell)$$

$$= \left[1 + \frac{i\Gamma_{\lambda n}}{E_\lambda + \Delta_\lambda - E - i\Gamma_\lambda/2}\right] \exp(2i\phi_\ell) ,$$

where $\Gamma_{\lambda n}$, Γ_λ, E_λ, and Δ_λ are the partial neutron width, the total width, the energy eigenvalue, and the level shift, respectively, for the λth level in the compound system, and E is the energy of relative motion in the center-of-mass system. After performing the necessary algebra, one can represent the quantities τ_λ and β_λ as

$$\tau_\lambda = \left[1 - \frac{\Gamma_{\lambda n}(\Gamma_\lambda - \Gamma_{\lambda n})}{(E_\lambda + \Delta_\lambda - E)^2 + \Gamma_\lambda^2/4}\right]^{1/2}$$

and

$$\tan \beta_\lambda = \frac{\Gamma_{\lambda n}(E_\lambda + \Delta_\lambda - E)}{[(E_\lambda + \Delta_\lambda - E)^2 + \Gamma_\lambda^2/4](\tau_\lambda + 1) - \Gamma_\lambda\Gamma_{\lambda n}/2} .$$

We constructed expressions relating the differential-scattering cross section $\sigma(\Theta)$ to the phase shifts δ_λ' from the general equations given in Blatt and Biedenharn (Bl52a). Terms corresponding to $\ell \neq \ell'$ and $s \neq s'$, where ℓ and ℓ' are the

incoming and outgoing angular momenta and s and s' are the incoming and outgoing channel spins, were omitted from the expressions to reduce the number of parameters. In the computer code used to fit the measured distributions, the resonance parameters were treated as fixed input and ϕ_ℓ for the $\ell = 0$ and $\ell = 1$ potential phase shifts were varied to fit the measurements.

The potential phase shifts for $\ell = 2$ and $\ell = 3$ were represented by hard-sphere values, given by

$$\phi_\ell = - \arctan [F_\ell(ka)/G_\ell(ka)] \quad ,$$

where k is the wave number for the incident neutrons, a is the nuclear radius used in the calculations, and F_ℓ and G_ℓ are the regular and irregular neutron wave functions, as given in Lane and Thomas (La58). The energy dependences of the Γ_λ and Δ_λ used in the calculations were represented in the usual manner by

$$\Gamma_\lambda = 2\gamma_\lambda^2 ka/(F_\ell^2 + G_\ell^2) \quad ,$$

$$\Delta_\lambda = - \gamma_\lambda^2 ka(F_\ell F_\ell' + G_\ell G_\ell')/(F_\ell^2 + G_\ell^2) \quad ,$$

where γ_λ^2 is the reduced width of the level designated by λ. We obtained the values for γ_λ^2 and E_λ from the resonance widths and energies derived from the total cross-section measurements.

APPENDIX C
LEGENDRE COEFFICIENTS AND ANGULAR DISTRIBUTIONS FOR NEUTRON INELASTIC SCATTERING

Complete graphs of the evaluated Legendre coefficients as functions of neutron energy are given in this appendix for angular distributions of (n,n') reactions to the first 12 excited states in ^{14}N. We have used the ENDF definitions of the coefficients throughout [i.e., the "natural" coefficients divided by $(2\ell + 1)$]. Sample angular distributions are also given for each of the levels at several neutron energies. The Legendre coefficients are presented in the odd figures, C1 through C23; the sample angular distributions are given in the even figures, C2 through C24. The calculated angular distributions have been normalized to the appropriate level-excitation cross sections. Almost all of the input data consisted of (p,p') rather than (n,n') measurements. None of the observed distributions that was adequately defined experimentally for $\theta > 90°$ was observed to be symmetric about 90°, as required by Hauser-Feshbach theory. Nevertheless, for lack of data to determine the complete distributions, we assumed the last two levels to have symmetric distributions.
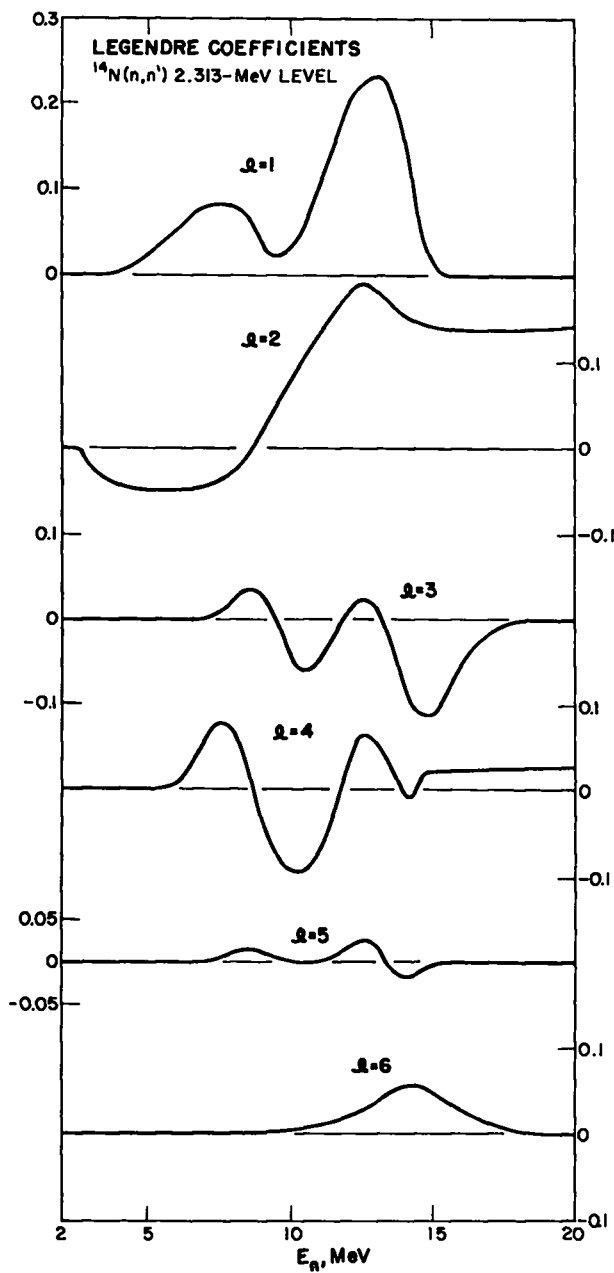
Fig. C1. Evaluated Legendre coefficients for inelastic scattering to the 2.313-MeV level in ^{14}N.
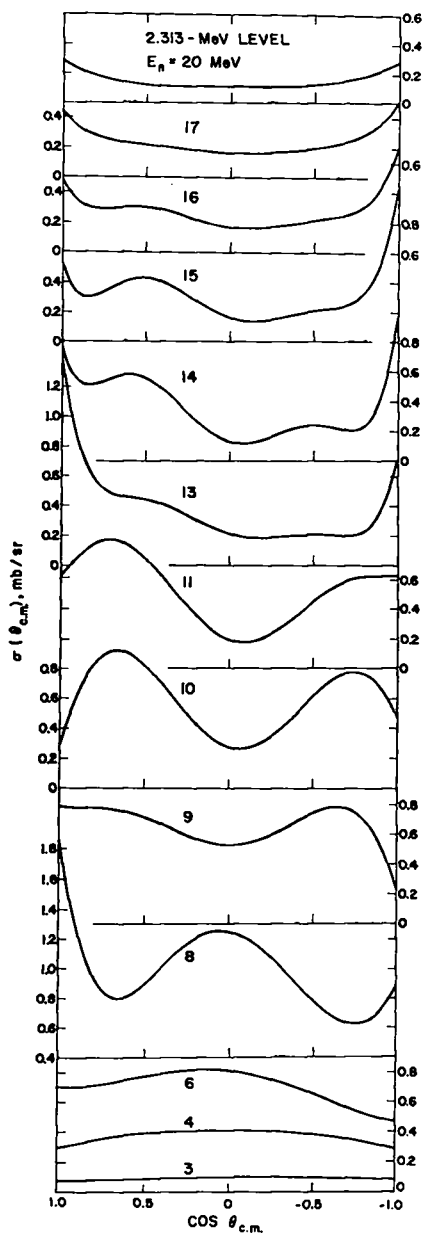
Fig. C2. Evaluated differential cross sections at selected energies for inelastic scattering to the 2.313-MeV level in ^{14}N. Note that the 8-MeV curve has a suppressed zero.

67
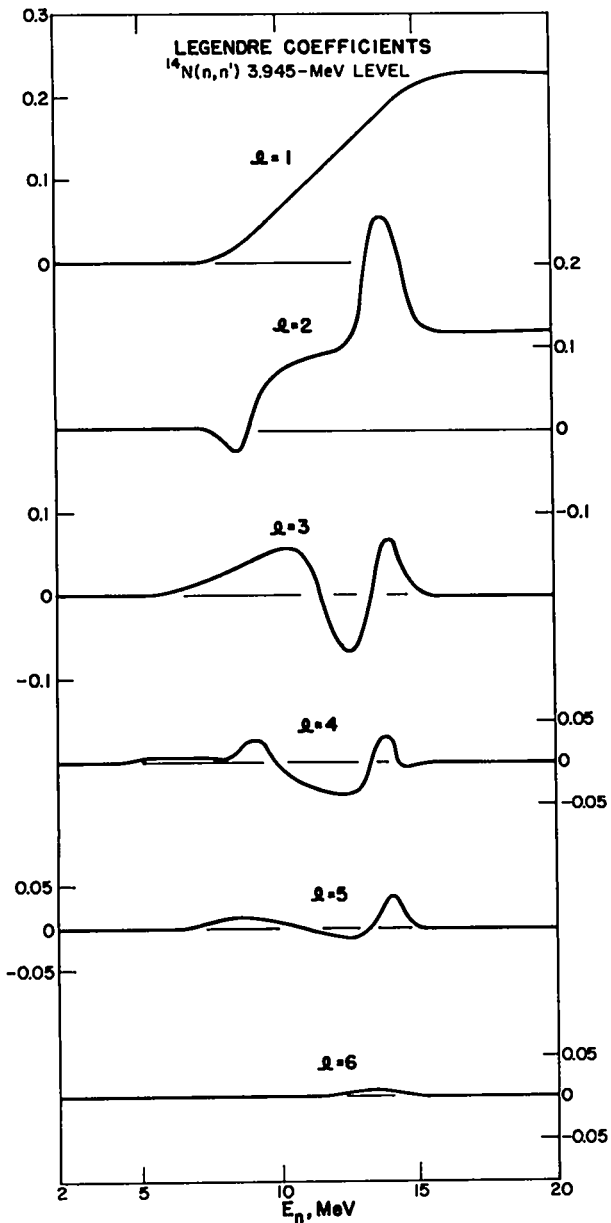
Fig. C3. Evaluated Legendre coefficients for inelastic scattering to the 3.945-MeV level in ^{14}N. This transition exhibits the largest ℓ=2 coefficient of any inelastic channel for nitrogen.
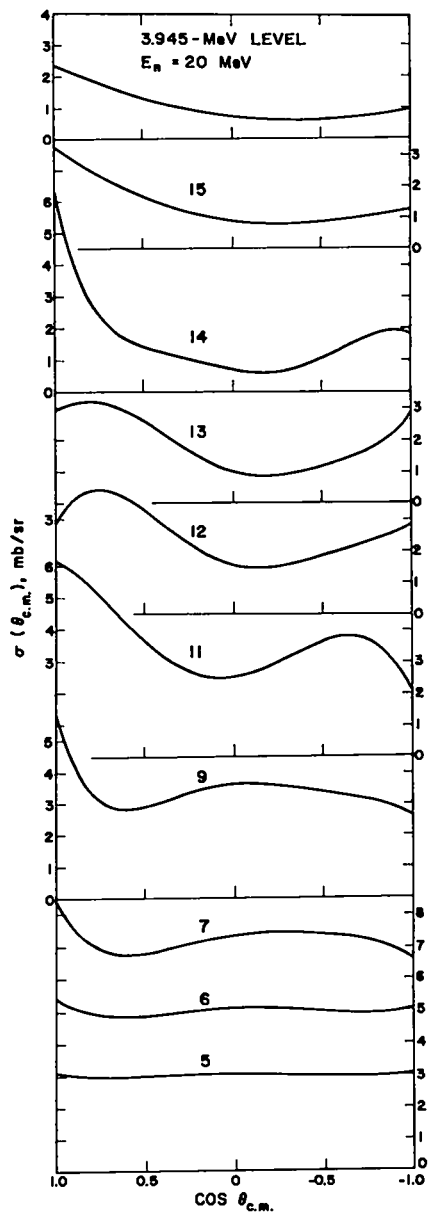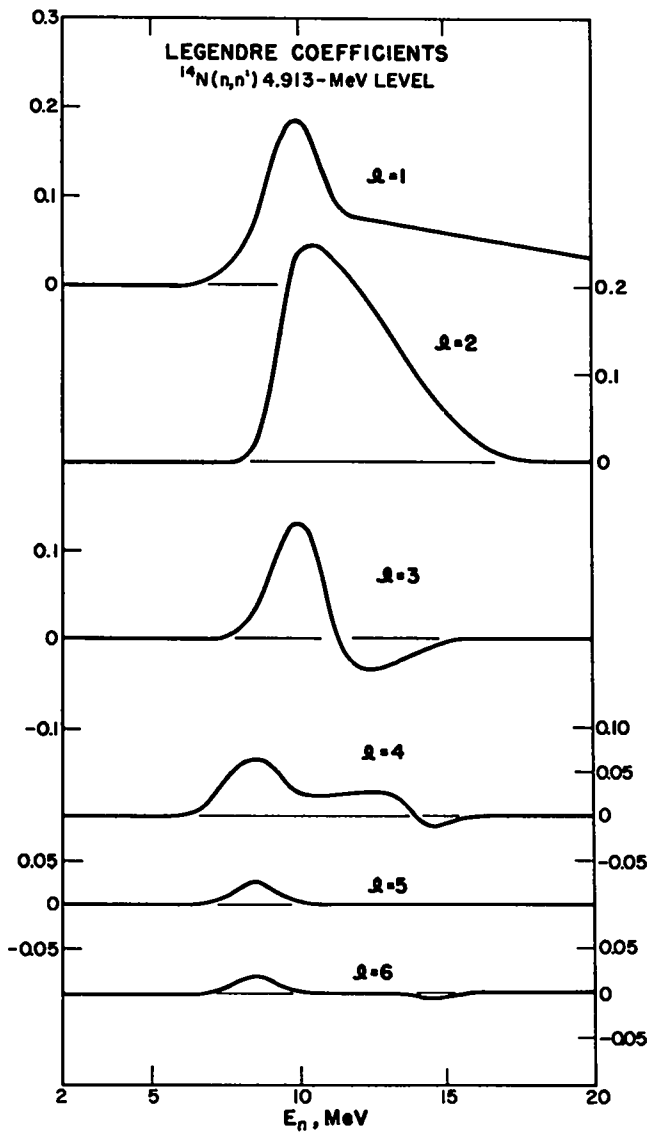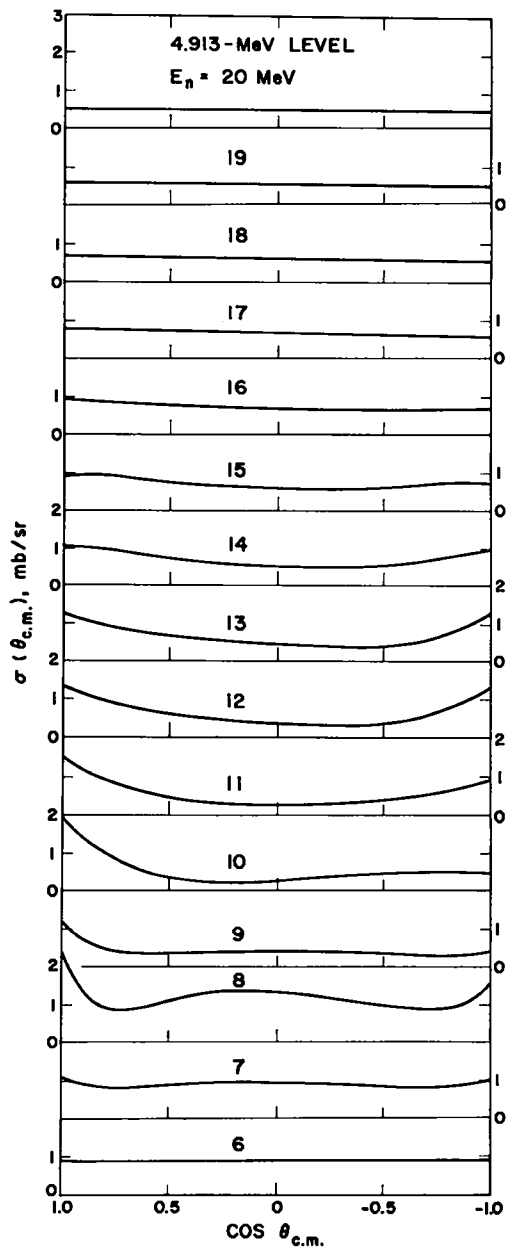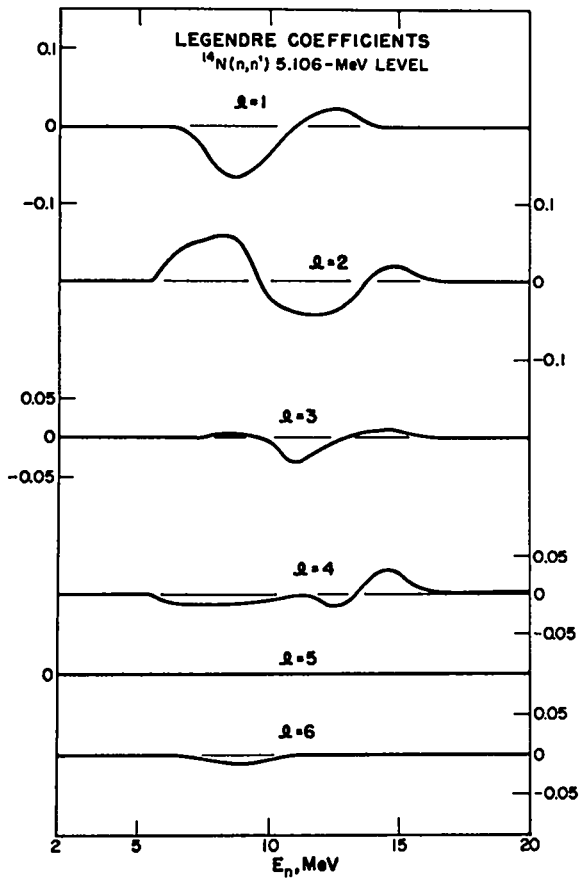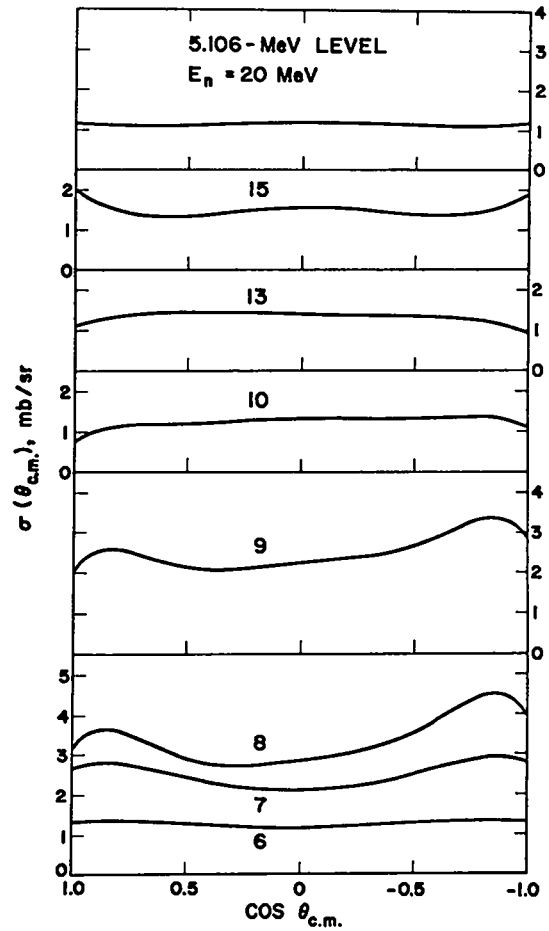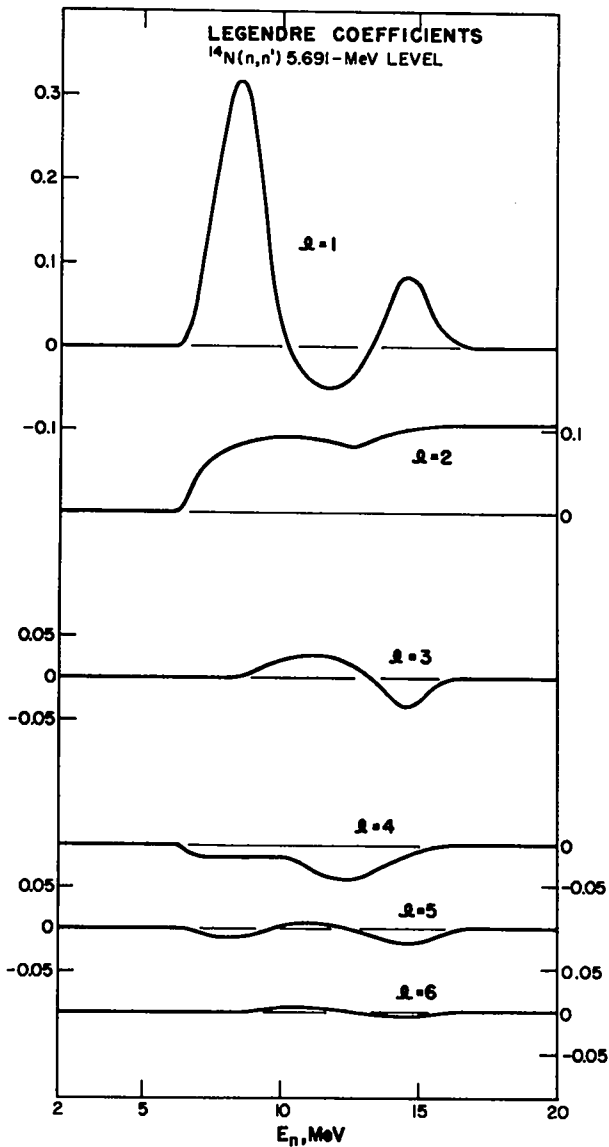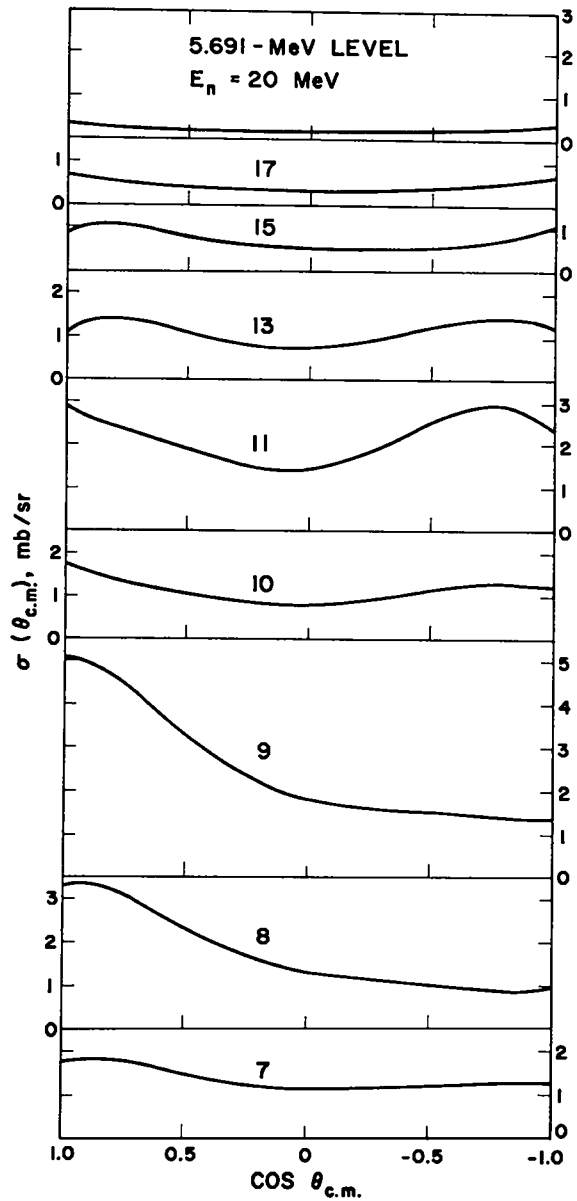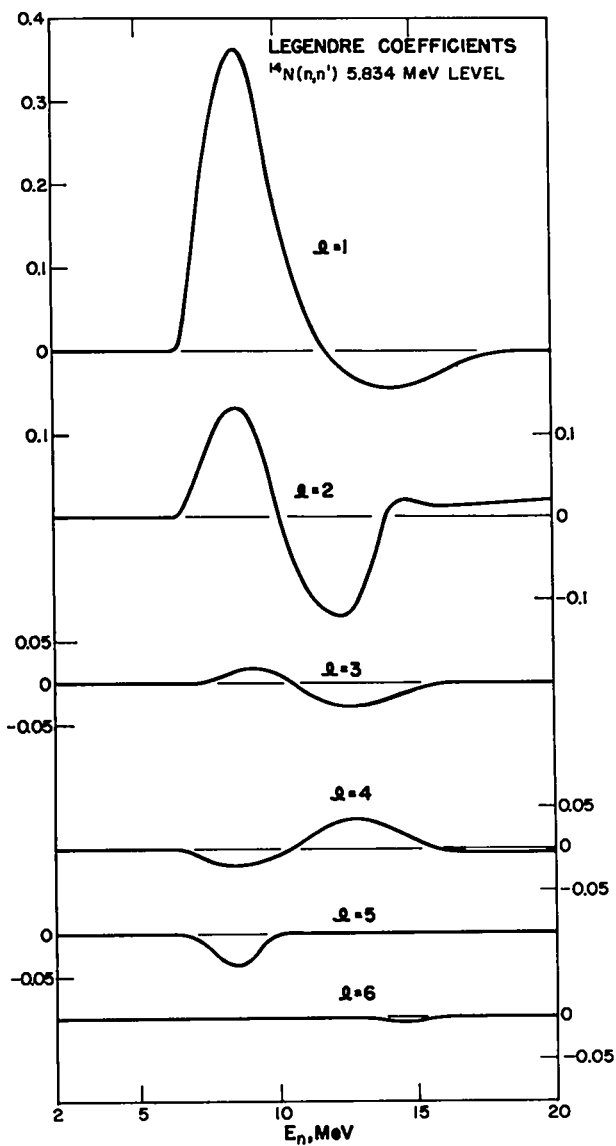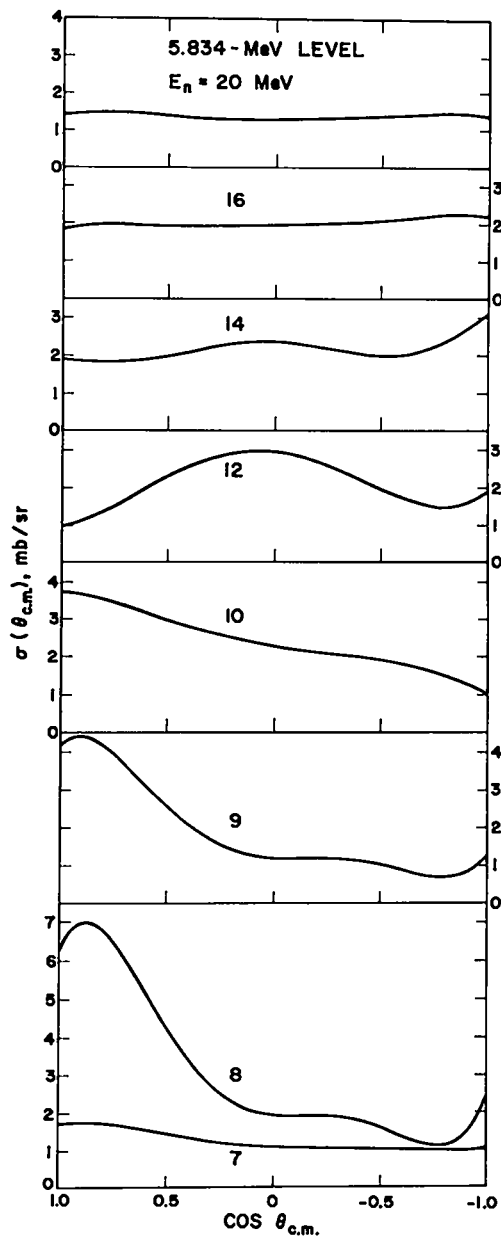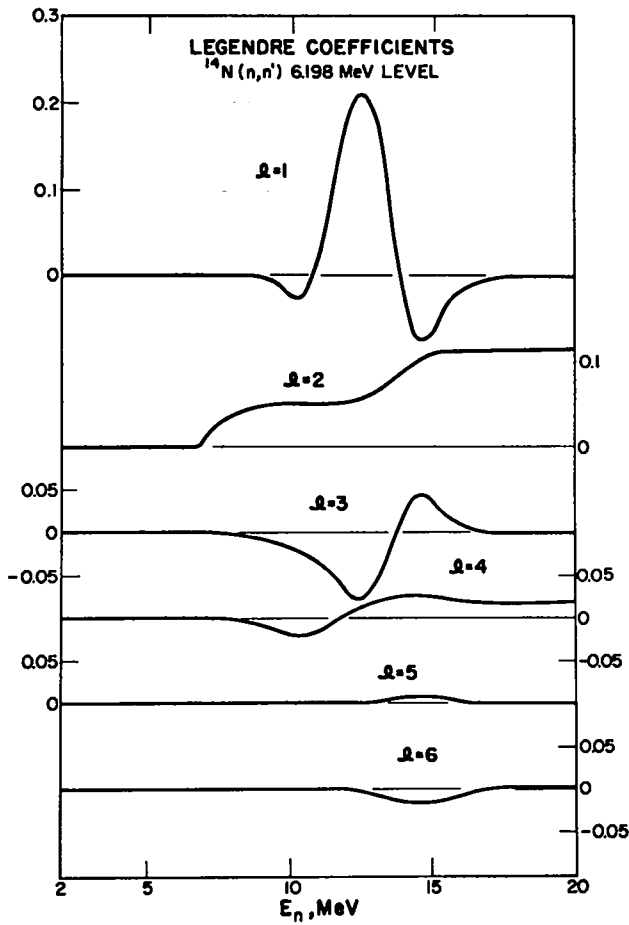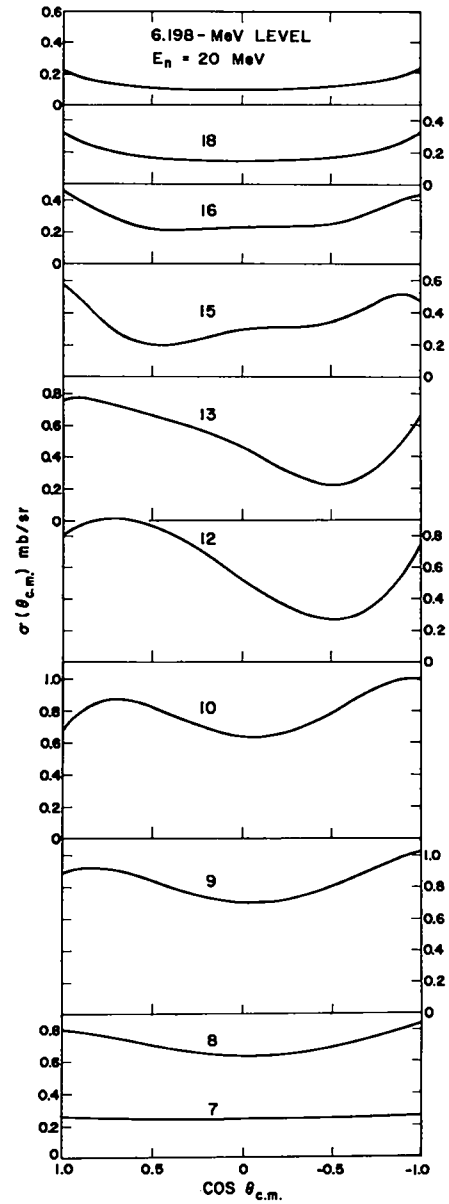
Fig. C4. Evaluated differential cross sections at selected energies for inelastic scattering to the 3.945-MeV level in ^{14}N.
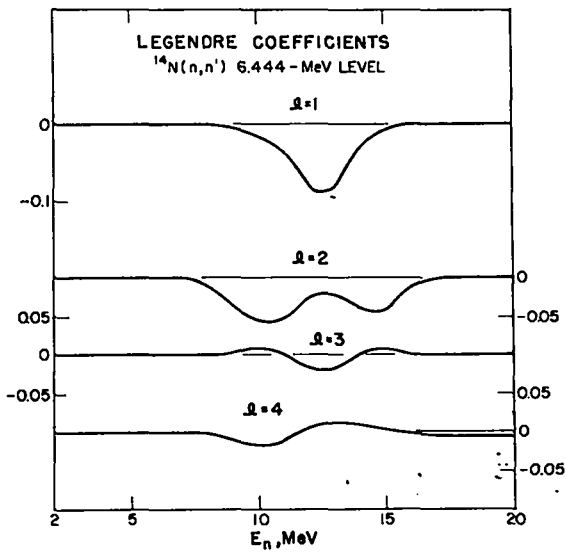
Fig. C5. Evaluated Legendre coefficients for inelastic scattering to the 4.913-MeV level in ^{14}N.

Fig. C6. Evaluated differential cross sections at selected energies for inelastic scattering to the 4.913-MeV level in ^{14}N.

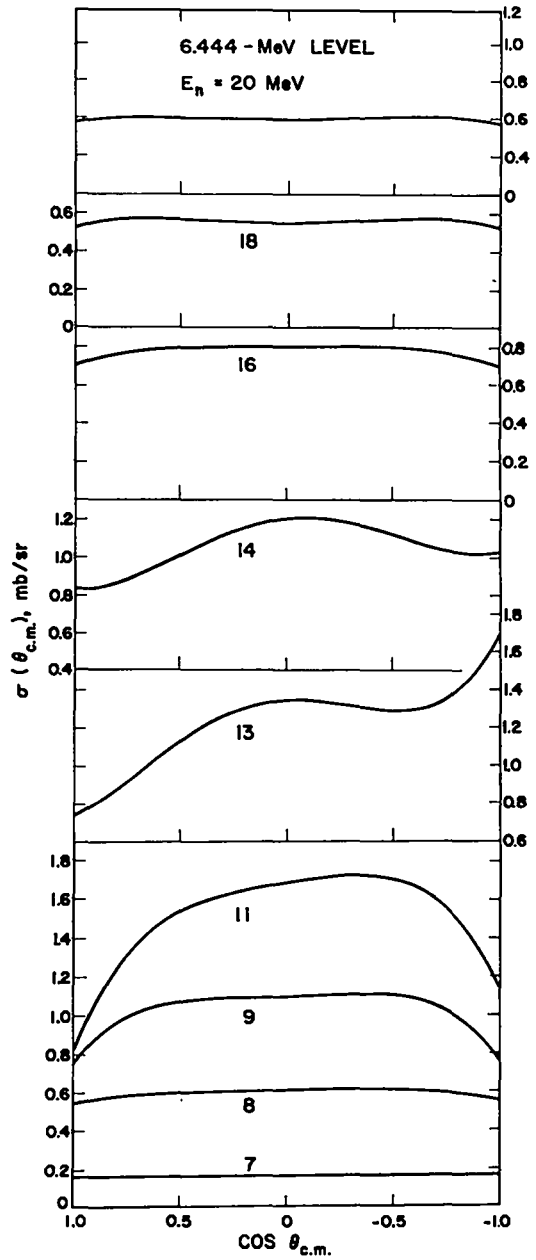**Fig. C7.** Evaluated Legendre coefficients for inelastic scattering to the 5.106-MeV level in ^{14}N.

Fig. C8. Evaluated differential cross sections at selected energies for inelastic scattering to the 5.106-MeV level in ^{14}N.
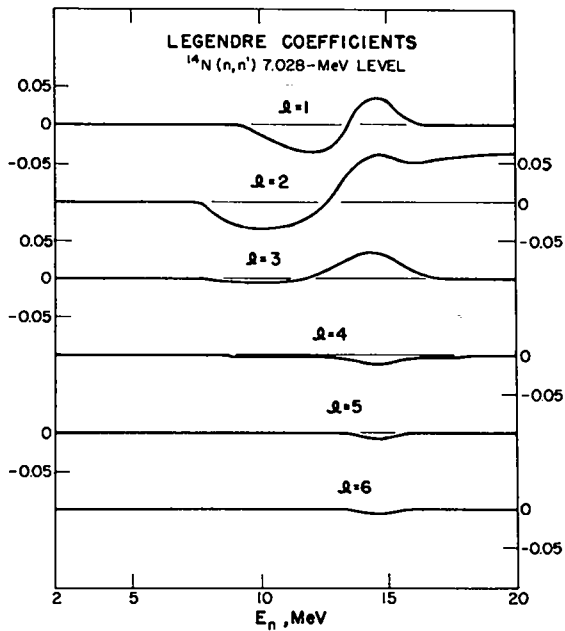
Fig. C9. Evaluated Legendre coefficients for in-
elastic scattering to the 5.691-MeV level
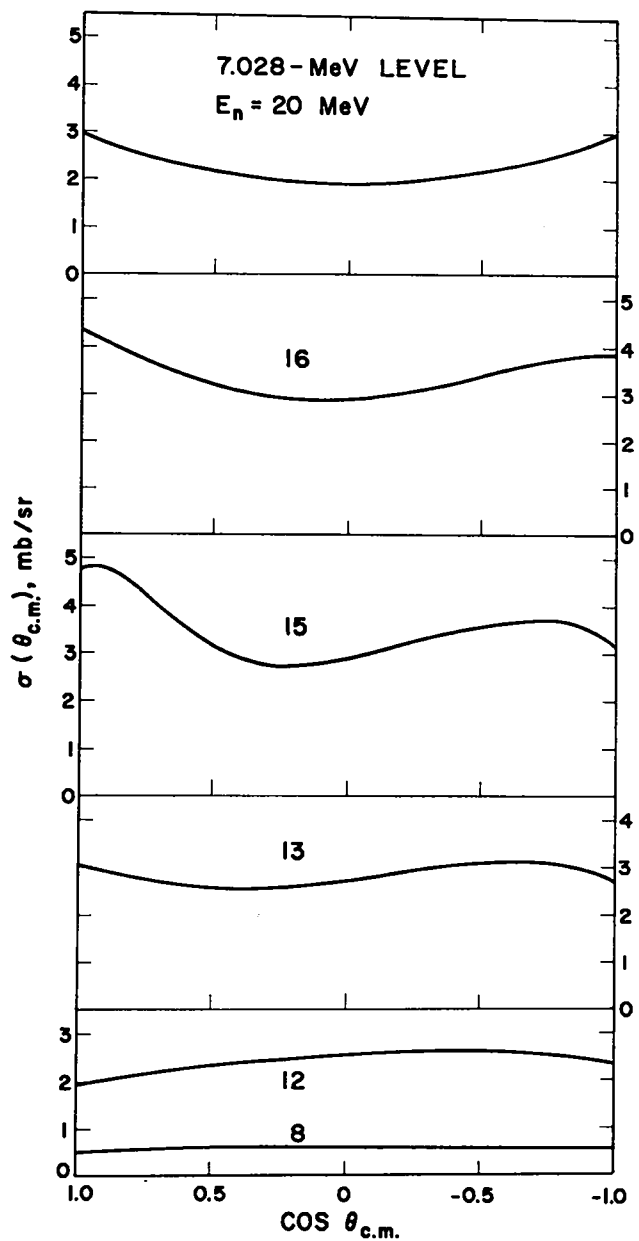in ^{14}N.

Fig. C10. Evaluated differential cross sections at
selected energies for inelastic scattering
to the 5.691-MeV level in ^{14}N.

Fig. C11. Evaluated Legendre coefficients for inelastic scattering to the 5.834-MeV level in ^{14}N. This transition exhibits the largest ℓ=1 coefficient of any of the inelastic channels for nitrogen.

Fig. C12. Evaluated differential cross sections at selected energies for inelastic scattering to the 5.834-MeV level in ^{14}N. Note that the maximum/minimum cross-section ratio is close to 7.
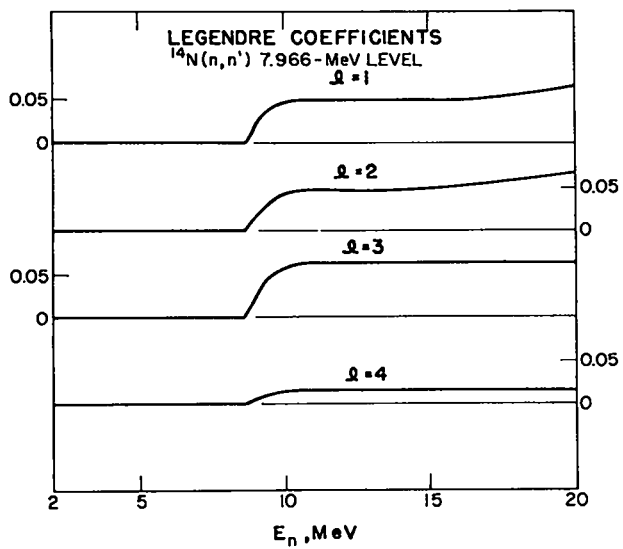
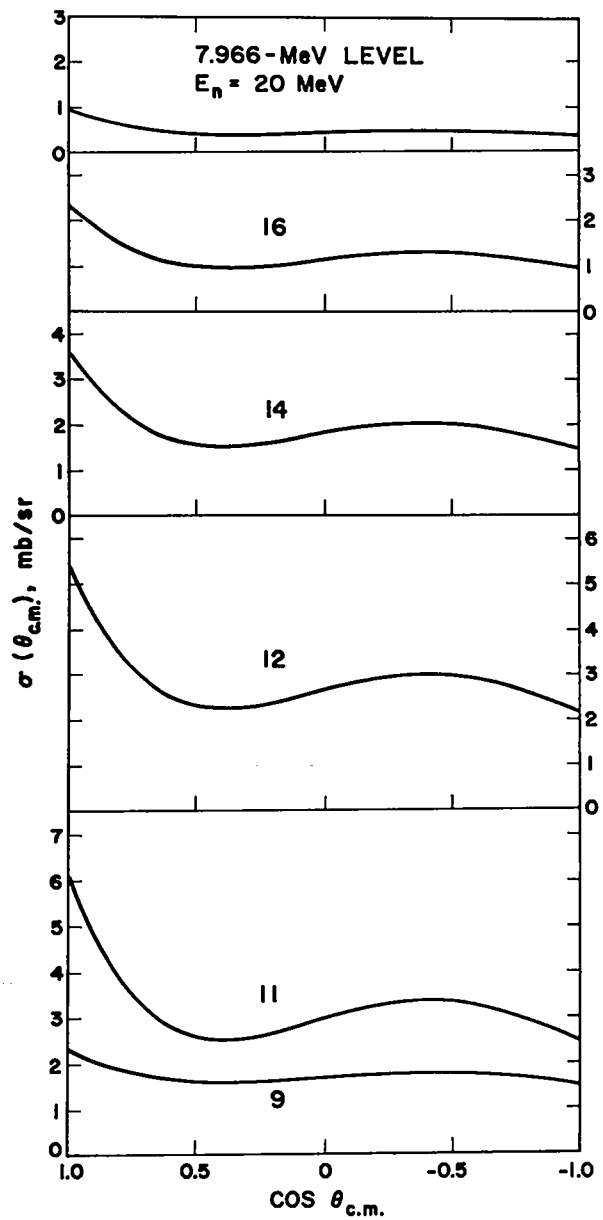Fig. C13. Evaluated Legendre coefficients for inelastic scattering to the 6.198-MeV level in ^{14}N.

Fig. C14. Evaluated differential cross sections at selected energies for inelastic scattering to the 6.198-MeV level in ^{14}N.

Fig. C15. Evaluated Legendre coefficients for inelastic scattering to the 6.444-MeV level in ^{14}N.

Fig. C16. Evaluated differential cross sections at selected energies for inelastic scattering to the 6.444-MeV level in ^{14}N. Note the suppressed zero for the 13-MeV curve.

Fig. C17. Evaluated Legendre coefficients for inelastic scattering to the 7.028-MeV level in ^{14}N.

Fig. C18. Evaluated differential cross sections at selected energies for inelastic scattering to the 7.028-MeV level in ^{14}N.
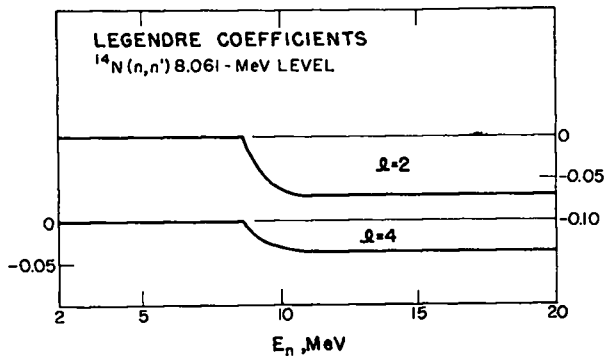
Fig. C19. Evaluated Legendre coefficients for in-
elastic scattering to the 7.966-MeV level
in ^{14}N.

Fig. C20. Evaluated differential cross sections at
selected energies for inelastic scatter-
ing to the 7.966-MeV level in ^{14}N.

Fig. C21. Evaluated Legendre coefficients for in-
elastic scattering to the 8.061-MeV level
in ^{14}N. There were not enough measured
points at back angles in the (p,p') data
from which these curves were constructed
to define the cross sections beyond 90°,
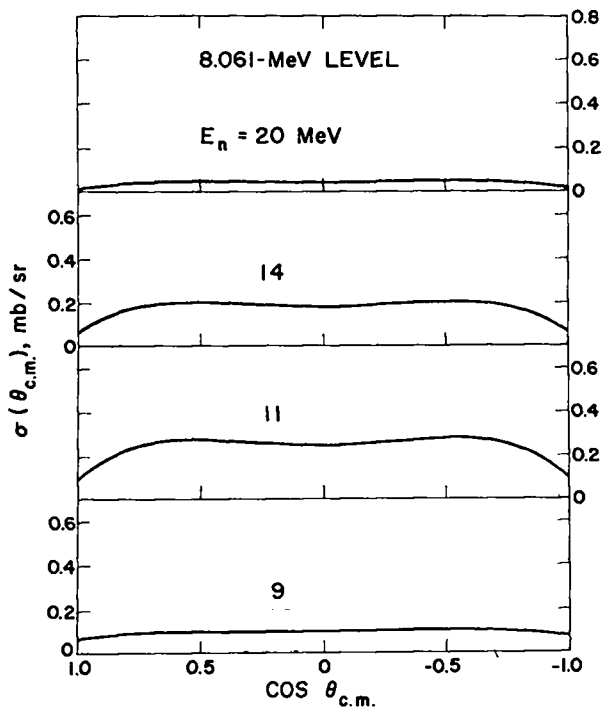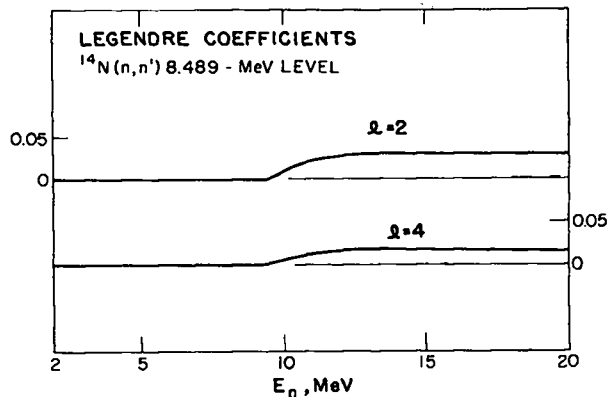so the distributions were assumed sym-
metric.

Fig. C23. Evaluated Legendre coefficients for in-
elastic scattering to the 8.489-MeV level
in ^{14}N, assumed symmetric in the absence
of adequate data.

Fig. C22. Evaluated differential cross sections at
selected energies for inelastic scatter-
ing to the 8.061-MeV level in ^{14}N, assumed
symmetric about 90° in the absence of suf-
ficient data to determine the entire dis-
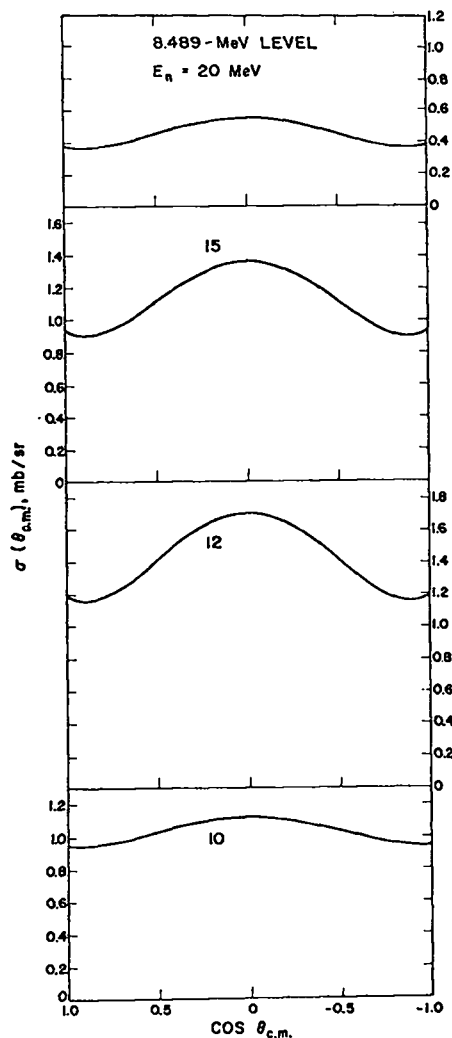tribution.

Fig. C24. Evaluated differential cross sections at
selected energies for inelastic scattering
to the 8.489-MeV level in ^{14}N. Symmetry
about 90° has been assumed.

77